UNIVERSITY
OF GÄVLE

DEPARTMENT OF TECHNOLOGY

Design a Highly Linear Power Amplifier Based on HBT

Paul Saad

June 2006

Master's Thesis in Electronics/Telecommunication

Examiner: Prof. Daniel Rönnow

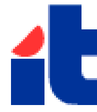

SAAD PAUL

M.Sc Thesis 05/06

Design a Highly Linear Power Amplifier Based on SiGe HBT

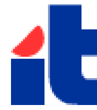

ABSTRACT

The RF power amplifier (PA) is one of the critical components in the 802.11 transceivers, and it is expected to provide a suitable output power at a very good gain with high efficiency and linearity.

However, present-day telecommunication device technology is not well suited to the requirements of optical data communication. Digital CMOS is the most used technology in RF applications, nowadays; nevertheless HBT gives more advantage in terms of higher power gain and better thermal capabilities.

In this thesis we are designing, manufacturing and testing a power amplifier based on HBT technology, in order to investigate its characteristics and performance for power amplifier applications and to prove that HBT power amplifiers can be widely used for this kind of applications.

Therefore we will study the HBT technology, as well as the transistor characteristics and HBT structure and properties. Since we are designing a power amplifier for WIFI applications, we will also give an overview of WIFI and present the IEEE 802.11 physical layer standard and applications and features of it, and then we will present the advantages and disadvantages of WIFI and the specifications of the power amplifier to be designed and manufactured.

This thesis will present a Class A PA design and discuss its performance. We will study parameters which quantify the various aspects of amplifier performance such as 1-dB compression point, 3rd order intercept point, intermodulation distortion; efficiency and adjacent channel power ratio.

The Class A amplifier was designed using NEC HBT (Heterojunction Bipolar Transistor) transistor models and its performance was simulated using ADS. Various procedures involved in the design of the Class A amplifier such as DC simulation, bias point selection, Load-pull characterization, input and output matching circuit design and the design of a bias network are explained. Memory effects in Power Amplifiers are also discussed and found to be very small, with less than 0.2 dB variation in the output at fundamental frequencies.

The power gain, linearity, efficiency, power added efficiency, the input and output reflection coefficients, the Adjacent Channel Power Ratio (ACPR) and the memory effects of the PA

were measured and have been found to be satisfying and meet the specifications for WIFI applications. The efficiency of 21% was found, which is in the practical efficiency range for class A PA. The Linearity of the power amplifier was measured by its two-tone intercept point and found to be satisfying.

All the results show that this technology can be widely used for this kind of applications and that HBT can replace CMOS with improve performance, which was our objective.

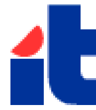

Acknowledgment

Working on this thesis was a very useful, important and memorable experience to me. I would like to thank all those people who made this thesis possible.

To my committee members in the University of Gävle for giving me the opportunity to do my thesis in Aveiro with such a wonderful committed group of researchers.

To Prof Nuno Borges Carvalho, my advisor at the Institute of Telecommunications, in Aveiro Portugal. The knowledge that I gained from his lectures and during personal discussions was invaluable.

To my family, without you, I would have nothing. Without you, I would be nothing. Without you, I would go nowhere. Thank you!

To my fellow students, I am grateful for the time that we have spent together. As usual I have learned far more than I expected because of you and will cherish the knowledge as much as the memories. Keep in touch!

To my friends, you never cease to amaze me. More importantly, you never cease to honor me with your presence and loyalty. I can hope I have been able to return the favor.

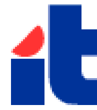

Table of Contents

1 CHAPTER 1 .... **1**

INTRODUCTION **1**

1.1 BACKGROUND 1
1.2 THE OBJECTIVE 1

2 CHAPTER 2 .... **3**

HBT TECHNOLOGY **3**

2.1 INTRODUCTION 3
2.2 P-N JUNCTION 3
2.3 P-N HETEROJUNCTION DIODES 4
2.4 THE TRANSISTOR ACTION 6
2.5 THE HETEROJUNCTION BIPOLAR TRANSISTOR 8
2.5.1 Current Gain in HBT *8*
2.5.2 Basic HBT Structures *12*
2.5.3 Advanced HBTs *13*
2.6 SI-GE HBT VERSUS CMOS 16
2.7 CONCLUSION 16

3 CHAPTER 3 .... **17**

WI-FI **17**

3.1 INTRODUCTION 17
3.2 WHAT IS WIFI? 17
3.3 STANDARDS OF WIFI 17
3.4 ADVANTAGES OF WI-FI 19
3.5 DISADVANTAGES OF WI-FI 19
3.6 SPECIFICATIONS FOR 802.11B 20

4 CHAPTER 4 .... **21**

RF POWER AMPLIFIER THEORY **21**

4.1 INTRODUCTION 21
4.2 EFFICIENCY 21

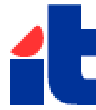

4.3 1-dB COMPRESSION POINT (P_{1-dB}) ... 22
4.4 INTERMODULATION DISTORSION (IMD) ... 23
4.5 ADJACENT CHANNEL POWER RATIO (ACPR) ... 24
4.6 INTERCEPT POINT (IP) ... 25
4.7 POWER AMPLIFIER CLASSIFICATION ... 26
4.7.1 Class A ... 26
4.7.2 Class B ... 27
4.7.3 Class AB ... 28
4.7.4 Class C ... 29

5 CHAPTER 5 ... 31

DESIGN AND IMPLEMENTATION ... 31

5.1 INTRODUCTION ... 31
5.2 MODEL OF THE NEC HBT TRANSISTOR ... 31
5.3 BIAS POINT SIMULATION ... 32
5.4 DETERMINATION OF THE S-PARAMETERS ... 35
5.5 STABILITY ... 36
5.6 LOAD PULL ... 38
5.7 MATCHING ... 40
5.7.1 Input Matching Network ... 40
5.7.2 Output Matching Network ... 41
5.8 BIAS ... 42
5.9 CURRENT SOURCE ... 43
5.10 CLASS A IMPLEMENTATION ... 44
5.11 RESULTS ... 45
5.11.1 Single-tone Simulation ... 45
5.11.2 Two-Tone Simulation ... 48
5.12 PERFORMANCE OF THE PA IN DIFFERENT CLASSES OF OPERATION ... 50
5.13 LAYOUT ... 57

6 CHAPTER 6 ... 59

MEMORY EFFECTS IN POWER AMPLIFIER ... 59

6.1 INTRODUCTION ... 59
6.2 SOURCES OF MEMORY EFFECTS ... 59

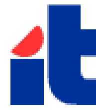

6.2.1 Self-Heating of Active Power Device *60*
6.2.2 Bias Network Construction *60*
6.2.3 Power Supply Properties *60*
6.3 SIMULATED RESULTS OF MEMORY EFFECTS IN THE POWER AMPLIFIER 62

7 CHAPTER 7 67

MEASUREMENTS 67

7.1 INTRODUCTION 67
7.2 MATCHING MEASUREMENT 67
7.3 POWER GAIN AND COMPRESSION CHARACTERISTIC MEASUREMENT 68
7.4 ADJACENT CHANNEL POWER RATIO MEASUREMENT 70
7.5 EFFICIENCY AND POWER ADDED EFFICIENCY MEASUREMENTS 71
7.6 LINEARITY MEASUREMENT 72
7.7 MEMORY EFFECTS 74

8 CHAPTER 8 77

CONCLUSION AND THE FUTURE WORK 77

8.1 INTRODUCTION 77
8.2 CONCLUSION 77
8.3 FUTURE WORK 77

APPENDIX 79

MANUFACTURING 79

REFERENCES 80

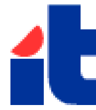

Table of Figures

FIGURE 2-1: P-N JUNCTION AND ITS ENERGY BAND DIAGRAM AT EQUILIBRIUM 3

FIGURE 2-2: DEPLETION REGION OF A P-N JUNCTION 4

FIGURE 2-3:ENERGY BAND DIAGRAMS FOR: (A) AN ISOLATED N-GE AND P-GAAS SEMICONDUCTOR IN EQUILIBRIUM, AND (B) N-GE AND P-GAAS BROUGHT INTO INTIMATE CONTACT TO FORM AN N-P HETEROJUNCTION DIODE. 6

FIGURE 2-4: PERSPECTIVE VIEW OF A SILICON P-N-P BIPOLAR TRANSISTOR... 6

FIGURE 2-5:(A) IDEALIZED ONE-DIMENSIONAL SCHEMATIC OF A P-N-P BIPOLAR TRANSISTOR AND (B) ITS CIRCUIT SYMBOL (C) IDEALIZED ONE-DIMENSIONAL SCHEMATIC OF AN N-P-N BIPOLAR TRANSISTOR AND (D) ITS CIRCUIT SYMBOL... 7

FIGURE 2-6: VARIOUS CURRENT COMPONENTS IN A P-N-P TRANSISTOR UNDER ACTIVE MODE OF OPERATION. THE ELECTRON FLOW IS IN THE OPPOSITE DIRECTION TO THE ELECTRON CURRENT 8

FIGURE 2-7:(A) SCHEMATIC CROSS SECTION OF AN N-P-N HETEROJUNCTION BIPOLAR TRANSISTOR (HBT) STRUCTURE. (B) ENERGY BAND DIAGRAM OF A HBT OPERATED UNDER ACTIVE MODE 13

FIGURE 2-8: CURRENT GAIN AS A FUNCTION OF OPERATING FREQUENCY FOR AN LNP-BASED HBT.B ... 14

FIGURE 2-9:(A) DEVICE STRUCTURE OF AN N-P-N SI/SIGE/SI HBT. (B) COLLECTOR AND BASE CURRENT VERSUS VEB FOR A HBT AND BIPOLAR JUNCTION TRANSISTOR (BJT). 14

FIGURE 2-10: ENERGY BAND DIAGRAMS FOR A HETEROJUNCTION BIPOLAR TRANSISTOR WITH AND WITHOUT GRADED LAYER IN THE JUNCTION, AND WITH AND WITHOUT A GRADED-BASE LAYER.... 15

FIGURE 4-1:1-DB COMPRESSION POINT 23

FIGURE 4-2: INTERMODULATION DISTORTION.. 24

FIGURE 4-3: PLOT OF ADJACENT CHANNEL POWER 24

FIGURE 4-4: PLOT SHOWING THIRD ORDER INTERCEPT POINT 25

FIGURE 4-5: BIASING FOR CLASS A 27

FIGURE 4-6: BIASING FOR CLASS B.. 28

FIGURE 4-7: BIAS FOR CLASS AB 29

FIGURE 4-8: BIAS FOR CLASS C 30

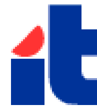

FIGURE 5-1: MODEL OF THE HBT TRANSISTOR 31

FIGURE 5-2: COLLECTOR CURRENT VS. COLLECTOR TO EMITTER VOLTAGE 32

FIGURE 5-3: SCHEMATIC THAT DETERMINES THE BIAS POINT 33

FIGURE 5-4: BIAS POINT SIMULATION FOR CLASS A 34

FIGURE 5-5: CIRCUIT THAT DETERMINES THE S-PARAMETERS 35

FIGURE 5-6: INPUT AND OUTPUT STABILITY CIRCLES 37

FIGURE 5-7: ONE TONE LOAD PULL SIMULATION 38

FIGURE 5-8: LOAD PULL ANALYSIS TO DETERMINE LOAD IMPEDANCE FOR MAXIMUM EFFICIENCY 39

FIGURE 5-9: SMITH CHART FOR THE DESIGN OF THE INPUT MATCHING NETWORK 40

FIGURE 5-10: SMITH CHART FOR THE DESIGN OF THE INPUT MATCHING NETWORK 41

FIGURE 5-11: BIAS CIRCUIT 42

FIGURE 5-12: CURRENT SOURCE 43

FIGURE 5-13: SCHEMATIC OF CLASS A DESIGN 44

FIGURE 5-14: SCHEMATIC OF THE ONE TONE HARMONIC BALANCE SIMULATION 45

FIGURE 5-15: CLASS-A POWER GAIN 46

FIGURE 5-16: CLASS-A PAE 46

FIGURE 5-17: CLASS-A PIN VS. POUT 47

FIGURE 5-18: FUNDAMENTAL AND THIRD HARMONIC 48

FIGURE 5-19: ZOOMED OUTPUT SPECTRUM SHOWING 3RD, 5TH AND 7TH ORDER IMD PRODUCTS 49

FIGURE 5-20: PLOT OF THE POWER TRANSDUCER GAIN AND THE PAE 49

FIGURE 5-21: PLOT OF THE FUNDAMENTALS AND THE THIRD ORDER INTERMODULATION 50

FIGURE 5-22: 3RD ORDER IMD VERSUS BASE CURRENT 51

FIGURE 5-23: POWER GAIN VERSUS INPUT POWER FOR DIFFERENT BASE CURRENT 52

FIGURE 5-24: FUNDAMENTAL AND THIRD HARMONIC FOR CLASS AB OPERATION 52

FIGURE 5-25: PLOT OF THE FUNDAMENTALS AND THE THIRD ORDER INTERMODULATION FOR CLASS AB 53

FIGURE 5-26: POWER GAIN VERSUS INPUT POWER FOR DIFFERENT BASE CURRENT 54

FIGURE 5-27: FUNDAMENTAL AND THIRD HARMONIC FOR CLASS B OPERATION 54

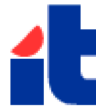

FIGURE 5-28: PLOT OF THE FUNDAMENTALS AND THE THIRD ORDER INTERMODULATION FOR CLASS B OPERATION 54

FIGURE 5-29: FUNDAMENTAL AND THIRD HARMONIC FOR CLASS C OPERATION 55

FIGURE 5-30: PLOT OF THE FUNDAMENTALS AND THE THIRD ORDER INTERMODULATION FOR CLASS C OPERATION 55

FIGURE 5-31: ARTWORK COMPONENT 57

FIGURE 5-32: PA LAYOUT DESIGN - ADS 58

FIGURE 6-1: TYPICAL LOCATION OF THE MEMORY EFFECTS POWER AMPLIFIER 59

FIGURE 6-2: MEMORY EFFECTS DUE TO POWER SUPPLY VARIATIONS 61

FIGURE 6-3: MEMORY EFFECTS DUE TO MISMATCHING OF EVEN HARMONICS 62

FIGURE 6-4: MEASURED UPPER AND LOWER IMD3 AS FUNCTION OF INPUT POWER AND FREQUENCY SPACING (ΔF) OF A TWO-TONE INPUT SIGNAL: (A) CLASS-A, (B) CLASS-AB 63

FIGURE 6-5: MEASURED OUTPUT SIGNAL AT (A) FUNDAMENTAL FREQUENCIES, (B) UPPER AND LOWER IMD3 AS FUNCTION OF FREQUENCY SPACING (ΔF) OF A TWO-TONE INPUT SIGNAL (INPUT POWER =-6 DBM). 64

FIGURE 6-6: SCHEMATIC OF THE LOAD IMPEDANCE 65

FIGURE 6-7: OUTPUT IMPEDANCE 65

FIGURE 6-8: SCHEMATIC OF THE SOURCE IMPEDANCE 66

FIGURE 6-9: INPUT IMPEDANCE 66

FIGURE 7-1: SETUP FOR THE MATCHING MEASUREMENT 68

FIGURE 7-2: INPUT, OUTPUT REFLECTION COEFFICIENTS (S11, S22) AND TRANSMISSION COEFFICIENT (S21) 68

FIGURE 7-3: POWER GAIN SETUP MEASUREMENTS 68

FIGURE 7-4: POWER GAIN VERSUS INPUT POWER 69

FIGURE 7-5: OUTPUT POWER VERSUS INPUT POWER 70

FIGURE 7-6: 3GPP ACPR MEASUREMENT 71

FIGURE 7-7: POWER EFFICIENCY AND PAE VERSUS OUTPUT POWER 72

FIGURE 7-8: TWO TONES MEASUREMENT SETUP 72

FIGURE 7-9: THE TWO FUNDAMENTALS AND THE THIRD ORDER INTERMODULATION PRODUCTS 73

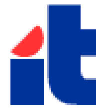

FIGURE 7-10: TWO-TONES INTERCEPT POINT 74

FIGURE 7-11: MEASURED OUTPUT SIGNAL AT (A) FUNDAMENTAL FREQUENCIES, (B) UPPER AND LOWER IMD3 AS FUNCTION OF FREQUENCY SPACING (ΔF) OF A TWO-TONE INPUT SIGNAL AND INPUT POWER SWEEPING 75

FIGURE 7-12: 3D VIEW OF THE DIFFERENCE MEASURED OUTPUT SIGNAL AT (A) FUNDAMENTAL FREQUENCIES, (B) UPPER AND LOWER IMD3 AS FUNCTION OF FREQUENCY SPACING (ΔF) OF A TWO-TONE INPUT SIGNAL AND INPUT POWER SWEEPING.. 76

FIGURE 8-1: MULTIPLE STAGE POWER AMPLIFIER 78

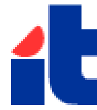

List of Tables

TABLE 3-1: DIFFERENT FEATURES OF STANDARDS IN WIFI 19

TABLE 3-2:SPECIFICATIONS FOR 802.11B..... 20

TABLE 5-1:PARAMETERS OF THE HBT TRANSISTOR..... 32

TABLE 5-2: SIMULATED S-PARAMETERS 35

TABLE 5-3: OUTPUT OF THE CURRENT SOURCE 43

TABLE 5-4: VALUES AT 1-DB COMPRESSION POINT 47

TABLE 5-5: HARMONIC LEVELS 48

TABLE 5-6:COLLECTOR CURRENT FOR DIFFERENT VALUES OF BASE CURRENT..... 51

TABLE 5-7: CHARACTERISTICS OF THE PA IN DIFFERENT CLASSES OF OPERATION 56

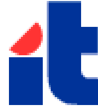

1 CHAPTER 1

INTRODUCTION

1.1 Background

Data communication using wireless networks such as IEEE 802.11 has found widespread use for the last few years. The RF power amplifier (PA) is one of the critical components in the 802.11 transceivers, expected to provide a suitable output power at a very good gain with high efficiency and linearity.

Present-day telecommunication device technology is not well suited to the requirements of data communication among and within computers because the computer environment is much more demanding. It imposes a higher ambient temperature on the devices, and requires denser packaging and smaller power dissipation per device, as well as a high degree of parallelism.

The GaAs/AlGaAs device technology is ideally suited to this task; nevertheless, the high performance follows the high price on the market, which suggests usage of alternative technologies.

LDMOS\GAN-based power amplifiers are used for very high power RF applications; therefore they are used for base station power amplifiers.

BJT transistors offer good performance, but are restricted for low frequency applications.

Due to the high volume of digital ICs using CMOS technology, digital CMOS is an extremely attractive candidate for realizing low-cost RF circuits; hence it is the most used technology in RF applications, nowadays. However, this process is geared toward optimizing digital circuit performance which imposes severe restrictions on realizing high-performance RF circuits in this technology, such as low power and low thermal capability.

1.2 The Objective

In this work we are designing, manufacturing and testing a power amplifier based on HBT technology, in order to investigate its characteristics and performance for power amplifier applications. If we can get good results that would prove that this technology can be widely used for this kind of applications we can show that HBT can replace

CMOS, which are mostly used nowadays, since HBT gives more advantage in terms of higher power gain and better thermal capabilities, i.e. for the same power, CMOS will dissipate more heat which increases the costs of the cooling systems and the DC power consumption.

2 CHAPTER 2

HBT TECHNOLOGY

2.1 Introduction

Since we are designing a power amplifier based on HBT (Hetero junction Bipolar Transistor) we will study in this chapter the HBT technology. We will start by giving an overview on the p-n Junction and p-n Hetero-junction since they form the HBT transistors. Then we move forward to study the transistor action and the HBT structure and properties. Since the only difference between HBT and BJT (Bipolar Junction Transistor) transistors is the difference in the emitter-base junction structure we will end this chapter by a comparison between the HBTs and BJTs transistors.

2.2 P-N Junction

One of the crucial keys to solid state electronics is the nature of the p-n junction. When p-type and n-type materials are placed in contact with each other, the junction behaves very differently than either type of material alone. Specifically, current will flow readily in one direction (forward biased) but not in the other (reverse biased), creating the basic diode. This non-reversing behavior arises from the nature of the charge transport process in the two types of materials [1].

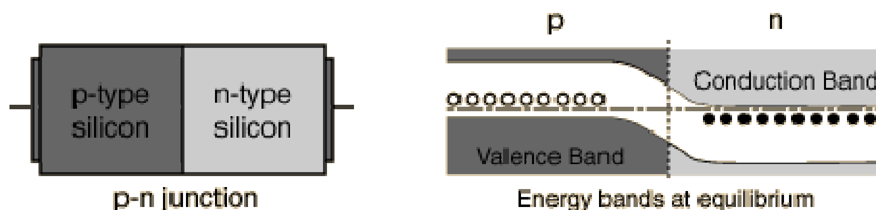

Figure 2-1: p-n junction and its energy band diagram at equilibrium

The open circles on the left side of the junction above represent "holes" or deficiencies of electrons in the lattice which can act like positive charge carriers. The solid circles on the right of the junction represent the available electrons from the n-type dopant. Near the junction, electrons diffuse across to combine with holes, creating a "depletion region".

The energy level sketch above right is a way to visualize the equilibrium condition of the p-n junction. When a p-n junction is formed, some of the free electrons in the n-region diffuse across the junction and combine with holes to form negative ions. In doing so they leave behind positive ions at the donor impurity sites [1].

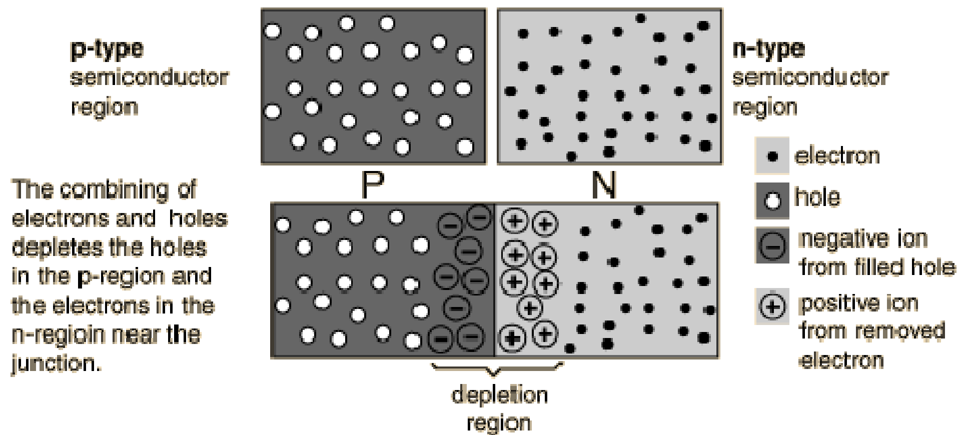

Figure 2-2: Depletion region of a p-n junction

2.3 P-N Heterojunction Diodes

A p-n heterojunction diode can be formed by using two semiconductors of different band gaps and with opposite doping impurities. Examples of p-n heterojunction diodes are Ge/GaAs, Si/SiGe, AlGaAs/GaAs, InGaAs/InAlAs, In-GaP/GaAs, InGaAs/InP, and GaN/InGaN heterostructures. The heterojunction diodes offer a wide variety of important applications for laser diodes, light-emitting diodes (LEDs), photodetectors, solar cells, junction field-effect transistors (JFETs), modulation-doped field-effect transistors (MODFETs or HEMTs), heterojunction bipolar transistors (HBTs).
Figure 1.3a shows the energy band diagram for an isolated n-Ge and p-GaAs semiconductor in thermal equilibrium, and Figure 2-3b shows the energy band diagram of an ideal n-Ge/p-GaAs heterojunction diode. As shown in Figure 2-3b, the energy band diagram for a heterojunction diode is much more complicated than that of a p-n homojunction due to the presence of energy band discontinuities in the conduction band (ΔEc) and valence band (ΔEv) at the metallurgical junction of the two materials. In Figure 2-3b, subscripts 1 and 2 refer to Ge and GaAs, respectively; the energy discontinuity step arises from the difference of band gap and work function in these two semiconductors. The conduction band offset at the heterointerface of the two materials is equal to ΔEc, and the valence band offset is ΔEv. The conduction and valence band offsets (ΔEc and ΔEv)

can be obtained from the energy band diagram shown in Figure 2-3a, and are given, respectively, by

$$\Delta E_c = q(\chi_1 - \chi_2) \quad (2.1)$$

$$\Delta E_v = (E_{g2} - E_{g1}) - \Delta E_c = \Delta E_g - \Delta E_c \quad (2.2)$$

This shows that the conduction band offset is equal to the difference in the electron affinity of these two materials, and the valence band offset is equal to the band gap difference minus the conduction band offset. From Eq. (2.2) it is noted that the sum of conduction band and valence band offset is equal to the band gap energy difference of the two semiconductors. When these two semiconductors are brought into intimate contact, the Fermi level (or chemical potential) must line up in equilibrium. As a result, electrons from the n-Ge will flow to the p-GaAs, and holes from the p-GaAs side will flow to the n-Ge side until the equilibrium condition is reached (i.e., the Fermi energy is lined up across the heterojunction). As in the case of a p-n homojunction, the redistribution of charges creates a depletion region across both sides of the junction. Figure 2-3b shows the energy band diagram for an ideal n-Ge/p-GaAs heterojunction diode in equilibrium, and the band offset in the conduction and valence bands at the Ge/GaAs interface is clearly shown in this figure. The band bending across the depletion region indicates that a built-in potential exists on both sides of the junction. The total built-in potential, V_{bi}, is equal to the sum of the built-in potentials on each side of the junction [2], i.e,

$$V_{bi} = V_{b1} + V_{b2} \quad (2.3)$$

Where V_{b1} are V_{b2} are the band bending potentials in p-Ge and n-GaAs, respectively.

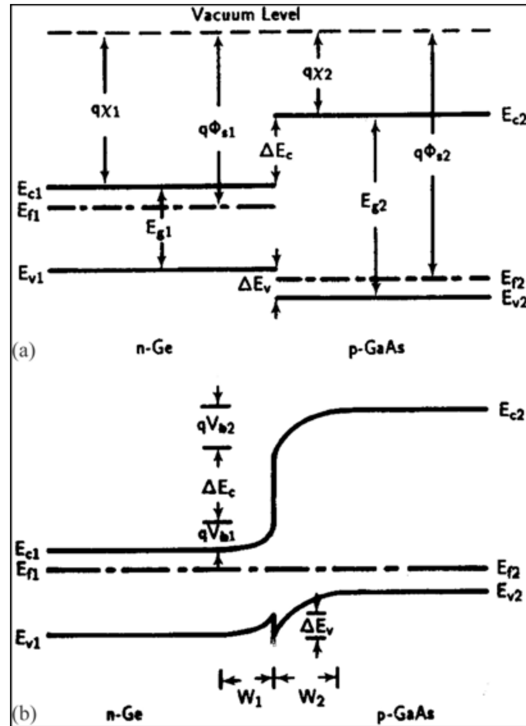

Figure 2-3:Energy band diagrams for: (a) an isolated n-Ge and p-GaAs semiconductor in equilibrium, and (b) n-Ge and p-GaAs brought into intimate contact to form an n-p Heterojunction diode.

2.4 The Transistor Action

A perspective view of a discrete p-n-p bipolar transistor is shown Figure 2.4 the transistor is formed by starting with a p-type substrate. An n-type region is thermally diffused through an oxide window into the p-type substrate. A very heavily doped p^+ region is then diffused into the n-type region. Metallic contacts are made to the p^+- and n-regions through the windows opened in the oxide layer and to the p-region at the bottom.

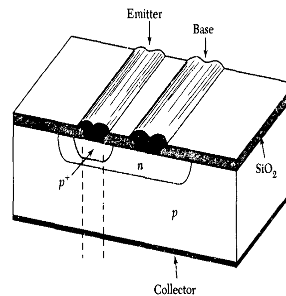

Figure 2-4: Perspective view of a silicon p-n-p bipolar transistor

An idealized, one-dimensional structure of a p-n-p bipolar transistor is shown in Figure 2-5a. Normally; the bipolar transistor has three separately doped regions and two p-n junctions. The heavily doped p^+-region is called the *emitter* (defined as symbol E in the figure). The narrow central n-region, with moderately doped concentration, is called the *base (*symbol *B).* The width of the base is small compared with the minority-carrier diffusion length. The lightly doped p-region is called the *collector (*symbol C).

Figure 2-5b illustrates the circuit symbol for a p-n-p transistor. The current components and voltage polarities are shown in the figure. The arrows of the various currents indicate the direction of current flow under normal operating conditions (also called the *active mode).* The + and - signs are used to define the voltage polarities. We can also denote the voltage polarity by a double subscript on the voltage symbol. In the active mode, the emitter-base junction is forward biased (V_{EB}>0) and the base-collector junction is reverse biased (V_{CB}<0).

The n-p-n bipolar transistor is the complementary structure of the p-n-p bipolar transistor. The structure and circuit symbol of an ideal n-p-n transistor are shown in Figures 2-5c and 2-5d, respectively. The n-p-n structure can be obtained by interchanging *p* for *n* and *n* for *p* from the p-n-p transistor. As a result the current flow and voltage polarity are all reversed.

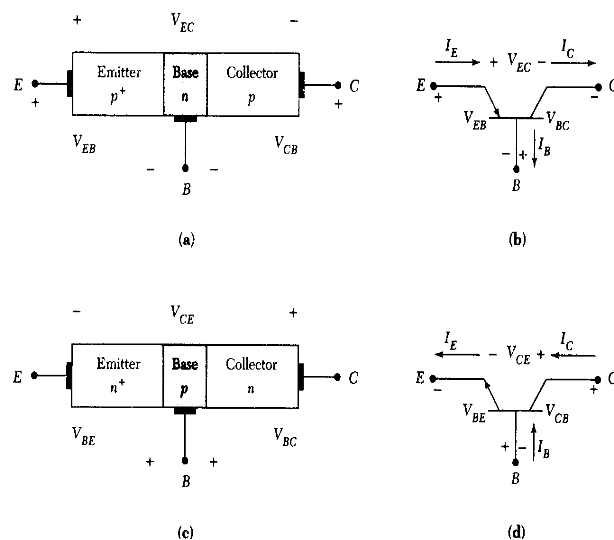

Figure 2-5:(a) Idealized one-dimensional schematic of a p-n-p bipolar transistor and (b) its circuit symbol (c) Idealized one-dimensional schematic of an n-p-n bipolar transistor and (d) its circuit symbol.

2.5 The Heterojunction Bipolar Transistor

We have considered the heterojunction in Sec.1.2 a heterojunction bipolar transistor (HBT) is a transistor in which one or both p-n junctions are formed between dissimilar semiconductors. The primary advantage of an HBT is its high emitter efficiency. The circuit applications of the HBT are essentially the same as those of bipolar transistors. However, the HBT has higher-speed and higher-frequency capability in circuit operation. Because of these features, the HBT has gained popularity in photonic, microwave, and digital applications. For example, in microwave applications, HBT is used in solid-state microwave and millimetre-wave power amplifiers, oscillators, and mixers.

2.5.1 Current Gain in HBT

Figure 2-6 shows the various current components in an ideal p-n-p transistor biased in the active mode (emitter-base junction is forward biased the collector-base junction is reverse biased). Note that we assume that there are no generation-recombination currents in the depletion regions. The holes injected from the emitter constitute the current I_{EP}, which is the largest current component in a well-designed transistor. Most of the injected holes will reach the collector junction and give rise to the current I_{CP}. There are three base current components, labelled I_{BB}, I_{En}, and I_{Cn}. I_{BB} corresponds to electrons that must be supplied by the base to replace electrons recombined with the injected holes (i.e., I_{BB} - I_{Ep} - I_{Cp}). I_{En} corresponds to the current arising from electrons being injected from the base to the emitter. However, I_{En} is not desirable. It can be minimized by using heavier emitter doping or a heterojunction. I_{Cn} corresponds to thermally generated electrons that are near the base-collector junction edge and drift from the collector to the base. As indicated in the figure, the direction of the electron current is opposite the direction of the electron flow [3].

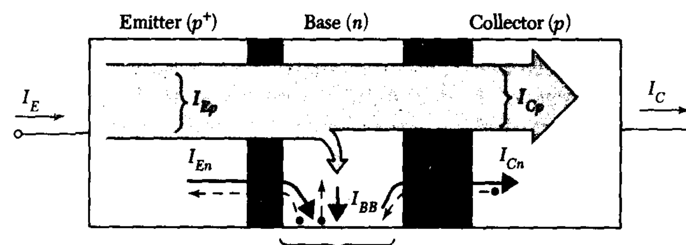

Figure 2-6: various current components in a p-n-p transistor under active mode of operation. The electron flow is in the opposite direction to the electron current

We can now express the terminal currents in terms of the various current components described above:

$$I_E = I_{Ep} + I_{En} \tag{2.4}$$

$$I_C = I_{Cp} + I_{Cn} \tag{2.5}$$

$$I_B = I_E - I_C = I_{En} + (I_{Ep} - I_{Cp}) - I_{Cn} \tag{2.6}$$

An important parameter in the characterization of bipolar transistors is the *common base current gain* α_0. This quantity is defined by

$$\alpha_0 \equiv \frac{I_{Cp}}{I_E} \tag{2.7}$$

Substituting Eq. (2.4) into Eq. (2.7) yields

$$\alpha_0 = \frac{I_{Cp}}{I_{Ep} + I_{En}} = \left(\frac{I_{Ep}}{I_{Ep} + I_{En}}\right)\left(\frac{I_{Cp}}{I_{Ep}}\right) \tag{2.8}$$

The first term on the right-hand side is called the *emitter efficiency y,* which is a measure of the injected hole current compared with the total emitter current:

$$\gamma \equiv \frac{I_{Ep}}{I_E} = \frac{I_{Ep}}{I_{Ep} + I_{En}} \tag{2.9}$$

The second term is called the *base transport factor* α_T, which is the ratio of the hole current reaching the collector to the hole current injected from the emitter:

$$\alpha_T = \frac{I_{Cp}}{I_{Ep}} \tag{2.10}$$

Therefore, Eq. (2.8) becomes

$$\alpha_0 = \gamma \alpha_T \tag{2.11}$$

For a well-designed transistor, because I_{En} is small compared with I_{Ep} and I_{Cp} is close to I_{EP}, both α_T and γ approach unity. Therefore, α_0 is close to 1.

We can express the collector current in terms of α_0: The collector current can be described by substituting Eqs. (2.9) and (2.10) into Eq. (2.5):

$$I_C = I_{Cp} + I_{Cn} = \gamma\alpha_T\left(\frac{I_{Ep}}{\gamma}\right) + I_{Cn} = \alpha_0 I_E + I_{Cn} \tag{2.12}$$

The collector current for the common-emitter configuration can be obtained by substituting Eq. (2.6) into Eq. (2.12):

$$I_C = \alpha_0\left(I_B + I_C\right) + I_{CBO} \tag{2.13}$$

Solving for I_C we obtain

$$I_C = \frac{\alpha_0}{\alpha_0 - 1} I_B + \frac{I_{Cn}}{1 - \alpha_0} \tag{2.14}$$

We now designate β_o as the *common-emitter current* gain, which is the incremental change of I_c with respect to an incremental change of I_B. From Eq. (2.14), we obtain

$$\beta_0 \equiv \frac{\Delta I_C}{\Delta I_B} = \frac{\alpha_0}{\alpha_0 - 1} \tag{2.15}$$

The second factor of (2.14) corresponds to the collector-emitter leakage current for I_B=0.

Let semiconductor 1 is the emitter and semiconductor 2 is the base of a HBT. We now consider the impact of the band gap difference between these two semiconductors on the current gain of a HBT.

When the base-transport factor α_T , is very close to unity, the common-emitter current gain can be expressed from Eqs. (2.11) and (2.15) as

$$\beta_0 \equiv \frac{\alpha_0}{1 - \alpha_0} \equiv \frac{\gamma\alpha_T}{1 - \gamma\alpha_T} = \frac{\gamma}{1 - \gamma} \quad (\text{For } \alpha_T = 1) \tag{2.16}$$

The emitter efficiency is given in function of the transistor physics dimensions [3] by Eq. (2.17)

$$\gamma = \frac{1}{1 + \frac{D_E}{D_P}\frac{n_{Eo}}{P_{n0}}\frac{W}{L_E}} \qquad (2.17)$$

Substituting from Eq. (2.16) in Eq. (2.17) yields (for *n-p-n* transistors)

$$\beta_0 = \frac{1}{\frac{D_E}{D_n}\frac{p_{E0}}{n_{p0}}\frac{W}{L_E}} \approx \frac{n_{p0}}{p_{E0}} \qquad (2.18)$$

Where $N_B = \frac{n_i^2}{p_{n0}}$ is the impurity doping in the base, $N_E = \frac{n_i^2}{n_{E0}}$ is the impurity doping in the emitter, D_E is the diffusion constant of the minority carriers in the emitter, D_P is the diffusion constant of the minority carriers in the collector, L_E is the diffusion length of the minority carriers in the Emitter and W is the width of the depletion region of the base-collector junction.

The minority carrier concentrations in the emitter and the base using the law of mass action [3] are given by

$$P_{E0} = \frac{n_i^2(emitter)}{N_E(emitter)} = \frac{N_C N_V \exp(-E_{gE}/KT)}{N_E} \qquad (2.19)$$

$$n_{p0} = \frac{n_i^2(base)}{N_B(base)} = \frac{N_C^{'} N_V^{'} \exp(-E_{gB}/KT)}{N_B} \qquad (2.20)$$

Where N_c and N_v are the densities of states in the conduction band and the valence band, respectively, and E_{gE} is the band gap of the emitter semiconductor. N'_c, N'_v, and E_{gB} are the corresponding parameters for the base semiconductor.

$$\beta_0 \approx \frac{N_E}{N_B} esp\left(\frac{E_{gE} - E_{gB}}{kT}\right) = \frac{N_E}{N_B}\exp\left(\frac{\Delta E_g}{kT}\right) \qquad (2.21)$$

This expression illustrates the advantage of a HBT over a BJT since in a homojunction BJT, $\Delta E_g = 0$ and the exponential factor is unity which means that we have higher common emitter gain in a HBT than for a BJT for the same doping.

2.5.2 Basic HBT Structures

Most developments of HBT technology are for the $Al_xGa_{1-x}As/GaAs$ material system. Figure 2-7a shows a schematic structure of a basic n-p-n HBT. In this device; the n-type emitter is formed in the wide band gap $Al_xGa_{1-x}As$ whereas the p-type base is formed in the lower band gap GaAs. The n-type collector and n-type sub collector are formed in GaAs with light doping and heavy doping, respectively. To facilitate the formation of ohmic contacts, a heavily doped n-type GaAs layer is formed between the emitter contact and the AlGaAs layer. Due to the large band gap difference between the emitter and the base materials, the common-emitter current gain can be extremely large. However, in homojunction bipolar transistors, there is essentially no band gap difference; instead the ratio of the doping concentration in the emitter and base must be very high. This is the fundamental difference between the homojunction and the heterojunction bipolar transistors [3].

Figure 2-7b shows the energy band diagram of the HBT under the active mode of operation. The band gap difference between the emitter and the base will provide band offsets at the heterointerface. In fact, the superior performance of the HBT results directly from the valence-band discontinuity ΔE_V, at the heterointerface. ΔE_V increases the valence band barrier height in the emitter-base heterojunction and thus reduces the injection of holes from the base to the emitter. This effect in the HBT allows the use of a heavily doped base while maintaining a high emitter efficiency and current gain. The heavily doped base can reduce the base sheet resistance. In addition; the base can be made very thin without concern about the *punch-through* effect in the narrow base region. The punch through effect arises when the base-collector depletion region penetrates completely through the base and reaches the emitter-base depletion region. A thin base region is desirable because it reduces the base transit time and increases the cut-off frequency.

We can prove that since the cutoff frequency f_t can be expressed by $(2\Pi\tau_T)^{-1}$ [3], where τ_T is the total time of the carrier transit from the emitter to the collector. τ_T Includes the emitter delay time τ_E, the base transit time τ_B, and the collector transit time τ_C. The most important delay is the base transit time and it can be expressed by equation (2.22) [3],

$$\tau_B = \frac{w^2}{2D_P} \qquad (2.22)$$

Where w is the base width and D_P is the diffusion of the minority carrier in the base. From equation (2.22) we can conclude that with small base width we can achieve high frequency transistors.

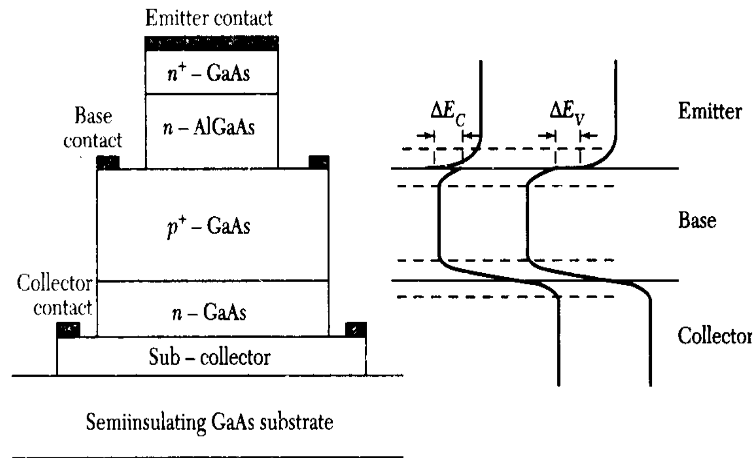

Figure 2-7:(a) Schematic cross section of an n-p-n heterojunction bipolar transistor (HBT) structure. (b) Energy band diagram of a HBT operated under active mode

2.5.3 Advanced HBTs

In recent years the InP-based (InP/InGaAs or AlInAs/ InGaAs) material systems have been extensively studied. The InP-based heterostructures had several advantages. The InP/InGaAs structure has very low surface recombination, and because of higher electron mobility in InGaAs than in GaAs, superior high-frequency performance is expected. A typical performance curve for an InP-based HBT is shown in Fig. 2-8. A very high cut-off frequency of 254 GHz is obtained. In addition, the InP collector region has higher drift velocity at high fields than that in the GaAs collector. The InP collector breakdown voltage is also higher than that in the GaAs [3].

Another heterojunction is in the Si/SiGe material system. This system has several properties that are attractive for HBT applications. Like A1GaAs/GaAs HBTs, Si/SiGe HBTs have high-speed capability since the base can be heavily doped because of the band gap difference. The small trap density at the silicon surface minimizes the surface recombination current and ensures a high current gain even at low collector current. Compatibility with the standard silicon technology is another attractive feature. Figure 2-

9a shows a typical Si/SiGe HBT structure. A comparison of the base and collector currents measured from a Si/SiGe HBT and a Si homojunction bipolar transistor is given by Fig. 2-9b. The results indicate that the Si/SiGe HBT has a higher current gain than the Si homojunction bipolar transistor. Compared with GaAs and InP-based HBTs, the Si/SiGe HBT, however, has a lower cut-off frequency because of the lower nobilities in Si.

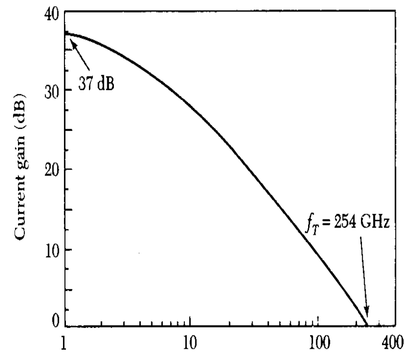

Figure 2-8: Current gain as a function of operating frequency for an lnP-based HBT.B

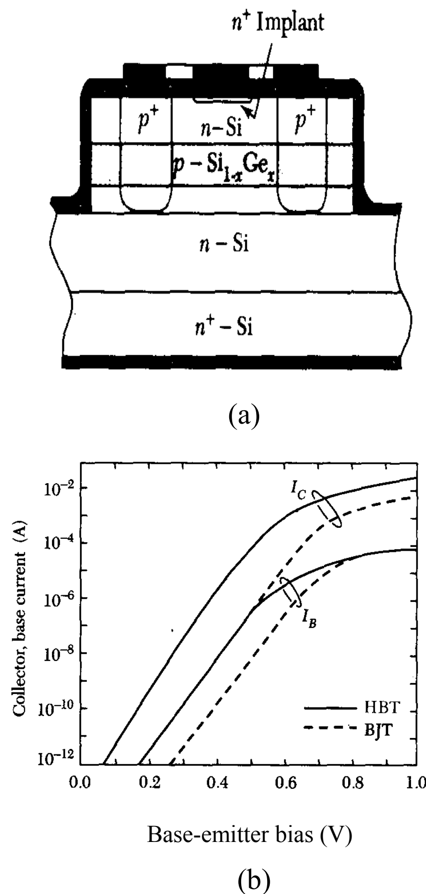

Figure 2-9:(a) Device structure of an n-p-n Si/SiGe/Si HBT. (b) Collector and base current versus VEB for a HBT and bipolar junction transistor (BJT).

The conduction band discontinuity ΔE_C, shown in Fig. 2-7b is not desirable, since the discontinuity will make it necessary for the carriers in the Heterojunction to transport by means of thermionic emission across a barrier or by tunnelling through it. Therefore, the emitter efficiency and the collector current will suffer. The problems can be alleviated by improved structures such as the graded-layer and the graded-base Heterojunction. Figure 2-10 shows an energy band diagram in which the ΔE_C is eliminated by a graded layer placed between the emitter and base Heterojunction. The thickness of the graded layer is W_g.

The base region can also have a graded profile, which results in a reduction of the band gap from the emitter side to the collector side. The energy band diagram of the graded base HBT is illustrated in figure 2-10 (dotted line). Note that there is a built-in electric field ε_{bi} ; in the quasi-neutral base. It results in a reduction in the minority-carrier transit time and, thus, an increase in the common-emitter current gain and the cut-off frequency of the HBT. ε_{bi} Can be obtained, for example, by varying linearly the Al mole fraction x of $Al_xGa_{1-x}As$ in the base from x = 0.1 to x = 0 [3].

For the design of the collector layer, it is necessary to consider the collector transit time delay and the breakdown voltage requirement. A thicker collector layer will improve the breakdown voltage of the base-collector junction but proportionally increase the transit time. In most devices for high-power applications, the carriers move through the collector at their saturation velocities because very large electric fields are maintained in this layer.

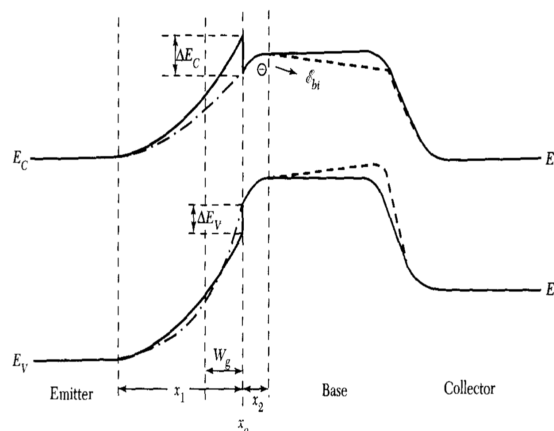

Figure 2-10: Energy band diagrams for a heterojunction bipolar transistor with and without graded layer in the junction, and with and without a graded-base layer

2.6 Si-Ge HBT versus CMOS

CMOS devices offer the advantages of high Ft and Fmax as well as good linearity and lower voltage operation, due to lower threshold voltages. HBT devices offer the advantages of excellent noise performance and an improved transconductance. For RF communications circuits, SiGe HBT consumes much less power than CMOS to achieve the same level of performance. The density differences for different circuit applications are also of practical interest. For RF amplifiers SiGe HBT occupy one-quarter to one-third the area of CMOS circuits of equivalent functionality.

Noise perhaps is the major advantage of SiGe HBT over CMOS for RF design. The 1/f noise due to carrier trapping –detrapping at interface states and thermal noise due to gate and channel resistances are both significantly higher in CMOS than in SiGe HBTs. To reduce them noise, very large CMOS devices and large operating current are often required.

2.7 Conclusion

After presenting the HBT structure and HBT properties we can summarize our study of the HBT technology by presenting the advantages of this technology over simple BJT.

The band gap difference between emitter and base in a HBT transistor results in higher speed, and thus higher operating frequency. The transistor gain is also increased compared to a BJT, which can then be traded for a lower base resistance, and hence lower noise.

For the same amount of operating current, HBT has a higher gain, lower RF noise, and low 1/f noise than an identically constructed BJT. The higher raw speed can be traded for lower power consumption as well. For the Same functionality HBT circuits occupy less area than BJT circuits.

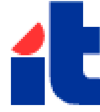

3 CHAPTER 3

WI-FI

3.1 Introduction

Since we are designing a power amplifier for WIFI applications, in this chapter we will give an overview of WIFI, the standard IEEE 802.11 and its corresponding improvements, defined by IEEE, applications and features of each standard, the advantages and disadvantages of WIFI and finally we will state the specifications of the power amplifier to be designed for WIFI applications.

3.2 What is WIFI?

WiFi is a set of product compatibility standards for wireless local area networks (WLAN) based on the IEEE 802.11specifications. New standards beyond the 802.11 specifications, such as 802.16(WiMAX), are currently in the specification period and offer many enhancements, anywhere from longer range to greater transfer speeds.

WiFi was intended to be used for mobile devices and LANs, but is now often used for Internet access. It enables a person with a wireless-enabled computer or personal digital assistant (PDA) to connect to the Internet when in proximity of an access point. The geographical region covered by one or several access points is called a **hotspot**. Hotspots can be found in airport lounges, coffee shops, corporate cafeterias or any other meeting area within range of a wireless LAN base station. There are thousands of hotspots all over the world—and more are being added every day [5].

3.3 Standards of WiFi

The Standards of WIFI is being standardized by the Institute of Electrical and Electronics Engineers (IEEE):

- IEEE 802.11a
- IEEE 802.11b
- IEEE 802.11g

Most Hotspots use 802.11b.

The WLAN standards started with the 802.11 definition, developed in 1997 by the IEEE. This base standard allowed data transmission of up to 2 Mbps. Over time, this standard has been enhanced. These extensions are recognized by the addition of a letter to the original 802.11 standard, including 802.11a and 802.11b [4].

3.3.1 802.11b

The 802.11b specification was ratified by the IEEE in July 1999 and operates at radio frequencies in the 2.4 to 2.497 GHz bandwidth of the radio spectrum. The 802.11b transmitter uses BPSK (Binary Phase Shift Keying) or QPSK (Quadrature Phase Shift Keying). The modulation method selected for 802.11b is known as complementary direct sequence spread spectrum (DSSS) using complementary code keying (CCK) making data speeds as high as 11 Mbps.

3.3.2 802.11a

The 802.11a specification was also ratified in July 1999, but products did not become available until 2001 so it isn't as widely deployed as 802.11b. 802.11a operates at radio frequencies between 5.15 and 5.875 GHz and a modulation scheme known as orthogonal frequency division multiplexing (OFDM) makes data speeds as high as 54 Mbps possible.

3.3.3 802.11g

The 802.11g employ also OFDM. The advantage of this system is that it reduces errors introduced by multi-path propagation at high data rates. Systems based on OFDM can offer higher data rates (54Mbps) or longer range at lower data rates compared with conventional single carrier systems.

The table below summarizes the differentiating features of each standard.

Standard	**802.11b**	**802.11g**	**802.11a**
Purpose	Wireless Internet Access	Wireless Internet Access	Wireless Internet Access
Frequency Band	2.4GHz	2.4GHz	5GHz
Maximum data rate/channel	11 Mbps	54 Mbps	54 Mbps

	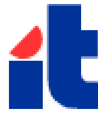		
Typical range	100 ft at 11 Mbps 300 ft at 1 Mbps	50 ft at 54 Mbps 150 ft at 11 Mbps	40 ft at 54 Mbps 300 ft at 6 Mbps
Devices	Laptop computers, PDAs, cell phones	Laptop computers	Laptop computers, PDAs, cell phones

Table 3-1: Different features of standards in WiFi

3.4 Advantages of WI-FI

- Allows LANs to be deployed without cabling, potentially reducing the costs of network deployment and expansion. Spaces where cables cannot be run, such as outdoor areas and historical buildings, can host wireless LANs.
- WiFi products are widely available in the market. Different brands of access points and client network interfaces are interoperable at a basic level of service.
- Competition amongst vendors has lowered prices considerably since their inception.
- WiFi networks support roaming, in which a mobile client station such as a laptop computer can move from one access point to another as the user moves around a building or area.
- Many access points and network interfaces support various degrees of encryption to protect traffic from interception.
- WiFi is a global set of standards. Unlike cellular carriers, the same WiFi client works in different countries around the world [5].

3.5 Disadvantages of WI-FI

- The 802.11b and 802.11g flavors of WiFi use the unlicensed 2.4 GHz spectrum, which is crowded with other devices such as Bluetooth, microwave ovens, cordless phones (900 MHz or 5.8 GHz are, therefore, alternative phone frequencies one can use if one has a WiFi network), or video sender devices, among many others. This may cause degradation in performance. Other devices that use microwave frequencies, such as certain types of cell phones, can also cause degradation in performance.
- Power consumption is fairly high compared to some other standards, making battery life and heat a concern.

- WiFi networks have limited range. A typical WiFi home router using 802.11b or 802.11g might have a range of 45 m (150 ft) indoors and 90 m (300 ft) outdoors. Range also varies, as WiFi is no exception to the physics of radio wave propagation, with frequency. WiFi in the 2.4 GHz frequency block has better range than WiFi in the 5 GHz frequency block, and less range than the oldest WiFi (and pre-WiFi) 900 MHz block.
- Access points could be used to steal personal information transmitted from WiFi users.
- Interoperability issues between brands or deviations in the standard can cause limited connection or lower throughput speeds [5].

3.6 Specifications for 802.11b

Since we are designing a power amplifier for WIFI applications (standard 802.11b), we will state in table 3-2 the typical characteristics of this standard defined by the IEEE.

Frequency	2.4 GHz
Bandwidth	97 MHz
Maximum Output Power	20 dBm
Linearity	Highly Linear (class A)
Power Added Efficiency	Maximum
Adjacent Channel Power Ratio (ACPR)	30 dBr
Type of Signals	QPSK signals

Table 3-2:Specifications for 802.11b

The power amplifier to be design is expected to meet these specifications stated in table 3-2.

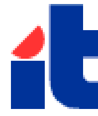

4 CHAPTER 4

RF Power Amplifier Theory

4.1 Introduction

The RF power amplifier (PA), a critical element in transmitter units of communication systems, is expected to provide a suitable output power at a very good gain with high efficiency and linearity. The output power from a PA must be sufficient for reliable transmission. High gain reduces the number of amplifier stages required to deliver the desired output power and hence reduces the size and manufacturing cost. High efficiency improves thermal management, battery lifetime and operational costs. Good linearity is necessary for bandwidth efficient modulation. However these are contrasting requirements and a typical power amplifier design would require a certain level of compromise. There are several types of power amplifiers which differ from each other in terms of linearity, output power or efficiency. This thesis will present a Class A PA design and discuss its performance. Parameters which quantify the various aspects of amplifier performance such as 1-dB compression point, 3rd order intercept point, intermodulation distortion; efficiency and adjacent channel power ratio are discussed in this chapter.

4.2 Efficiency

Commercial RF power amplifiers are designed for high efficiency, resulting in longer battery life and less complex thermal management. A few figures of merit regarding efficiency are defined here.

1. *Collector efficiency*

Collector efficiency η is defined as the ratio of the RF output power and the total DC consumption power in Eq. 4.1.

$$\eta = \frac{P_{out}}{P_{DC}} \quad (4.1)$$

Where Pout is the total RF output power and P_{DC} is the total DC power consumption.
The collector efficiency is independent of the power gain of the amplifier.
Different classes of operation will have different collector efficiency. The ideal drain efficiency for Class A is 50%, and 78.5% for Class B. Class C and switching mode amplifiers have ideally 100% collector efficiency.

2. *Power Added Efficiency (PAE)*

The power added efficiency (PAE) is defined as

$$\text{PAE} = \frac{P_{out} - P_{in}}{P_{DC}} \tag{4.2}$$

Where P_{in} is the RF input power. PAE gives the overall efficiency of the power amplifier. Since

$$P_{out} = P_{in} * Gain \tag{4.3}$$

$$PAE = \left(1 - \frac{1}{Gain}\right)\frac{P_{out}}{P_{DC}} = \left(1 - \frac{1}{Gain}\right)\eta \tag{4.4}$$

This shows that power gain has a large impact on the overall efficiency. The higher the power gain, the closer PAE is to η. [4]
The PAE is a better figure of merit since in the previous case we can have 100% efficiency when we have an input of 1 W, an output power of 1 W and a DC power of 1 W which clearly gives a wrong measure of efficiency, the PAE will be 0% in this case.

4.3 1-dB compression point ($P_{1\text{-dB}}$)

When a power amplifier is operated in its linear region, the gain is a constant for a given frequency. However when the input signal power is increased, there is a certain point beyond which the gain is seen to decrease. As it's shown in figure 4-1.The input 1-dB compression point is defined as the power level for which the

input signal is amplified 1 dB less than the linear gain. The 1-dB compression point can be input or output referred and is measured in terms of dBm. A rapid decrease in gain will be experienced after the 1-dB compression point is reached. This gain compression is due to the non-linear behavior of the device and hence the 1-dB compression point is a measure of the linear range of operation.

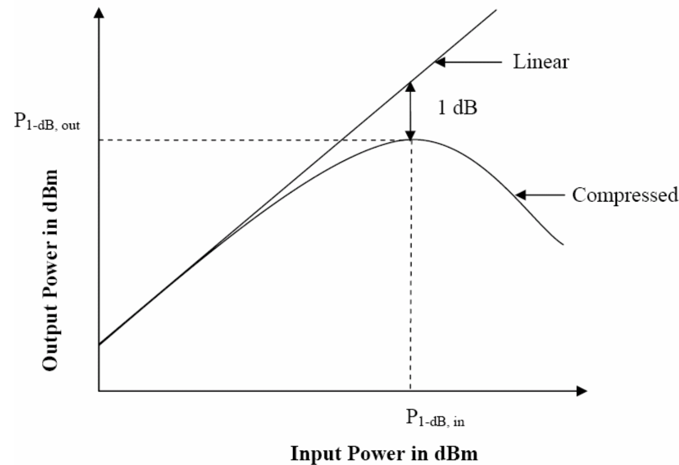

Figure 4-1:1-dB compression point

4.4 Intermodulation Distorsion (IMD)

Intermodulation distortion is a nonlinear distortion characterized by the appearance, in the output of a device, of frequencies that are linear combinations of the fundamental frequencies and all harmonics present in the input signals [5]. A very common procedure to measure the intermodulation distortion is by means of a two-tone test. In a two-tone test a nonlinear circuit is excited with two closely spaced input sinusoids. This would result in an output spectrum consisting of various intermodulation products in addition to the amplified version of the two fundamental tones and their harmonics. If $\mathbf{f_1}$ and $\mathbf{f_2}$ are the fundamental frequencies then the intermodulation products are seen at frequencies given by $\mathbf{f_{IMD} = mf_1 \pm nf_2}$, Where m and n are integers from 1 to ∞.

The ratio of power in the intermodulation product to the power in one of the fundamental tones is used to quantify intermodulation. Of all the possible intermodulation products usually the third order intermodulation products (at frequencies $\mathbf{2f_1\text{-}f_2}$ and $\mathbf{2f_2\text{-}f_1}$) are typically the most critical as they have the highest strength. Furthermore they often fall in the receiver pass band making it difficult to filter them out. The fundamentals, the second, third, fifth and seventh orders are shown in figure 4-2.

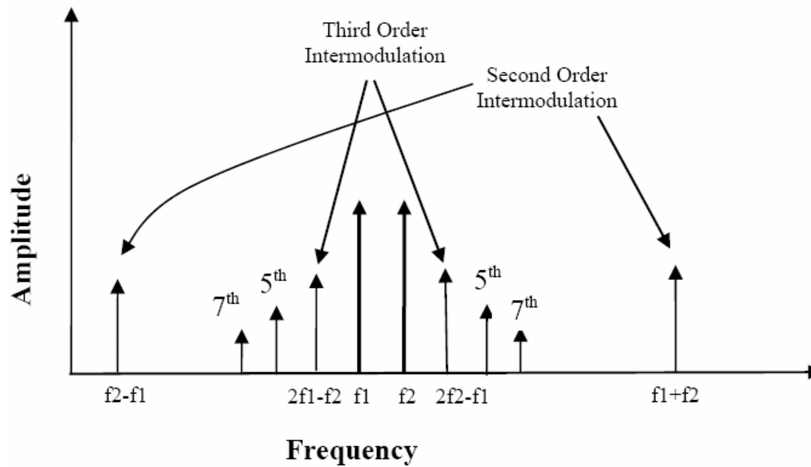

Figure 4-2: Intermodulation Distortion

4.5 Adjacent Channel Power Ratio (ACPR)

In many modern communication systems, the RF signal typically has a modulation band that fills a prescribed bandwidth on either side of the carrier frequency. Similarly the intermodulation products also have a bandwidth associated with them. The IM bandwidth is three times the original modulation band limit for third order products, five times the band limit for fifth order products and so on. Thus the frequency band of the intermodulation products from the two tones stretches out, leading to leakage of power in the adjacent channel. This leakage power is referred to as adjacent channel power. The adjacent channel power ratio (ACPR) is the ratio of power in the adjacent channel to the power in the main channel. ACPR values are widely used in the design of power amplifiers to quantify the effects of intermodulation distortion and hence also serve as a measure of linearity in real system.

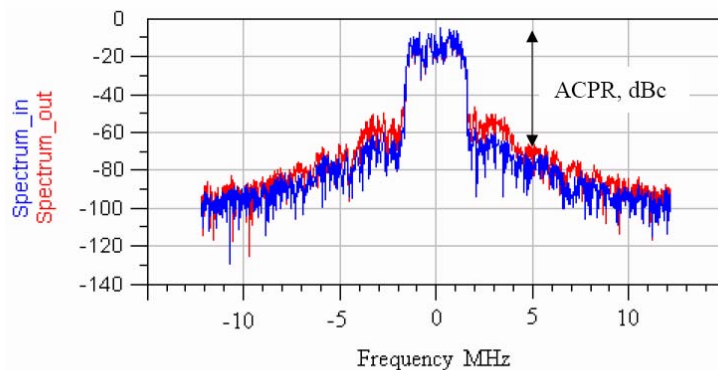

Figure 4-3: Plot of Adjacent Channel Power

4.6 Intercept Point (IP)

The intercept point is the point where the slope of the fundamental linear component meets the slope of the intermodulation products on a logarithmic chart of output power versus input power. Intercept point can be input or output referred. Input intercept point represents the input power level for which the fundamental and the intermodulation products have equal amplitude at the output of a nonlinear circuit. In most practical circuits, intermodulation products will never be equal to the fundamental linear term because both amplitudes will compress before reaching this point. In those cases intercept point is measured by a linear extrapolation of the output characteristics for small input amplitudes. Since the third order intermodulation products, among the IM products, are of greatest concern in power amplifier design, the corresponding intercept point called the third order intercept point (IP3) is an important tool to analyze the effects of third order nonlinearities [5].

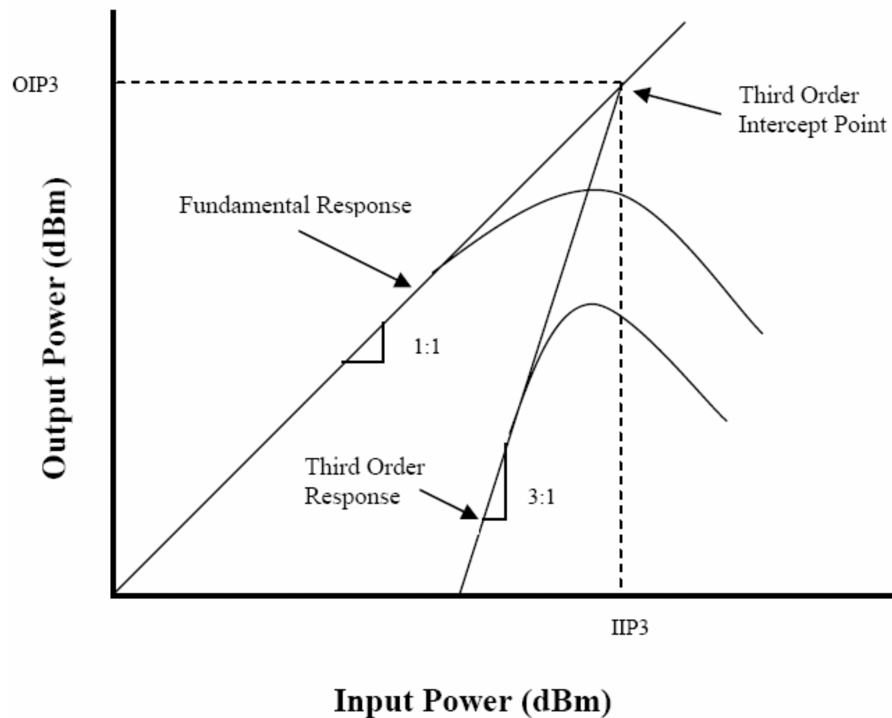

Figure 4-4: Plot showing Third Order Intercept point

4.7 Power Amplifier Classification

There are several types of power amplifiers and they differ from each other in terms of their linearity, efficiency and power output capability. The first step in designing a power amplifier is to understand the most important design factor and choose the power amplifier type most suited for that purpose. For example, linearity and efficiency are the most important characteristics of the power amplifier design for mobile communication systems. Beside that high linearity results in poor efficiency and vice versa.

Depending on the linearity and efficiency requirements in the application, the operation classes of amplifier can be divided into two groups: the first covers high linear amplifiers such as Pas in mobile communication applications, and the second group belongs to high efficient amplifiers such as high PAs in satellite applications.

Four operation classes under the first group: class-A, class-B, class –AB and class-C. These classes are intensively used in power amplifier design for microwave and wireless mobile communication based on non-constant envelope modulation which use multi-carrier signals. For this reason, such systems demand highly linear amplification. Beside that class-D, class-E, class-F, and others, also known as switched mode amplifiers [7], belong to the second group. These classes are intensively used in power amplifier design for satellite applications in which very high power is required. Therefore, the efficiency must be very high in order to avoid high power dissipation in the active device.

In this paragraph, we will consider the first group. These discussions based on BJT transistor viewpoint.

4.7.1 Class A

Class A is the simplest power amplifier type in terms of design and construction. The Class A amplifier has a conduction angle of 2π radians or 360°. Conduction angle refers to the time period for which a device is conducting. Thus a conduction angle of 360º tells us that in Class A operation the device conducts current for the entire input cycle. Class A amplifiers are considered to be the most linear since the transistor is biased in the center of the load line to allow for maximum voltage and current swings without cut-off or saturation. However the problem with Class A amplifiers is their very poor efficiency. This is because the device is conducting current at all times which translates to higher power loss. In fact it can be shown that the maximum efficiency achievable from a Class A power amplifier is only 50% [8]. However this is a theoretical number and the actual

efficiency is typically much less. In fact commercial Class A amplifiers have efficiency as low as 20%. Hence Class A amplifiers are usually used only in places where linearity is a stringent requirement and where efficiency can be compromised.

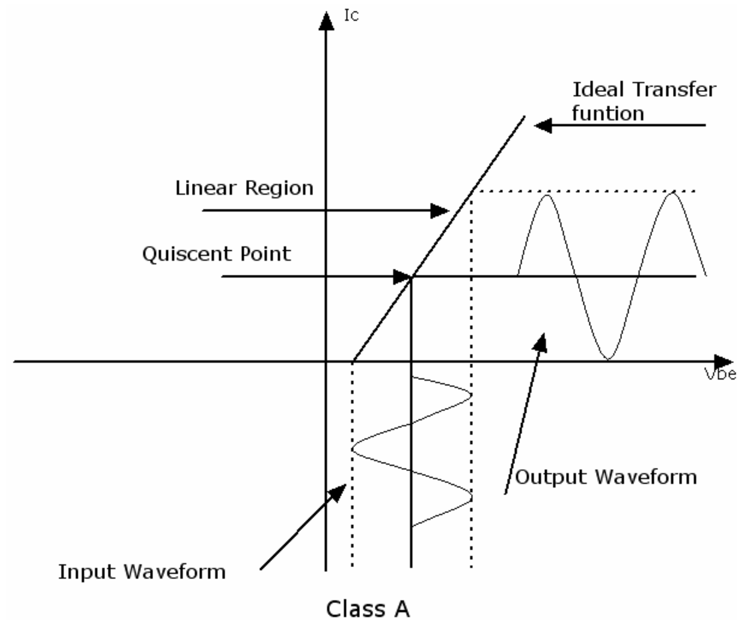

Figure 4-5: Biasing for class A

4.7.2 Class B

The next class of power amplifiers is Class B. The transistor is biased at the threshold voltage point of the transistor for Class B operation. Hence there is a current flowing at the output of the device only when there is a signal at the input. Moreover the device would conduct current only when the input signal level is greater than the threshold voltage. This occurs for the positive half cycle of the input signal and during the negative half cycle the device remains turned off. Hence the conduction angle for Class B operation is 180º or π radians. Due to this behavior; there is a large saving in the power loss. It can be shown that the maximum theoretical efficiency achievable with Class B operation is about 78.5% [8]. Commercial Class B amplifiers typically have an efficiency of 40-60%. However, the increased efficiency comes at the cost of reduced linearity. The reduction in the output power occurs because the output current flows for only one half cycle of the input signal. The poor linearity is primarily attributed to an effect called the crossover distortion [8]. Whenever the transistor is turned on (at the start of positive half cycle) and turned off (at the start of negative half cycle) the transistor does not change abruptly from one state to the other. Instead the transition is gradual and nonlinear, and results in an offset voltage. This voltage alters the output waveform (crossover distortion)

thereby reducing the linearity. Sometimes a Class B amplifier is realized in “push-pull” configuration. In this configuration the two transistors are driven 180º out-of-phase so that each transistor is conducting for one half cycle of the input signal and turned off for the other half cycle.

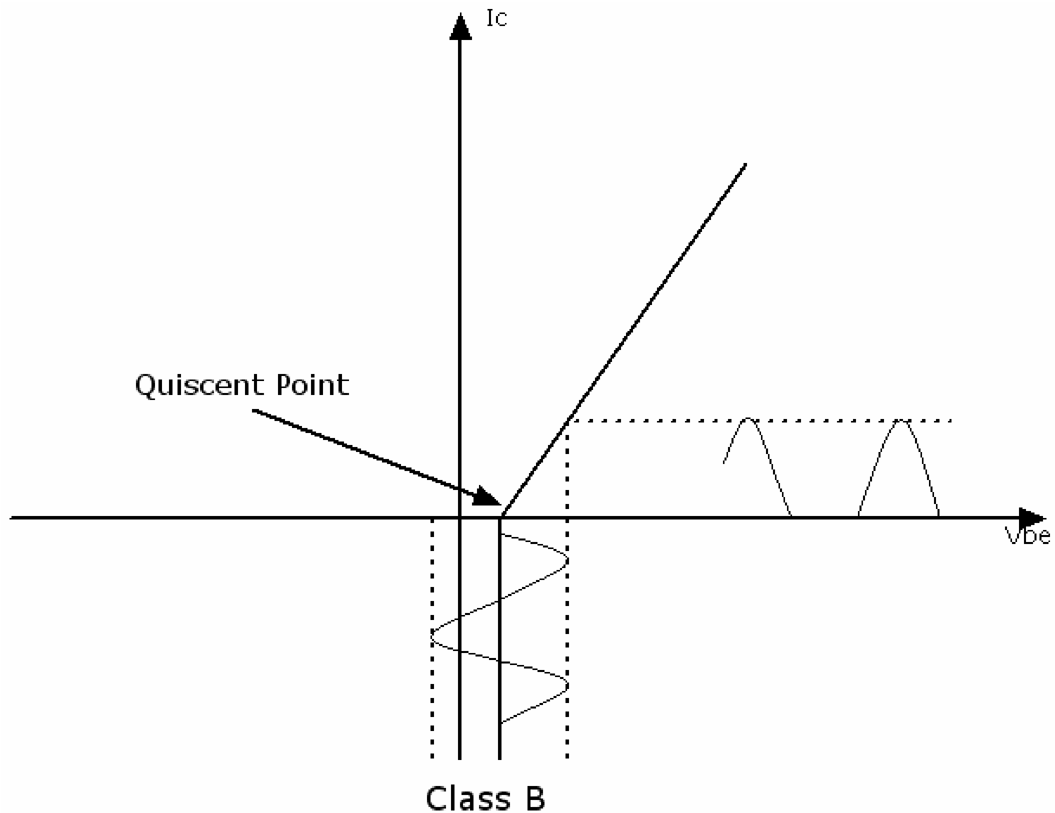

Figure 4-6: Biasing for class B

4.7.3 Class AB

The crossover distortion effect in Class B amplifiers can be minimized by biasing the base in such a way so as to produce a small quiescent collector current. This leads to the type of amplifiers called Class AB, where the transistor is biased between class-A and class-B. Class AB amplifier operation, as the name suggests, can be considered to be a compromise between Class A and Class B operation. The conduction angle of a Class AB amplifier lies between 180º and 360º. By varying the conduction angle the amplifier can be made to behave more as a Class A or Class B amplifier. Hence the theoretical maximum efficiency of a Class AB amplifier is between 50% and 78.5%. But commercial Class AB amplifiers typically have much lower efficiency in the order of 40-55%. Thus a trade-off between linearity and efficiency can be achieved by simply changing the base bias. Class AB amplifiers can also be realized in push-pull configurations even though single transistor configuration is preferred for high frequency linear operation.

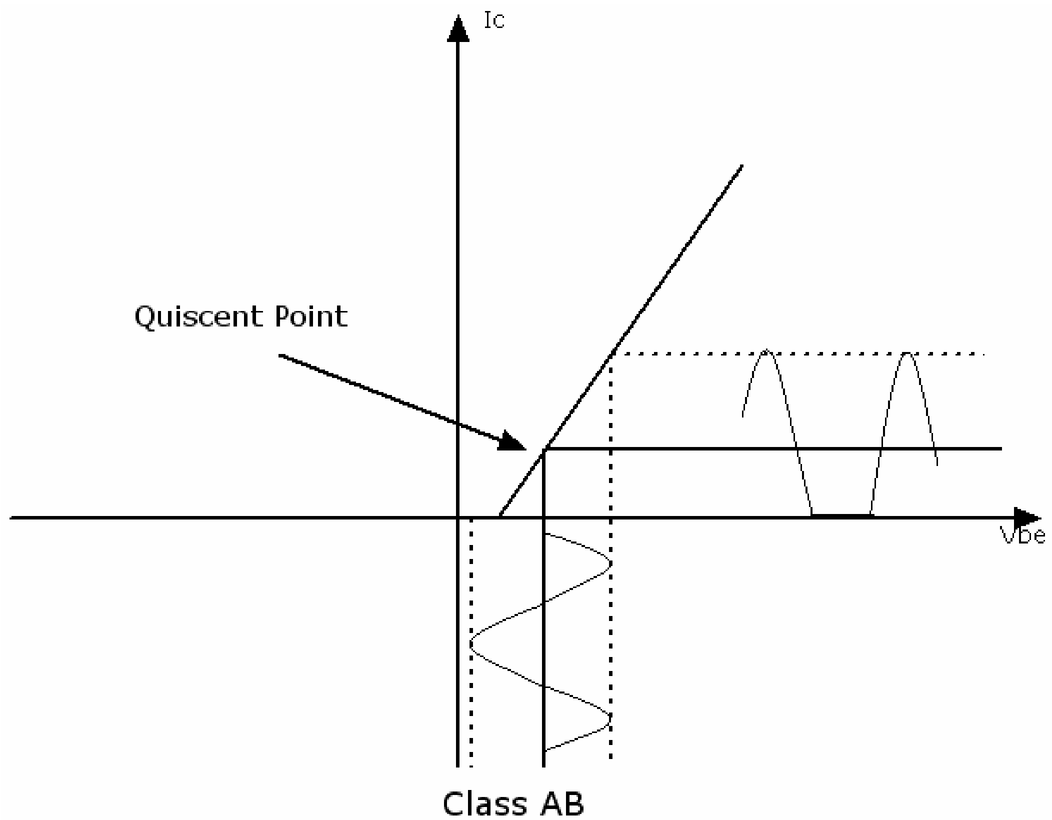

Figure 4-7: Bias for class AB

4.7.4 Class C

In class-C amplifier, the transistor operation point is chosen so that the output current (I_C) is zero for more than one-half duration of the input signal cycle, which means the conduction angle is less than 180 degree resulting in a good efficiency but on other hand a poor linearity compared to the previous amplifier classes. The efficiency of a Class C amplifier depends on the conduction angle. The efficiency increases for decreasing conduction angle. The maximum theoretical efficiency of a Class C power amplifier is 100%. However this is obtainable only for a conduction angle of 0º which means that no signal is applied and this condition is of no interest. Commercially Class C amplifiers typically show an efficiency of 60% or more. Class C amplifiers are widely used in constant envelope modulation systems where linearity is not an issue.

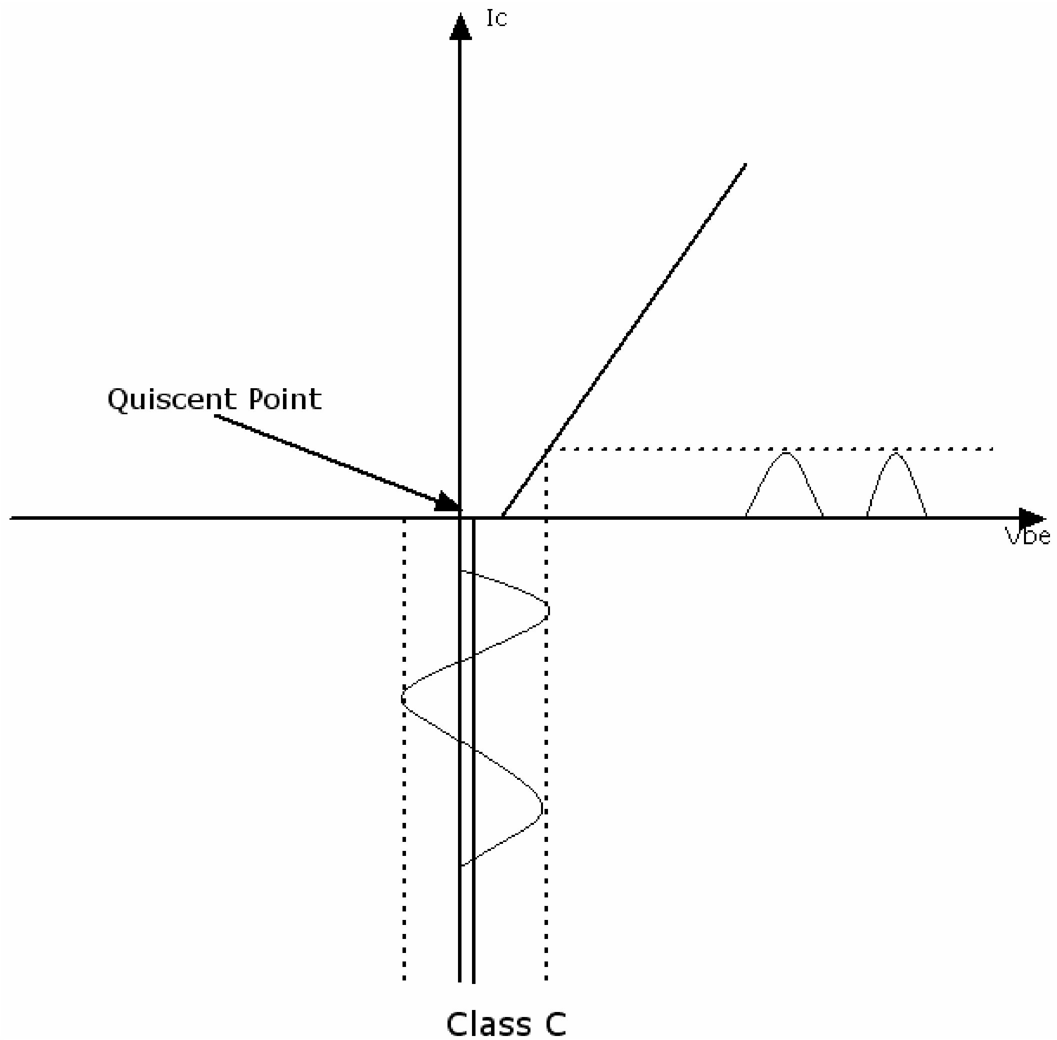

Figure 4-8: Bias for class C

As conclusion, increasing the bias current for better linearity (closer to class-A operation) results in lower efficiency and more heat dissipation. Conversely, lowering the bias current to improve efficiency (closer to class-B operation) results in reduced linearity. As soon as the envelope of the signal begins to vary, the linearity of the amplifier becomes more important so that a more linear amplifier than class-C must be used. In this case class-A or class-AB is preferred. Although more linear than class-C, the output of class-AB and class-A amplifiers is still a distorted version of the input.

5 CHAPTER 5

Design and Implementation

5.1 Introduction

A Class A power amplifier design is described in this section. The Class A amplifier was designed using NEC HBT (Heterojunction Bipolar Transistor) transistor models and its performance was simulated using ADS. Various procedures involved in the design of the Class A amplifier such as DC simulation, bias point selection, Load-pull characterization, input and output matching circuit design and the design of a bias network are explained.

5.2 Model of the NEC HBT transistor

To represent the transistor in ADS we need a model. We got the ADS model from the data sheet of the transistor [18]. The model used is shown in figure 5-1 and the value of the parameters is shown in table 5-1.

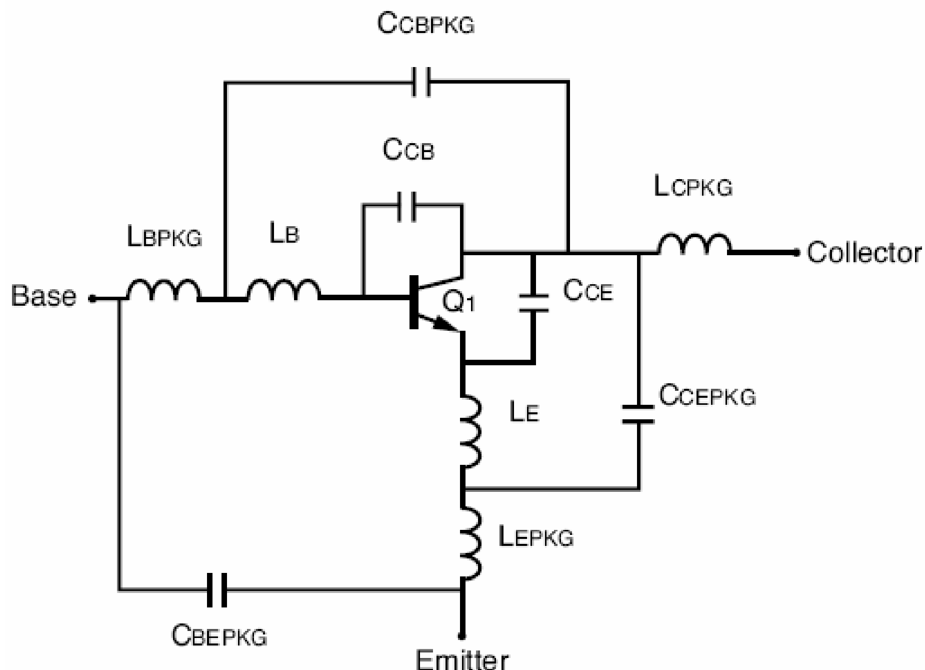

Figure 5-1: Model of the HBT transistor

Parameters	NESG2031M05
C_{CB}	0.01 pF
C_{CE}	0.07 pF
L_B	0.25 nH
L_E	0.15 nH
C_{CBPKG}	0.13 pF
C_{CEPKG}	0.01 pF
C_{BEPKG}	0.03 pF
L_{BPKG}	0.9 nH
L_{CPKG}	1.0 nH
L_{EPKG}	0.19 nH

Table 5-1:Parameters of the HBT transistor

5.3 Bias Point Simulation

The first step towards designing the class A amplifier was to select a suitable bias point for operation. The transistor should be biased for class A operation and maintained comfortably inside the rectangle limited by the nonlinearity borders which are the collector-emitter voltage, Knee voltage, V_k, and collector-base breakdown, V_{BR}, and in current, by collector current cut-off. In that respect, the best quiescent point is the one exactly located at the geometrical center of the saturation zone rectangle, (point Q in figure 5-2, since it will allow maximized output linear power, when associated to the diagonal load-line depicted in the same figure. Such a strategy leads to the widely accepted rule of thumb that states that a linear power amplifier has its device biased for class A, at a current close to $I_C/2$ and $V_{CE} = (V_K+V_{BR})/2$, and is loaded by the output termination that allows maximized signal excursion without clipping [i.e., an intrinsic R_L not far from $R_L = (V_{CE} - V_K)/I_C$].

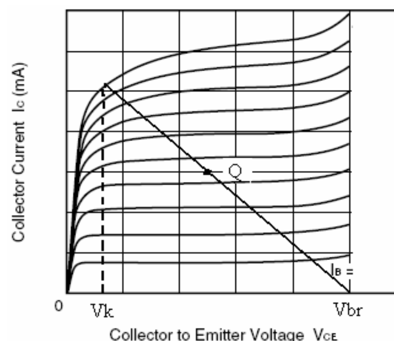

Figure 5-2: Collector current vs. collector to emitter voltage

In order to determine the bias point simulation a DC bias point simulation was performed. Figure 5-4 shows that the bias point for a class A should be:

$$V_{CE} = \frac{v_K + v_{BR}}{2} = \frac{0.5+5}{2} = 2.75\ \text{V}$$

$I_C = \frac{I_{C\max}}{2} = \frac{27.62}{2} = 13.81$ mA which lead to an approximate value of $I_B = 75\ \mu A$.

If we look in figure 5-4 we notice that this point is in the safe operating area of the transistor. The Safe Operating Area (SOA) of the transistor is defined as the voltage and current conditions over which the device can be expected to operate without self-damage due to thermal heating.

The Load at optimal bias $R_L = \frac{V_{CE} - V_K}{I_C} = \frac{5-0.5}{13.81} = 162.9\Omega$

The Efficiency $\eta = \frac{P_{out}}{P_{DC}} = \frac{15.54}{2.75 * 13.81} = 40.91\%$

All these values are summarized in figure 5.4.

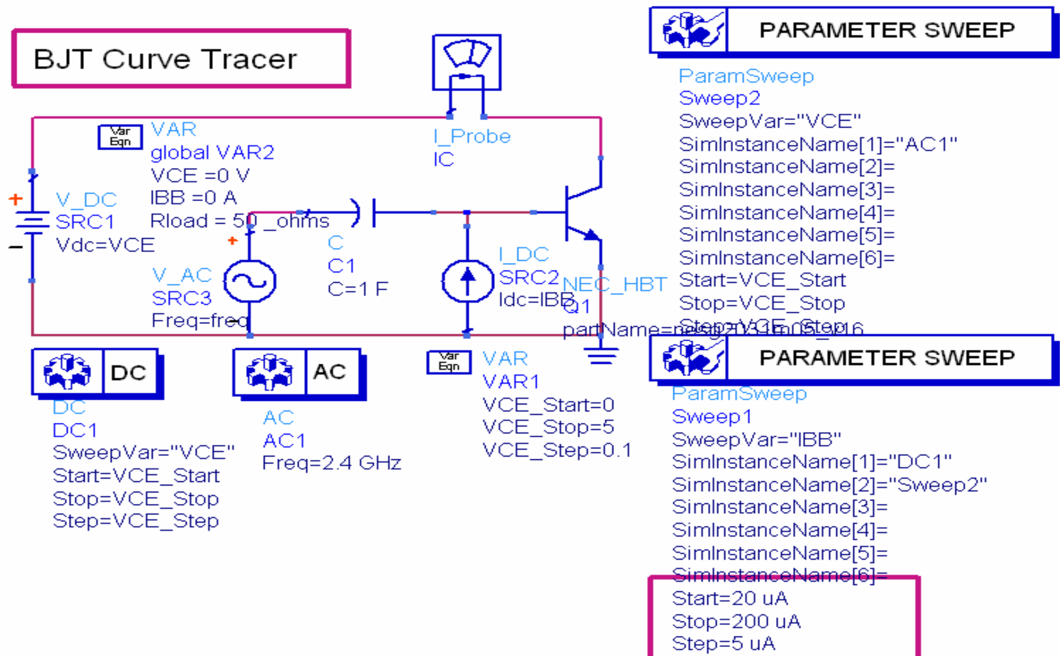

Figure 5-3: Schematic that determines the Bias Point

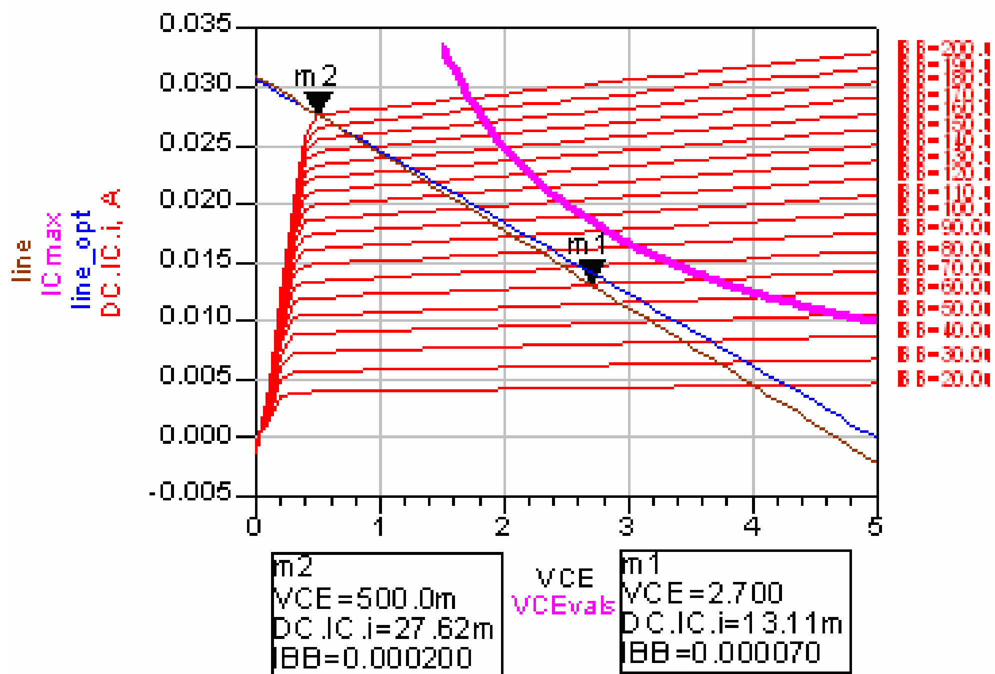

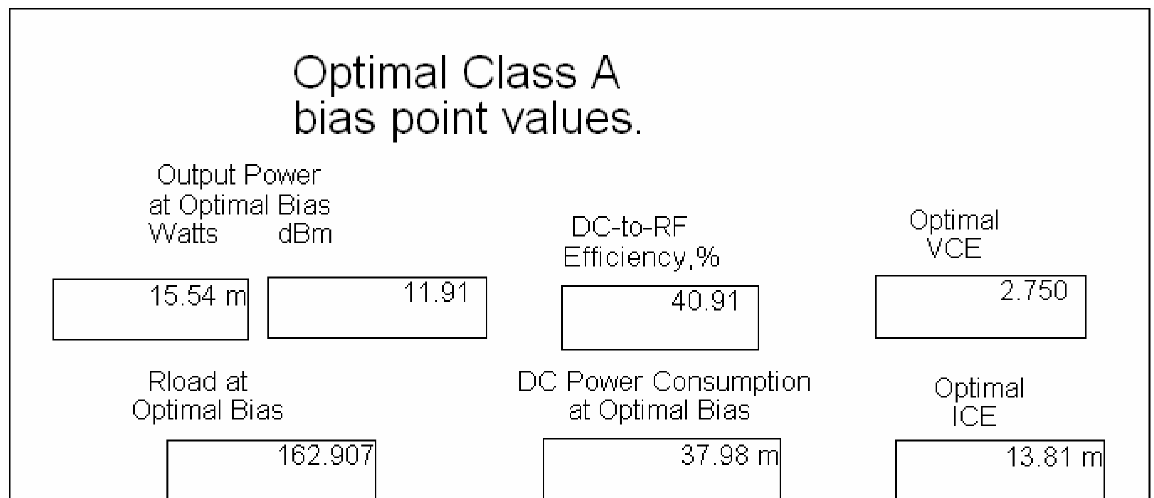

Figure 5-4: Bias point simulation for Class A

5.4 Determination of the S-Parameters

Due to the fact that a class A PA is highly linear, we are able to use S parameters. Therefore before we start designing the power amplifier we have to determine the S-parameters of the HBT transistors. The S-parameters are necessary to study the stability of the transistor by determining the stable and unstable region in the smith chart. We also need the S-parameters of the transistor to determine the input matching network that maximizes the power gain. Since the data sheet doesn't contain the S-Parameters for our specific bias point, we have to determine the S-parameters. In order to determine the S-parameters a simulation of the circuit shown in Figure 5-5 was performed.

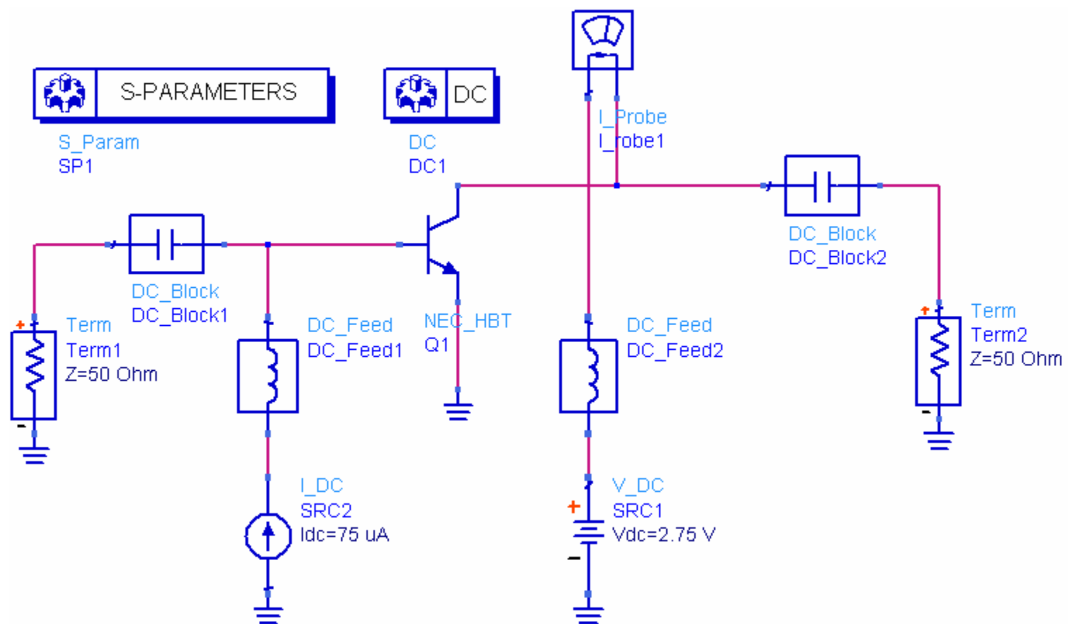

Figure 5-5: Circuit that determines the S-Parameters

After simulation of the circuit in figure 5.5 we get the S-parameters that are summarized in the following table.

freq	S(1,1)	S(1,2)	S(2,1)	S(2,2)
2.400 GHz	0.539 / 168.393	0.117 / 36.784	4.583 / 65.788	0.137 / -138.537

Table 5-2: Simulated S-parameters

5.5 Stability

To study the stability of the transistor amplifier we can apply the K – Δ test, where it can be shown that a device will be unconditionally stable if Rollet's condition, defined as

$$K = \frac{1 - |S_{11}|^2 - |S_{22}|^2 + |\Delta|^2}{2|S_{12}S_{21}|} > 1 \quad (5.1)$$

Along with auxiliary condition that

$$\Delta = S_{11}S_{22} - S_{12}S_{21} < 1 \quad (5.2)$$

are simultaneously satisfied.

We get the S-Parameters of the Transistor from table 5-2

$$S_{11} = 0.539\angle 168.393°$$
$$S_{21} = 4.583\angle 65.788°$$
$$S_{12} = 0.117\angle 36.784°$$
$$S_{22} = 0.137\angle -138.537°$$

$$\Delta = 0.539\angle 168.393 * 0.137\angle -138.537 - 0.117\angle 36.784 * 4.583\angle 65.788 = 0.519\angle -69.62$$

$$K = \frac{1 - (0.539)^2 - (0.137)^2 + (0.519)^2}{2(0.536211)} = 0.8952$$

Thus we have Δ < 1, but K < 1, so the unconditional stability criteria are not satisfied, and the device is potentially unstable.

To find the stability of the transistor we should plot the input and output stability circles in the Smith Chart.

The input stability circle is defined for $\Gamma_{out} = \left| S_{22} + \frac{S_{12}S_{21}\Gamma_S}{1 - S_{11}\Gamma_S} \right| = 1$ and plotted in the Γ_S plane. The centers and radii of the input stability circles are given respectively by:

$$C_S = \frac{(S_{11} - \Delta S_{22}^*)^*}{|S_{11}|^2 - |\Delta|^2} = 26.236\angle -175.65$$

$$R_S = \left| \frac{S_{12}S_{21}}{|S_{11}|^2 - |\Delta|^2} \right| = 25.34$$

The stable region is defined for $|\Gamma_{out}| < 1$ so if we set $Z_S = Z_0$, then $\Gamma_S = 0$ and $|\Gamma_{out}| = |S_{22}|$.

We have $|S_{22}| = 0.137 \Rightarrow |\Gamma_{out}| = 0.137 < 1$ so $\Gamma_S = 0$ (centre of the Smith chart) is in the stable region. The output stability circle is defined for $\Gamma_{in} = \left| S_{11} + \frac{S_{12}S_{21}\Gamma_L}{1 - S_{22}\Gamma_L} \right| = 1$ and plotted in the Γ_L plane. The centers and radii of the input stability circles are given respectively by:

$$C_L = \frac{(S_{22} - \Delta S_{11}{}^*)^*}{|S_{22}|^2 - |\Delta|^2} = 1.32\angle -97.9$$

$$R_L = \left| \frac{S_{12}S_{21}}{|S_{22}|^2 - |\Delta|^2} \right| = 2.14$$

The stable region is defined for $|\Gamma_{in}| < 1$ so if we set $Z_S = Z_0$, then $\Gamma_S = 0$ and $|\Gamma_{in}| = |S_{11}|$.

We have $|S_{11}| = 0.539 \Rightarrow |\Gamma_{in}| = 0.539 < 1$ so $\Gamma_S = 0$ (centre of the Smith chart) is in the stable region. The input and output stability circles are shown in the right side of figure 5-6.

The same process is done at other frequencies. We performed a frequency sweeping from 100 MHz to 10 GHz with a step of 100 MHz and we plotted the stability circles at these frequencies as it is shown in the left side of figure 5-6. We should note that this analysis is only valid for pure class A power amplifier.

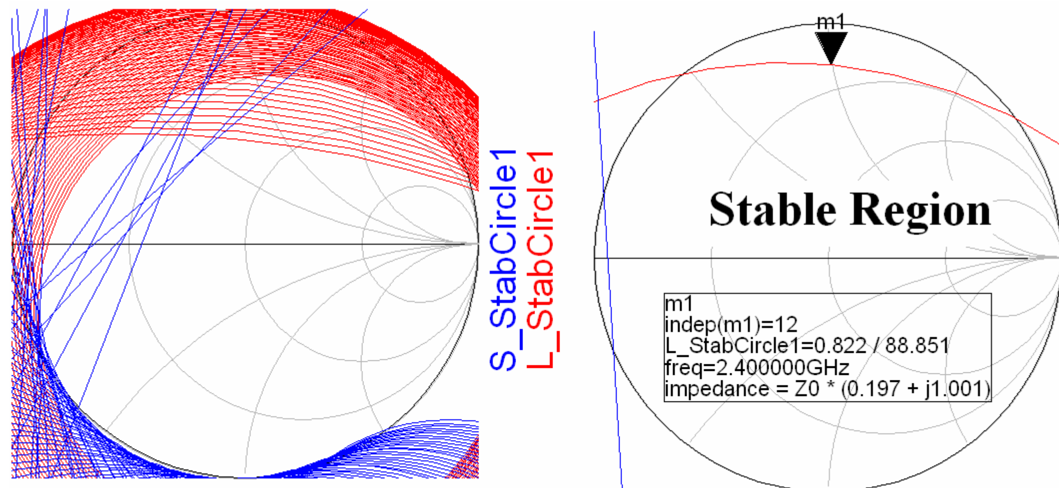

Figure 5-6: Input and output stability circles

5.6 Load Pull

Load pull is a technique wherein the load impedance seen by the device under test (DUT) is varied and the performance of the DUT is simultaneously measured [5]. Similarly in source pull the performance of the DUT for varying source impedances is measured. The measured results are very useful in determining the optimum load and source impedance which the device must see to give the best performance. Load pull, in particular, is commonly used to determine the load impedance required for maximizing efficiency. The input of a power amplifier is usually conjugate matched to optimize the gain and the source pull is not always required. It should be noted that the impedance values calculated vary with bias. In this design, load pull is performed to obtain maximum efficiency. The load pull schematic is shown in figure 5.7. The results obtained from these simulations shows that the transistor needs to see an impedance of 65.954 + j*49.007 ohms at the output in order to get a PAE of 48.81% and get an output power of 11.91 dBm. These results are shown in figure 5.8.

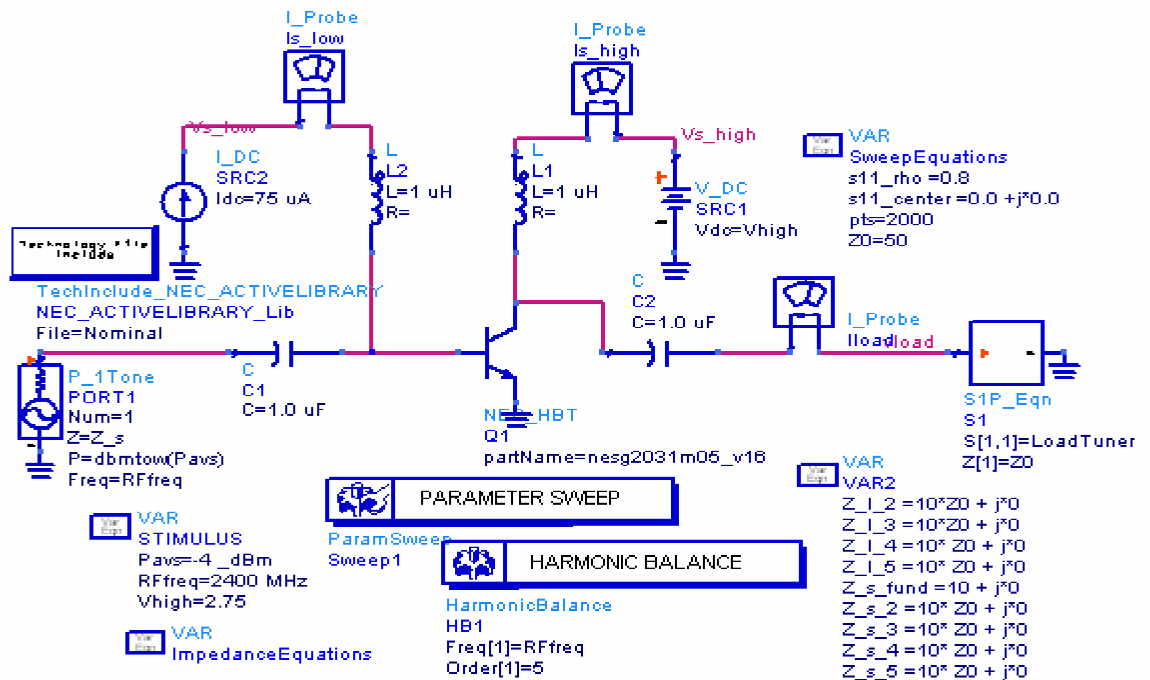

Figure 5-7: One tone load pull simulation

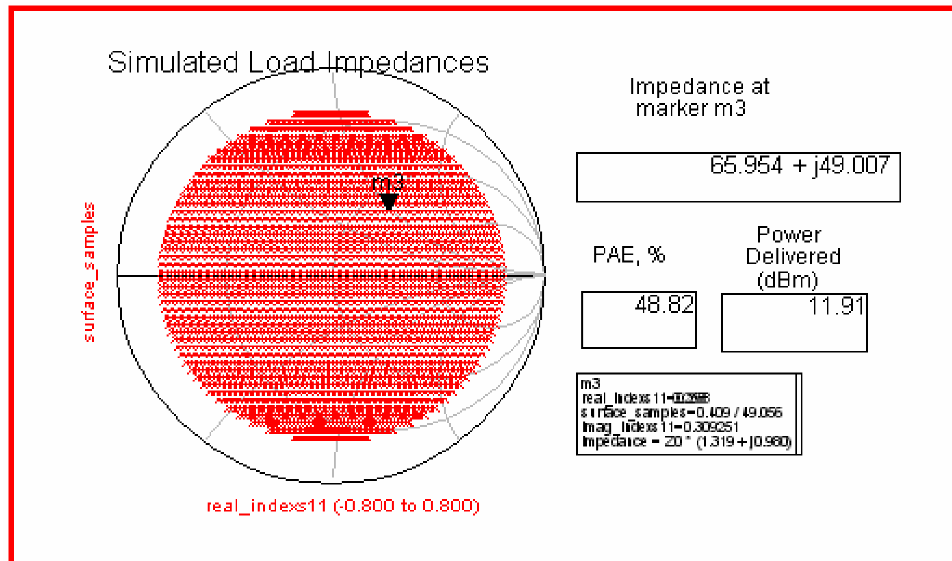

Figure 5-8: Load pull analysis to determine load impedance for maximum efficiency

Since we have found the load impedance, we can calculate Γ_L. Γ_L is given by

$$\Gamma_L = \frac{z_l - 1}{z_l + 1} = |\Gamma| e^{j\theta} = 0.41 \angle 49^\circ$$ where $z_l = Z_l/50$ is the normalized load impedance.

The reflection coefficient seen looking at the input of the transistor is given by

$$\Gamma_{in} = S_{11} + \frac{S_{12} S_{21} \Gamma_L}{1 - S_{22}\Gamma_L} = 0.75 \angle 162.63^\circ$$

Since we have calculated Γ_{in} and in order to get the maximum power transfer from the input matching network to the transistor we choose $\Gamma_S = \Gamma_{in}^* = 0.75 \angle -162.63$.

We notice that Γ_L and Γ_S are in the stable region of figure 5.6 which implies that the transistor will be stable and not oscillating. In the next section we will design the input and output matching sections of the power amplifier.

5.7 Matching

To match the network we will use an open-circuited shunt stub followed by a length of transmission line. So, the best way is to work with admittances. It is possible to go from $Z|_{50\Omega}$ to $Y|_{50\Omega}$ just by rotating the point 180°. We move toward the load on the smith chart until the circumference whose real part is equal to 1. This will bring us to the 1 +jb circle. Then we move toward generator from the open circuit point on the smith chart jb to get the length of the required stub.

5.7.1 Input Matching Network

We plot $\Gamma_S = 0.75\angle 162.63$ and we do as mention above, we get

Distance to Stub: 0.226λ-0.193 λ=**0.033 λ**

Length of Stub: **0.184 λ**

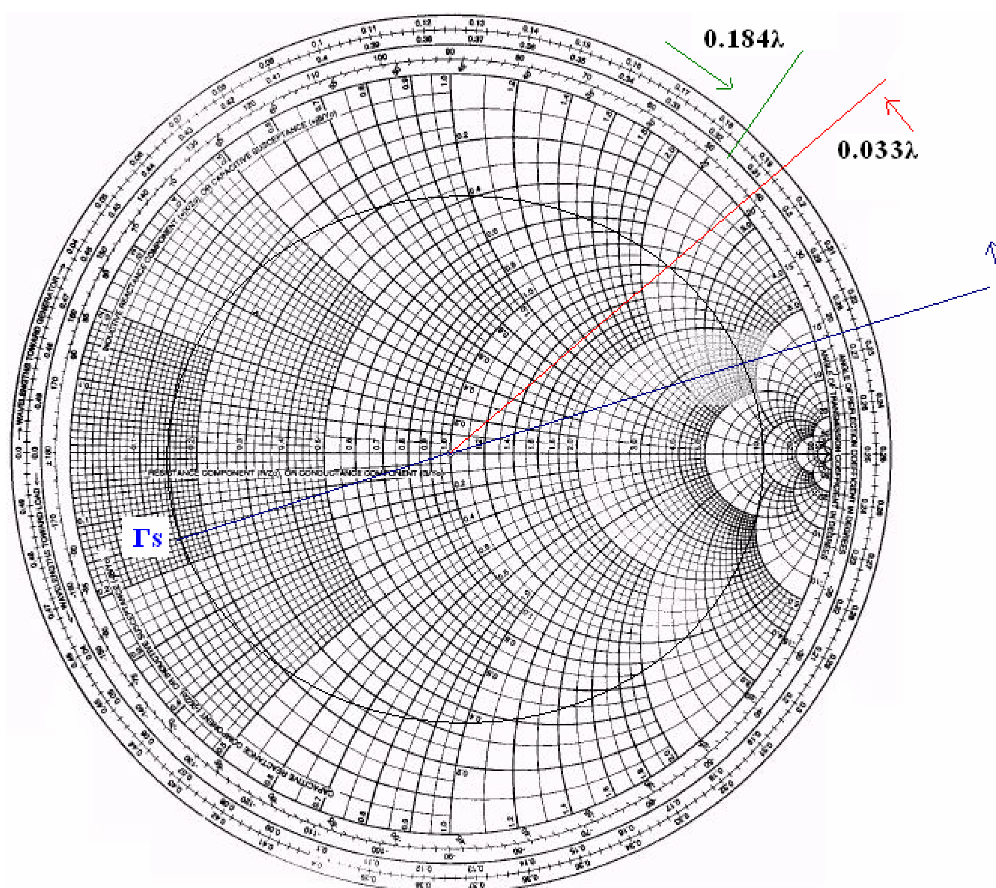

Figure 5-9: Smith Chart for the design of the input matching network

5.7.2 Output Matching Network

We plot $\Gamma_L = 0.41\angle 49.32$ and we do as mention above, we get

Distance to Stub: 0.431λ-0.159λ=**0.272λ**

Length of Stub: **0.116λ**

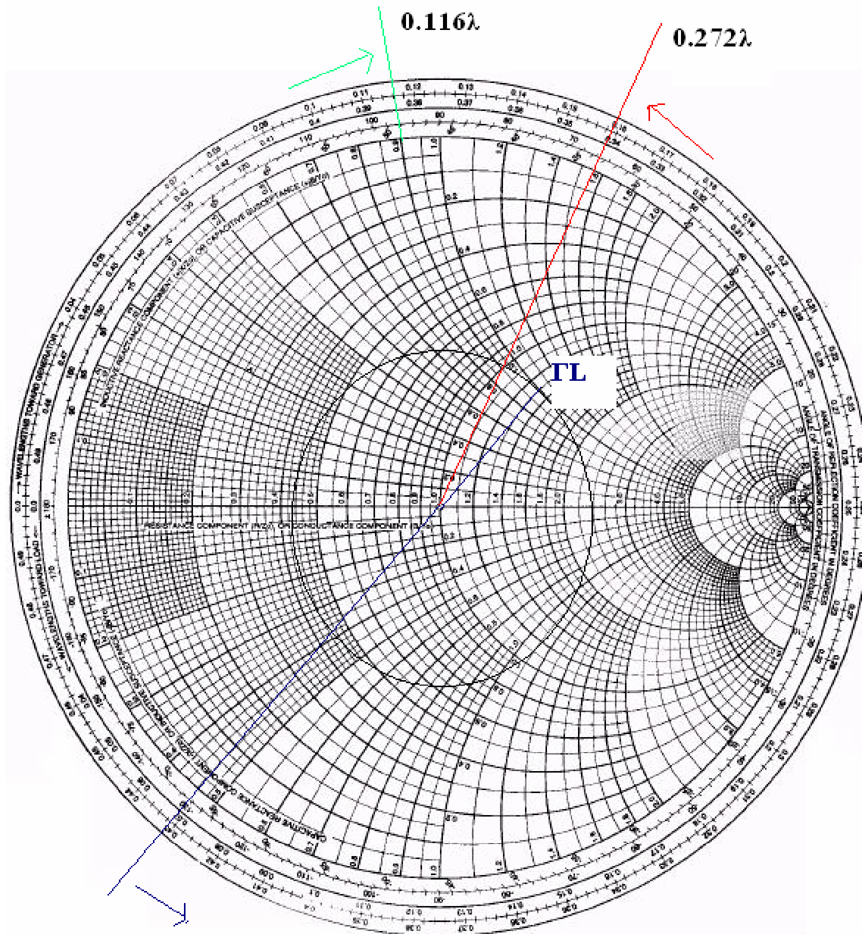

Figure 5-10: Smith Chart for the design of the input matching network

5.8 Bias

The SiGe HBT we are using can be biased in several ways. The Bias configuration that we have chosen for the PA design is represented in the following figure.

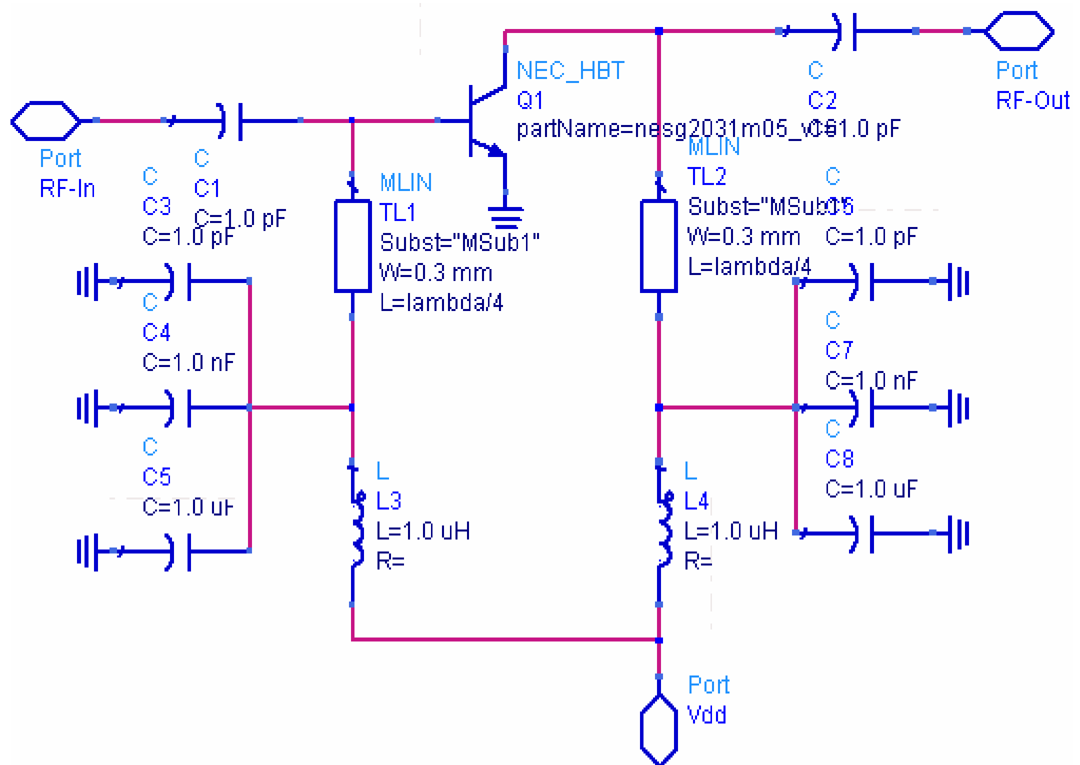

Figure 5-11: Bias circuit

In this circuit, the capacitors C1 and C2 represent the DC-Block capacitors.

The capacitors C3, C4 and C5 are used to short the bias feed end. The λ/4 line, TL1, transforms the short into an open at the frequency 2.4 GHz.

The capacitors C6, C7 and C8 are used to short the bias feed end. The λ/4 line, TL2, transforms the short into an open at the frequency 2.4 GHz.

The inductors L3 and L4 are used to increase the low frequency stability; if low frequency passes it will pass to the collector creating a feedback and then the Power Amplifier could start oscillating at low frequency.

5.9 Current Source

In order to bias the transistor we need a base current of 75 μA. Since we don't have a source current in the laboratory we have to design one. The current source that I have designed is formed by one npn transistor, one pnp transistor and three resistors as shown in figure 5.12. The same source voltage that will bias the HBT transistor will bias also this circuit.

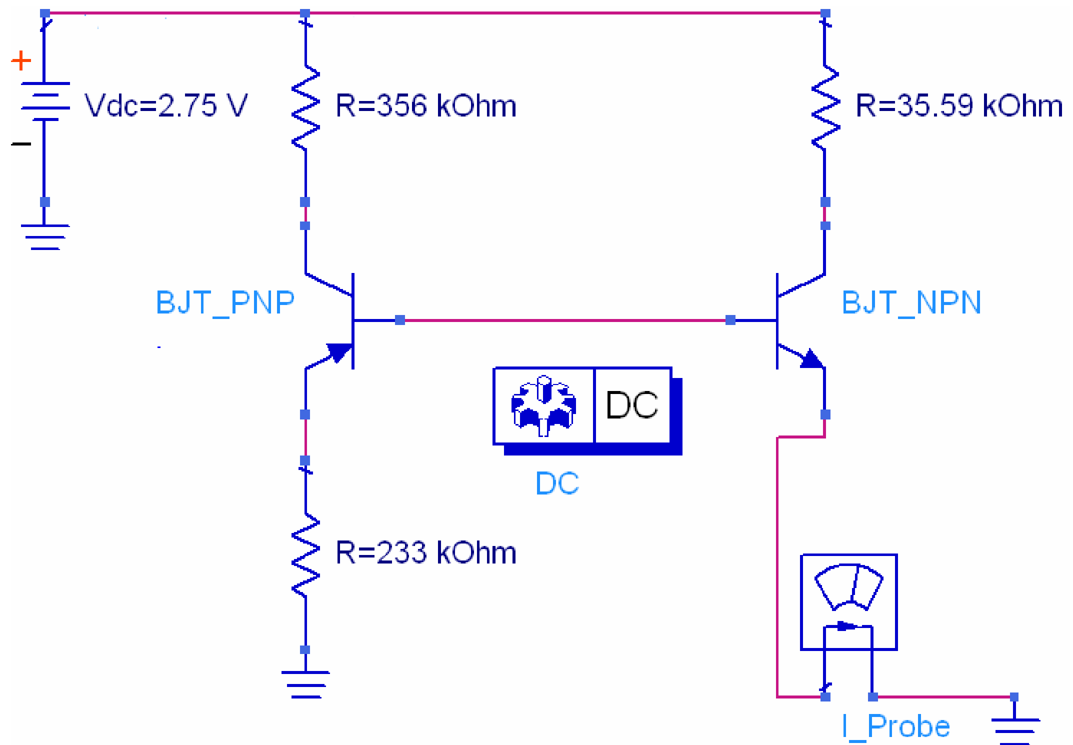

Figure 5-12: Current source

After simulation of this circuit we get the 75 μA at the emitter of the npn transistor, this will current will bias the base of the HBT transistor.

freq	I_Probe1.i
0.0000 Hz	75.00 uA

Table 5-3: Output of the current source

5.10 Class A Implementation

The various design blocks Matching, Bias and current source of the Class A amplifier were explained in the previous sections. Figure 5-13 shows the final realization of the class A power amplifier.

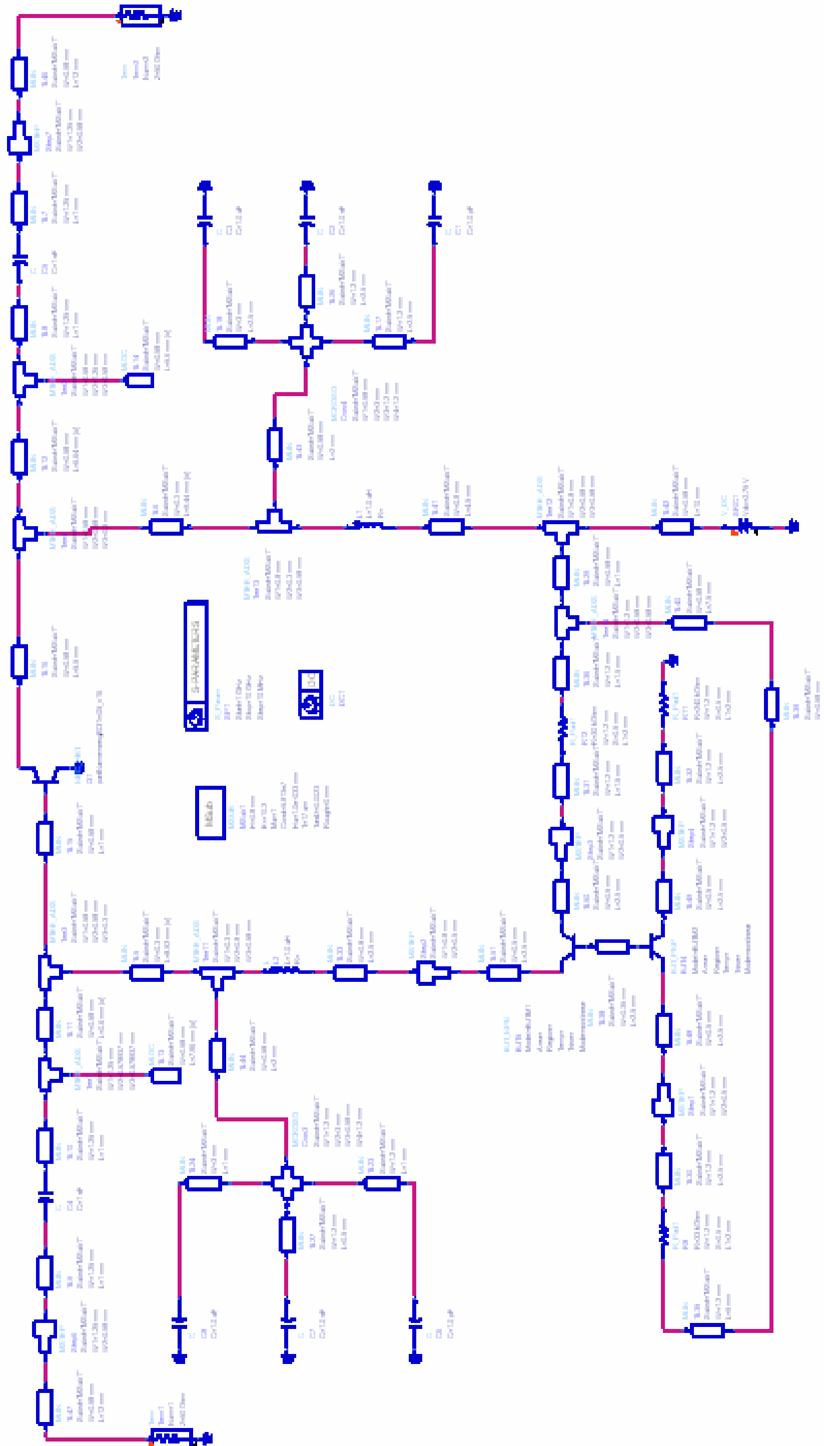

Figure 5-13: Schematic of class A design

5.11 Results

The Class A amplifier showed in figure 5.13 was simulated in ADS to evaluate its performance. This was done by means of single-tone and two-tone harmonic balance simulations.

5.11.1 Single-tone Simulation

A single tone harmonic balance simulation was done to plot the transducer power gain, the Power Added Efficiency PAE, input power P_{in}, output power P_{out} and the harmonic levels. Figure 5-14 shows the schematic of the one tone harmonic balance simulation.

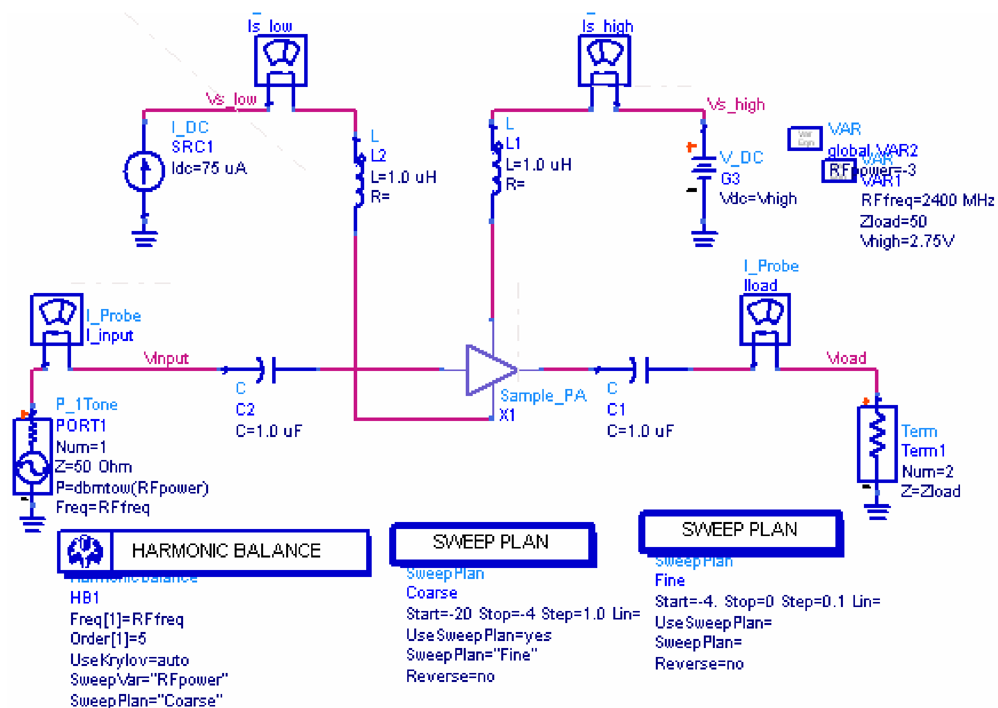

Figure 5-14: Schematic of the one tone harmonic balance simulation

Figure 5-15 shows the transducer power gain. As expected, gain decreases as the output power increases. At 1-dB compression point, the gain is about 14.58 dB at 11.57 dBm output power.

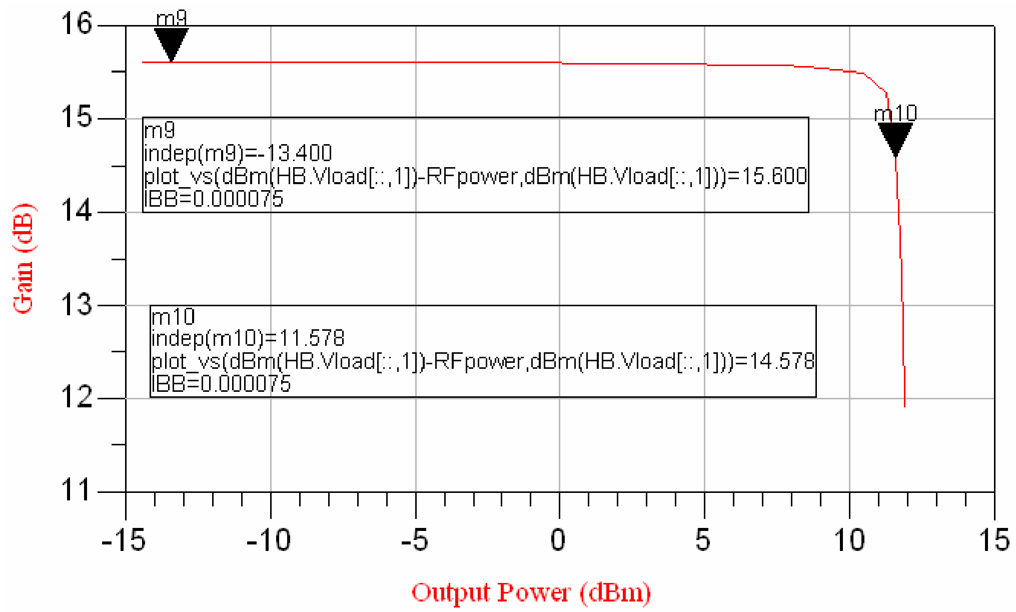

Figure 5-15: Class-A Power Gain

Figure 5-16 shows the Power Added Efficiency PAE. PAE is directly proportional with output power, it takes a maximum value of 45.171 at 2 dBm input power and it takes a value of 42.341 at the 1-dB compression point. Figure 5-17 shows P_{out} vs. P_{in}, RF power means input power and at 10 dBm input power, P_{out} becomes 10.3 dBm which means 0.3 dB gain. This expected since the amplifier is totally compressed.

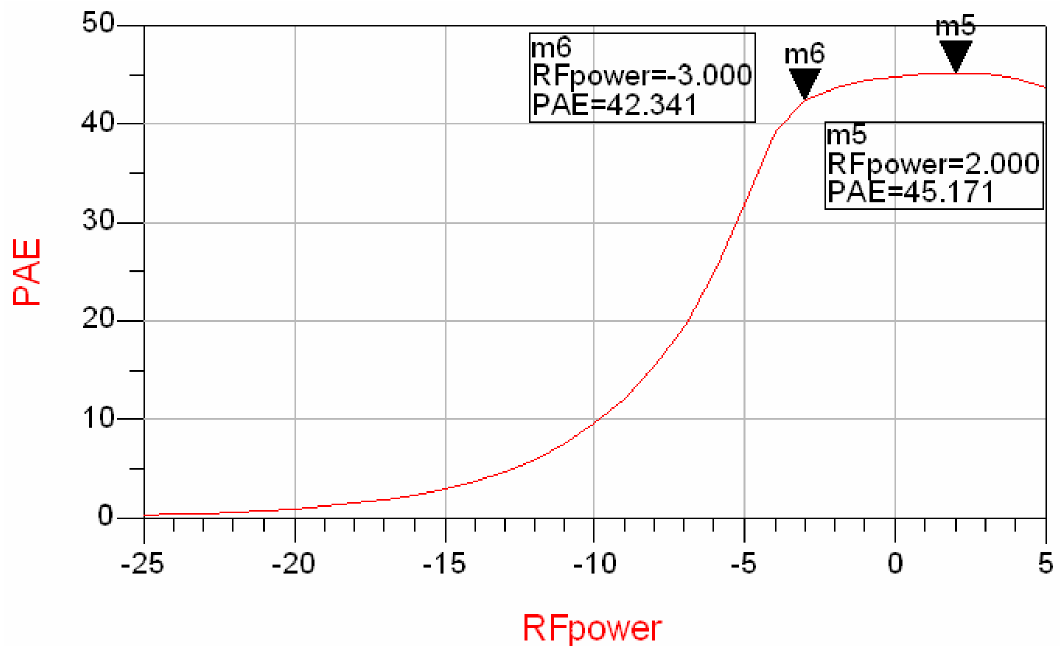

Figure 5-16: Class-A PAE

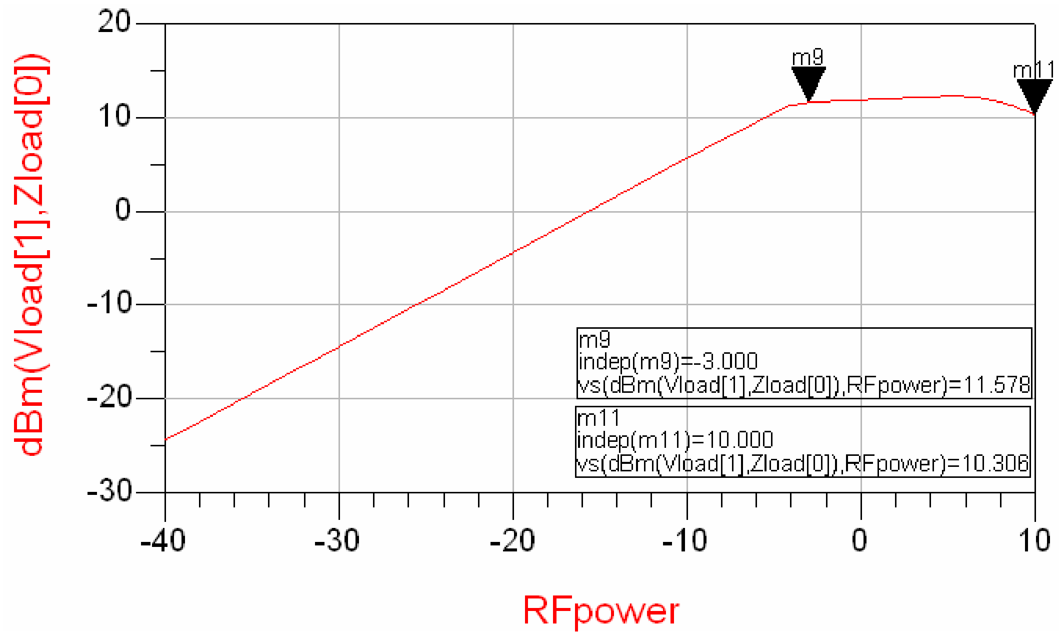

Figure 5-17: Class-A Pin vs. Pout

All the values at 1-dB compression point are summarized in table 5-4.

Available Source Power dBm	Fundamental Output Power dBm	Transducer Power Gain	Power- Added Efficiency, %	DC Power Consumpt. Watts	High Supply Current	Thermal Dissipation Watts
-3.020	11.573	14.593	42.252	0.033	0.012	0.019

Table 5-4: Values at 1-dB compression point

Figure 5-18 shows the spectrum of the fundamental and the Third Harmonic. There is an important characteristic of the third-order products which makes their presence more of a problem than one might first imagine. If we look to figure 5.18 in the linear region where no compression is, we notice that the output from the fundamental signal is proportional to input, i.e. for 30 dB rise in input level (-40 dBm to -10 dBm) there is 30 dB rise in output level (-25 dBm to 5dBm). However, the output of the third order product is proportional to the cube of signal input level and, for a 30 dB change in input level, the product increases by 90 dB (-140 dBm to -50 dBm).

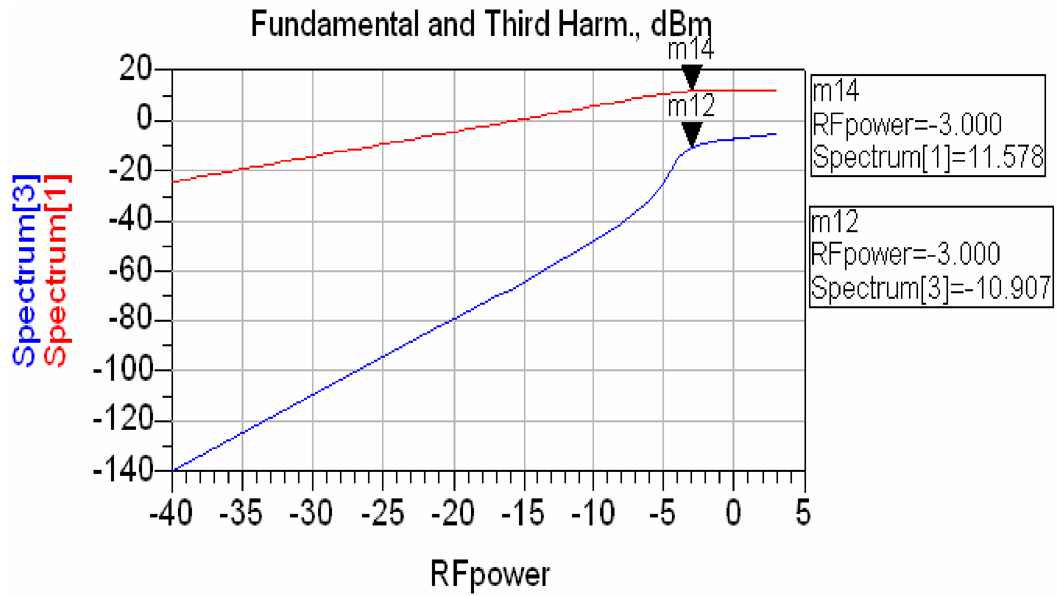

Figure 5-18: Fundamental and Third Harmonic

Table 5-5 presents the second, third, fourth and fifth harmonic levels at the output. The harmonic must be as low as possible in order to avoid unnecessary power loss and matching issues.

Available Source Power dBm	Second Harmonic dBc	Third Harmonic dBc	Fourth Harmonic dBc	Fifth Harmonic dBc
-3.020	-40.53	-22.44	-36.90	-51.45

Table 5-5: Harmonic Levels

5.11.2 Two-Tone Simulation

Two-tone harmonic balance simulations were performed on the Class A design. Harmonic balance is a frequency-domain analysis technique for simulating distortion in nonlinear circuits. Harmonic balance determines the spectral content of voltages and currents in the circuit. It is very useful to compute intercept point and intermodulation distortion. Here the two tone frequencies were chosen to be 2400.05 MHz and 2339.95 MHz. Seventh order harmonic balance simulation was performed to account for all harmonics up to the seventh harmonic. Fig 5-19 is a zoomed output spectrum of the Class A PA.

Figure 5-20 shows the Power Gain and the Power Added Efficiency, at the 1-dB compression point the PAE is 40.047 and is the input power is -4.3 dBm.

Figure 5-21 shows the two fundamentals, the lower and the upper third intermodulation distortion. At 1-dB compression point we have the intermodulation distortion is 27 dB below the fundamentals.

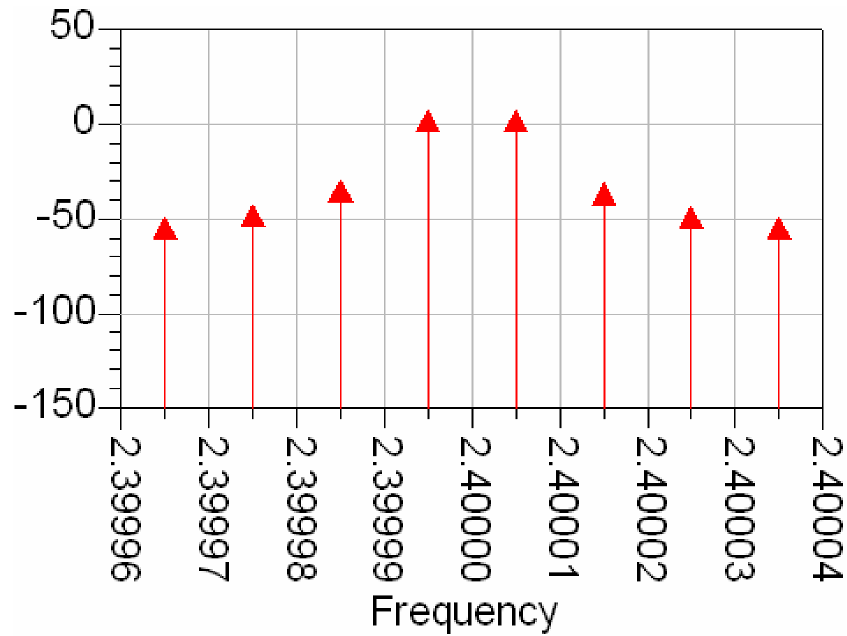

Figure 5-19: Zoomed output spectrum showing 3rd, 5th and 7th order IMD products

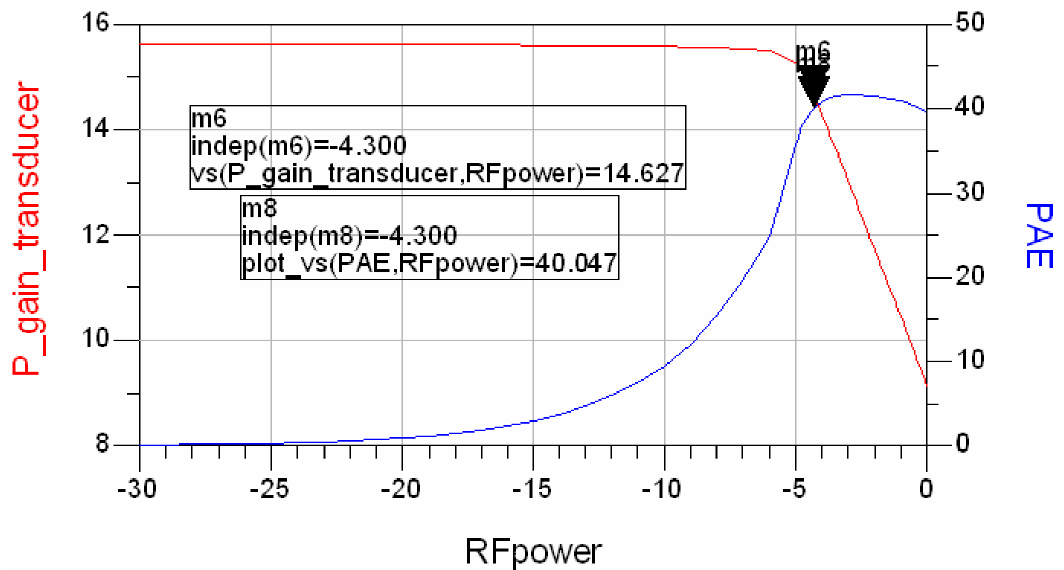

Figure 5-20: Plot of the power transducer gain and the PAE

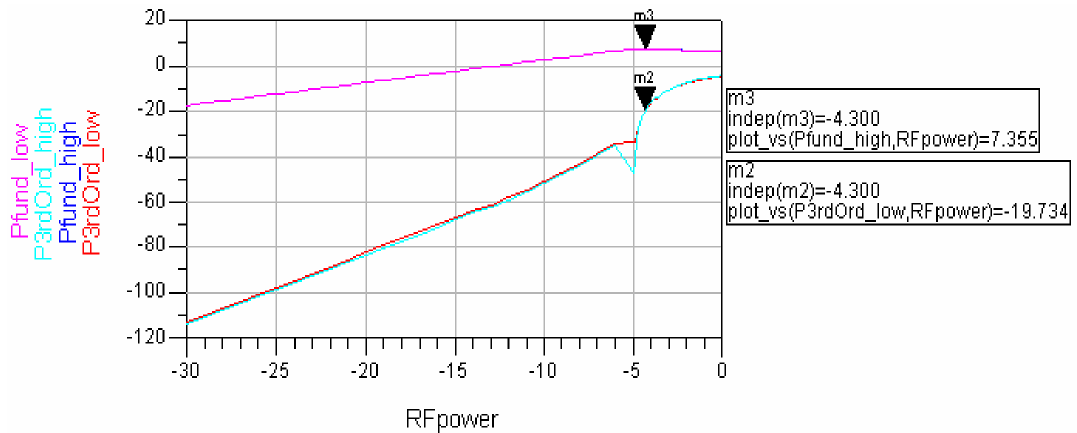

Figure 5-21: Plot of the fundamentals and the third order intermodulation

5.12 Performance of the PA in different classes of operation

In this section we will study the performance of this power amplifier in other classes of operation like Classes AB, B and C by changing the bias point only. Since we don't change the input and output matching networks of the class A power amplifier, the amplifier is class A but we will study its characteristics if we let it work in classes AB, B and C. in order to get a fair comparison between classes we will change the base current and leave the collector voltage constant and equal to 2.75 V.

We have from figure 5.4 that the maximum collector current is 27.63 mA. The class C is defined for a collector current less than 1% of this value. This gives that for class C.

$$I_C < 0.2734 \text{ mA}$$

Table 6.1 gives that the class C is for a base current

$$I_B < 1.2 \text{ µA}$$

The class B is defined for a collector current between one and 5 percent of this value. Table 5.6 gives that for class B we have:

$$0.2734 < I_C < 1.381 \text{ mA}$$

This gives that class B is for a current base between:

$$1.2 < I_B < 6.2\ \mu A$$

V_{CE}	I_B=1 μA	I_B=1.2 μA	I_B=4 μA	I_B=5 μA	I_B=6 μA	I_B=6.2 μA
2.75 V	I_C=0.23 mA	I_C=0.276 mA	I_C=0.908 mA	I_C=1.131 mA	I_C=1.351 mA	I_C=1.395 mA

Table 5-6:Collector current for different values of base current

It is shown in [16] that the PA third harmonic change with the bias point. Class B is defined for where we have a null in the output third order IMD. Class C would then be the operating regime of a PA biased below that bias point and classes A and AB would be the operating regimes of PAs biased above that point. Figure 5.22 shows us the variation of the third order IMD versus the base current and it is clearly that class B is obtained by biasing the base by a current of 4 μA. Since class C is for a base current less 1.2 μA we will choose 1 μA and for class AB we will choose a base current of 20 μA.

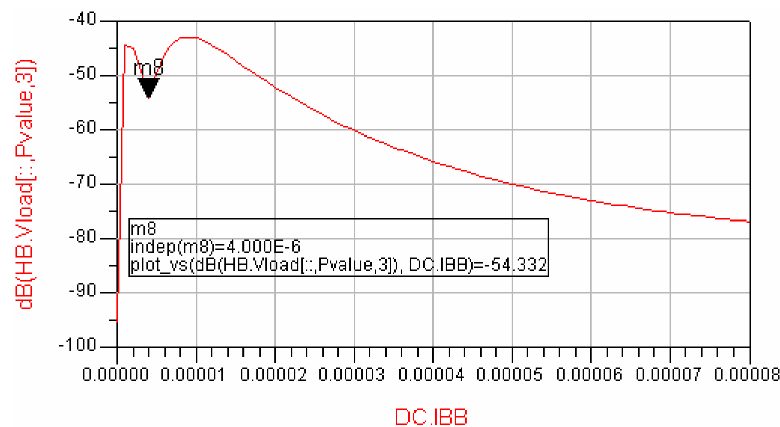

Figure 5-22: 3rd order IMD versus Base current

5.12.1 Class AB

For class AB operation the bias point is:

V_{CE} = 2.75 V

I_B =20 μA

A single tone and two tones simulations were done to study the characteristics of the PA in this class. Figure 5-23 shows the transducer power gain in function of the input power

for different base current. For I_B =20 μA the 1-dB compression point is for -13 dBm input power and 14.18 dB gain. Figure 5-24 shows the fundamental and the third harmonic which is 29.9 dB below carrier at the 1-dB compression point.

Figure 5.25 shows the two fundamentals, the lower and the upper third intermodulation distortion. At 1-dB compression point we have the intermodulation distortion is 50.3 dB below the fundamentals

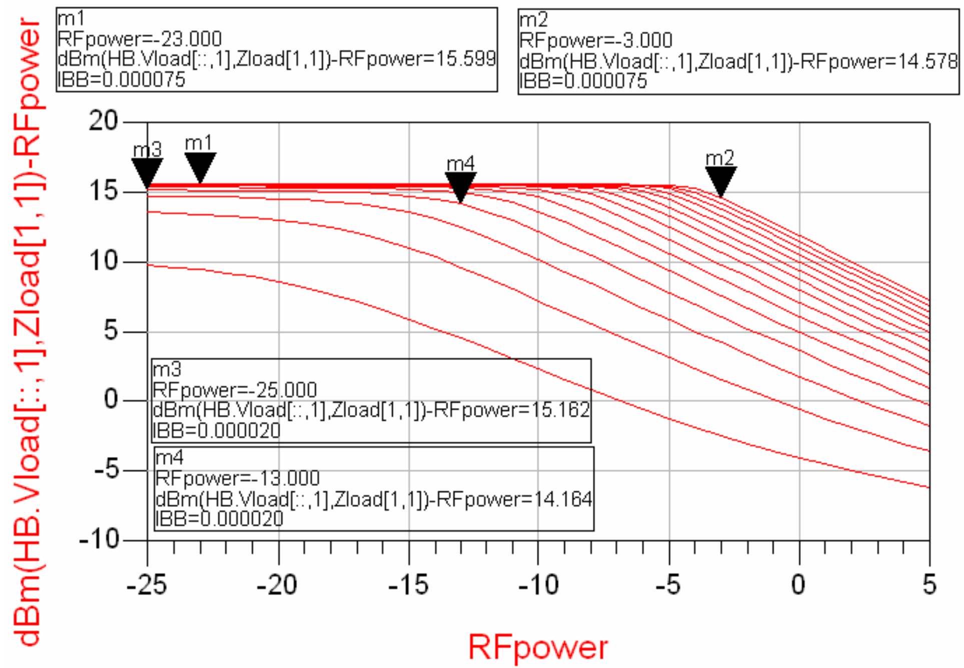

Figure 5-23: Power gain versus input power for different base current

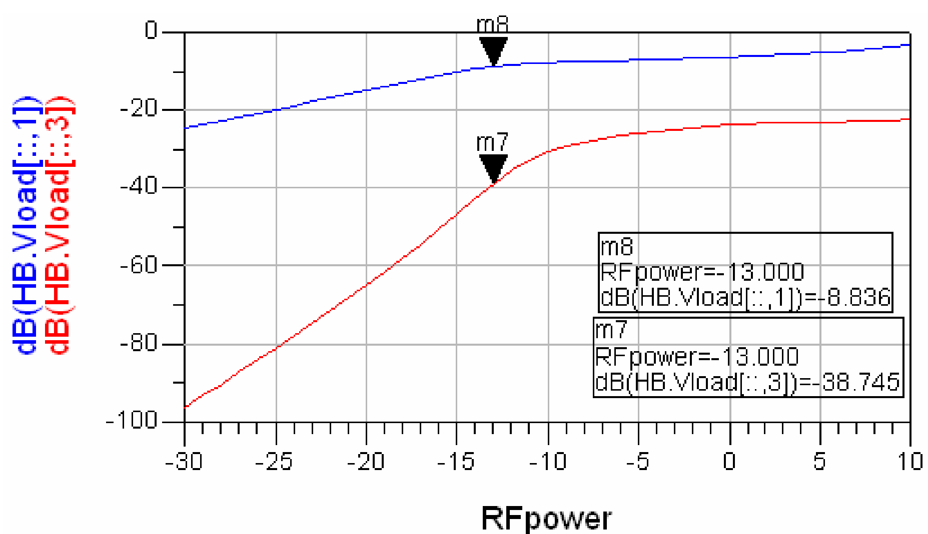

Figure 5-24: Fundamental and third harmonic for class AB operation

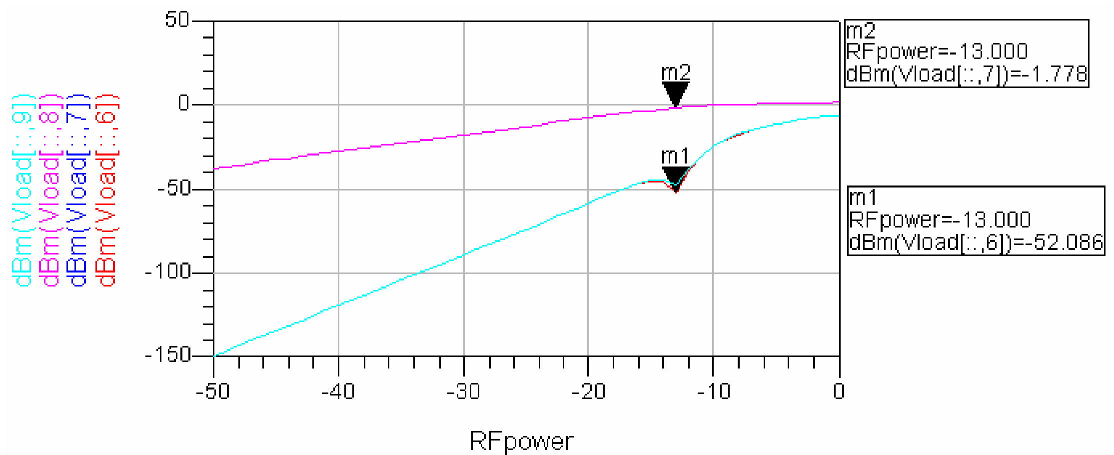

Figure 5-25: Plot of the fundamentals and the third order intermodulation for class AB

5.12.2 Class B

For class B operation the bias point is:

$$V_{CE} = 2.75 \text{ V}$$

$$I_B = 4 \text{ µA}$$

A single tone and two tones simulations were done to study the characteristics of the PA in this class. Figure 5-26 shows the transducer power gain in function of the input power for different base current. For I_B =4 µA the 1-dB compression point is for -23 dBm input power and 7.9 dB gain. Figure 5-27 shows the fundamental and the third harmonic which is 37.31 dB below carrier at the 1-dB compression point.

Figure 5.28 shows the two fundamentals, the lower and the upper third intermodulation distortion. At 1-dB compression point we have the intermodulation distortion is 46.4 dB below the fundamentals

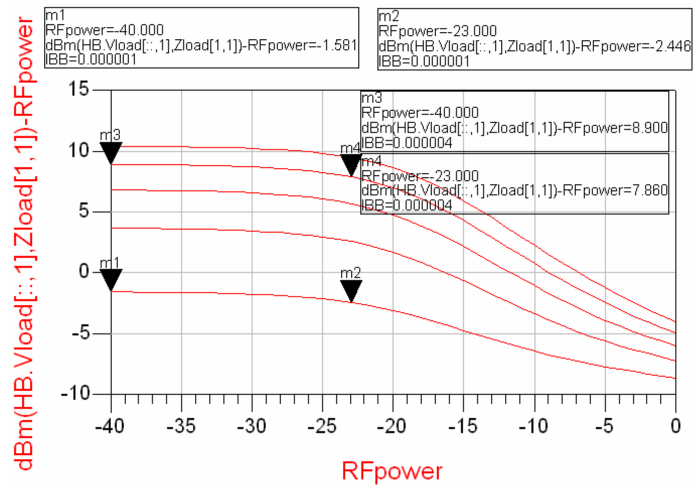

Figure 5-26: Power gain versus input power for different base current

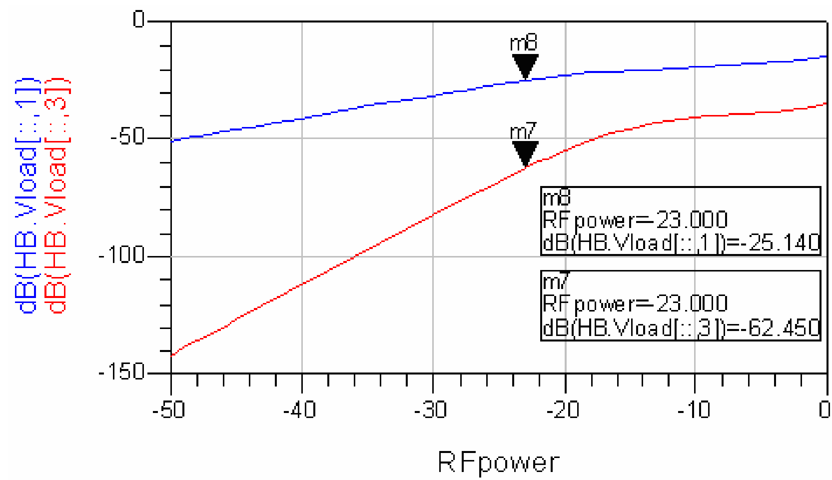

Figure 5-27: Fundamental and third harmonic for class B operation

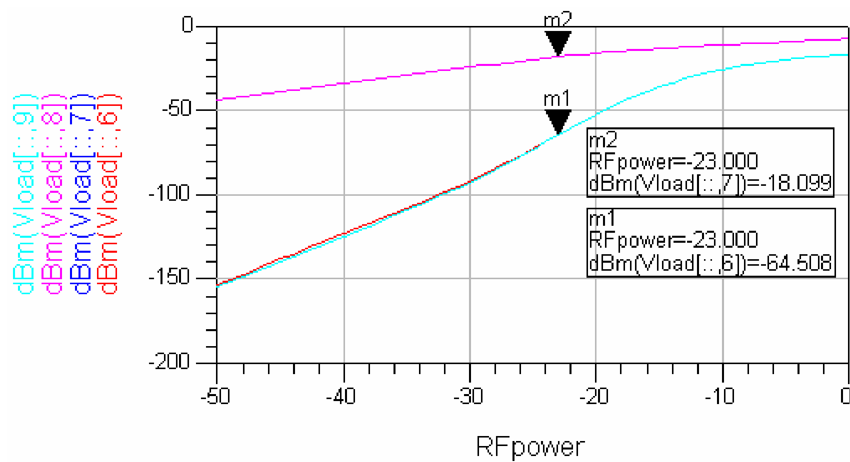

Figure 5-28: Plot of the fundamentals and the third order intermodulation for class B operation

5.12.3 Class C

For class C operation the bias point is:

$$V_{CE} = 2.75 \text{ V}$$

$$I_B = 1 \ \mu\text{A}$$

A single tone and two tones simulations were done to study the characteristics of the PA in this class. Figure 5-26 shows the transducer power gain in function of the input power for different base current. For $I_B = 1$ µA the 1-dB compression point is for -23 dBm input power and -2.5 dB gain. Figure 5-29 shows the fundamental and the third harmonic which is 40.6 dB below carrier at the 1-dB compression point.

Figure 5-30 shows the two fundamentals, the lower and the upper third intermodulation distortion. At 1-dB compression point we have the intermodulation distortion is 35.8 dB below the fundamentals

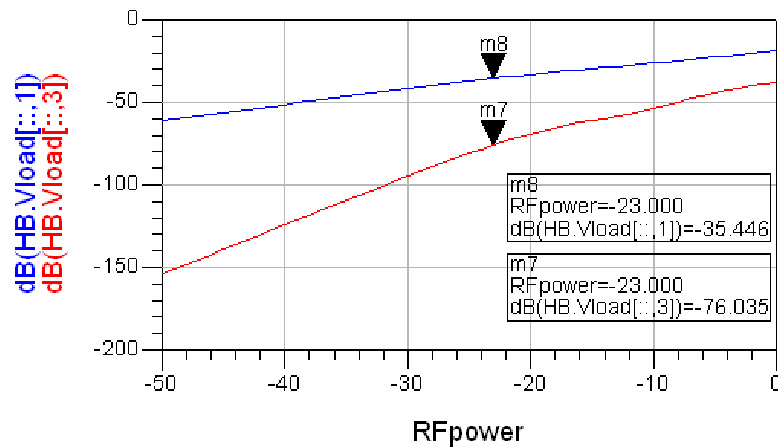

Figure 5-29: Fundamental and third harmonic for class C operation

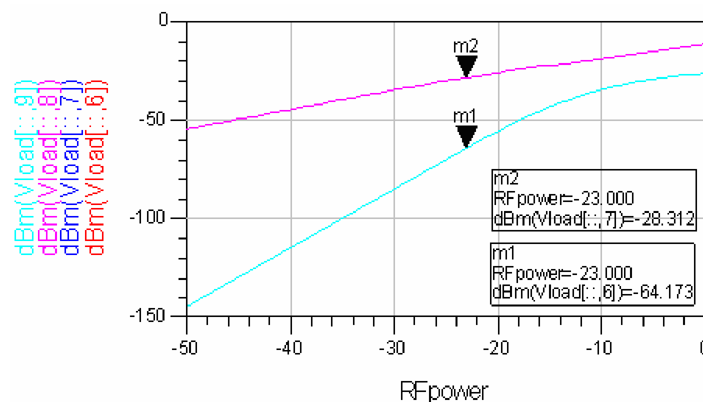

Figure 5-30: Plot of the fundamentals and the third order intermodulation for class C operation

Table 5-7 shown below summarizes all the values for different classes.

	Class A	**Class AB**	**Class B**	**Class C**
Power Supply	V_{CE} = 2.75 V I_B = 75 μA I_C = 13.9 mA	V_{CE} = 2.75 V I_B = 20 μA I_C = 5.262 mA	V_{CE} = 2.75 V I_B = 4 μA I_C = 0.908 mA	V_{CE} = 2.75 V I_B = 1 μA I_C = 0.23 mA
1-dB compression point	-3 dBm input power	-13 dBm input power	-23 dBm input power	-23 dBm input power
Power Gain @ 1-dB compression point	14.6 dB	14.16 dB	8.9 dB	-2.45 dB
3rd Harmonic	22.45 dBc	29.9 dBc	37.31 dBc	40.6 dBc
Third Intermodulation Distortion	27 dBc	50.3 dBc	46.4 dBc	35.8 dBc

Table 5-7: Characteristics of the PA in different classes of operation

5.13 Layout

The first step in layout design is to create the footprints for each component that is used in the design. Since we know which components we use, we take the dimensions of these components from the manufacturer's data sheet.

Since the 1nF and 1 pF Capacitors have the same dimensions, they are replaced by C_PAD capacitors from Lumped Artwork with the following characteristics:

$$W = 1.2mm$$
$$L = 2mm$$
$$S = 0.5mm$$

The 1 μF Capacitors are replaced by C_PAD capacitors from Lumped Artwork with the following characteristics:

$$W = 3mm$$
$$L = 4mm$$
$$S = 1mm$$

The 1 μH Inductors are replaced by L_PAD inductors from Lumped Artwork with the following characteristics:

$$W = 0.8mm$$
$$L = 1.6mm$$
$$S = 0.4mm$$

Since the Resistors have the same dimensions, they are replaced by R_PAD resistors from Lumped Artwork with the following characteristics:

$$W = 1.2mm$$
$$L = 2mm$$
$$S = 0.5mm$$

Where W is the width of the PAD, L is the pin-to-pin distance and S is the spacing.

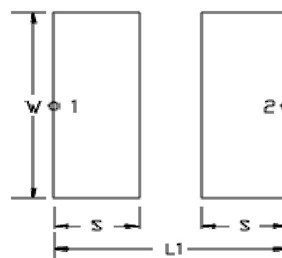

Figure 5-31: Artwork component

The HBT transistor is replaced by the transistor pb_nec_NE68518 _19931201 from the Library; the transistor used for the current source will be replaced by the transistor pb_hp_AT32063 _19961111.

The terminations and the voltage source are replaced by the Port component. Port is the standard port component offered and used to define networks. The number of ports of a network is the same as the number of Port components connected in it.

After doing the steps described above we start placing the components from the schematic to the Layout window. The complete Layout is represented in the following figure.

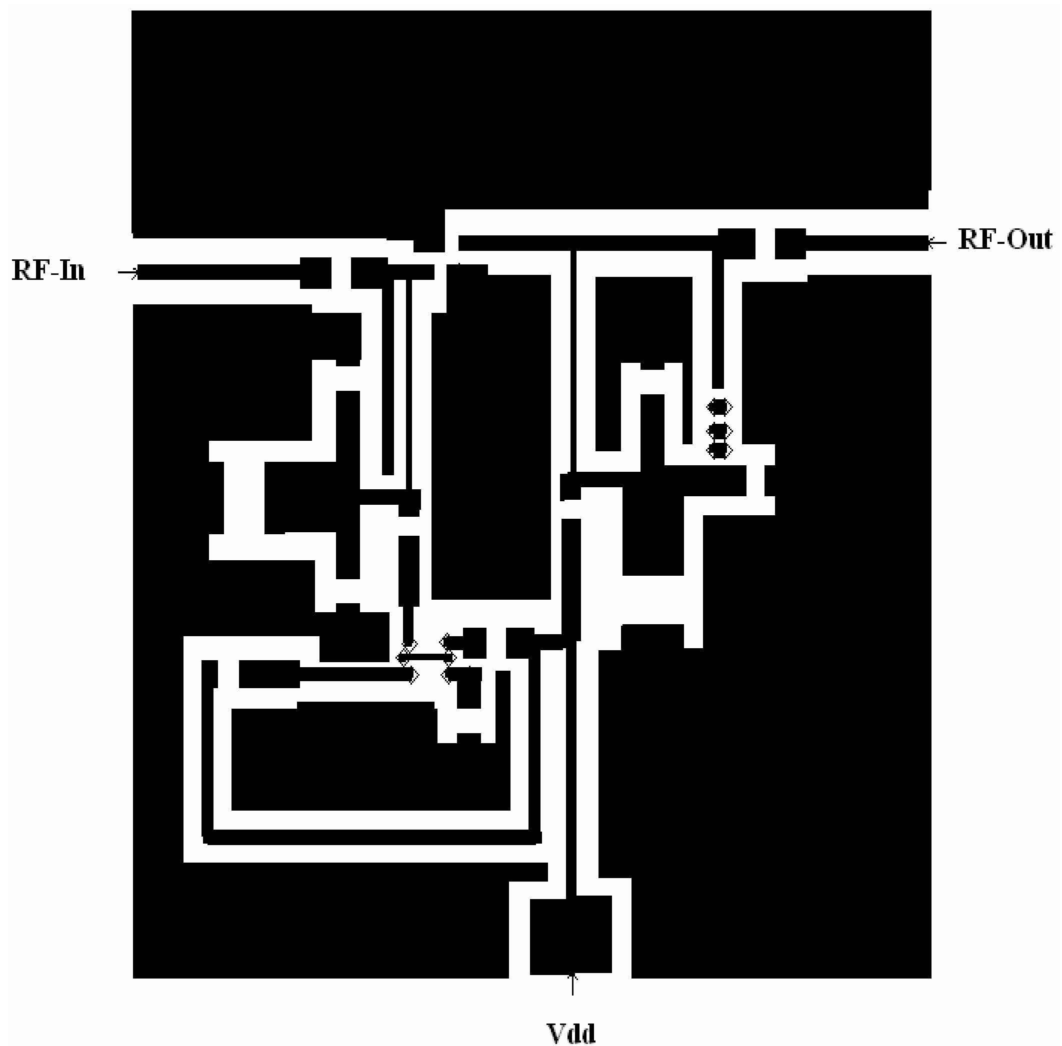

Figure 5-32: PA Layout Design - ADS

6 CHAPTER 6

MEMORY EFFECTS IN POWER AMPLIFIER

6.1 Introduction

Electrical systems can be divided into memory less systems and systems with memory. In Memory less systems, the output signal is only a function of the instantaneous input signal.

In systems with memory the output signal is a function of both the instantaneous and previous input signals.

In this chapter we will discuss the sources of the memory effects in Power Amplifiers and present the simulations done in ADS on our power amplifier to see its performance against memory effects.

6.2 Sources of Memory Effects

In some references [13], [14], memory effects are categorized as electrical and thermal. The main source of electrical memory effects is given by bias network impedance variation. Self-heating effect in the main source of thermal memory effects [13].

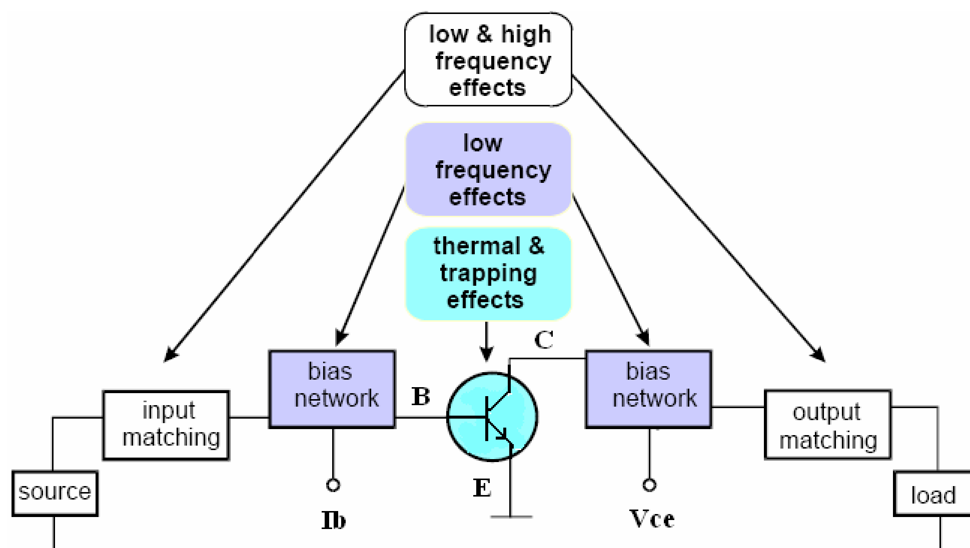

Figure 6-1: Typical location of the memory effects power amplifier

Practically, there are many other additional reasons, which contribute to the memory effect problem such as dispersion and trapping effects in the power active device.
Mixing all these effects: self-heating, dispersion and trapping effects as well as amplifier non linearity with additional mismatching, impedance variations and decoupling effects in the external circuits around amplifier like input and output matching networks, bias networks and power supply results in that the amplifier output signal is not only a function of instantaneous input signal value but also a function of previous values.

6.2.1 Self-Heating of Active Power Device

The dissipated power in active devices is the main source of thermal memory effect since the temperature changes due the dissipated power do not occur instantaneously. The thermal memory effects can be neglected in low power amplifiers. But this is not the case for the power amplifiers that are used in the base stations for mobile communications.

6.2.2 Bias Network Construction

The bias networks are required to isolate the RF signal to feed into the bias supply and avoiding active device instability.
In traditional bias network design, the bias circuit is usually designed to provide relatively high impedance at RF frequency as compared to the impedances of the input and output of the device and the matching circuits. In the case of the input signal with non-constant envelope, the envelope frequency variations cause variation in the impedance of the bias network which causes nonlinearity variation as a function of envelope frequency (memory effects).
In an ideal case, to avoid envelope frequency dependent bias network, the impedance should be a short circuit at envelope frequency and an open circuit at RF frequency to isolate the RF signal from the bias supply [15]. Practically, it is difficult to realize such an impedance, which has two requirements that tend to conflict with each other.

6.2.3 Power Supply Properties

In general, the amplifier power supplies are applied to the base and the collector sides in order to provide the necessary dc voltage or current for active device operation. Moreover, as described in (chapter 3), different amplifier operation classes give different output current waveforms with different conduction angles [7].

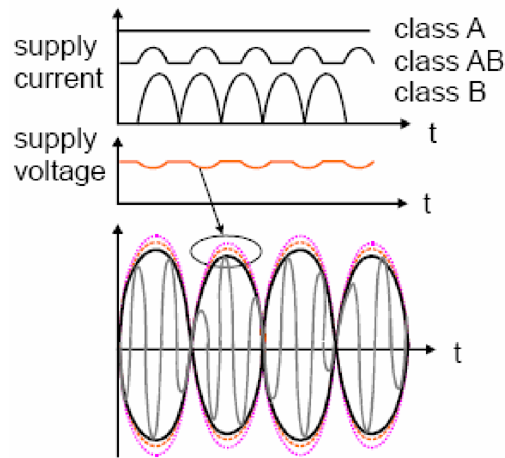

Figure 6-2: Memory effects due to power supply variations

Particularly, in the case of the input signal with a non-constant envelope, a current variation drew from the dc power supply causes dc voltage variations [7]. These voltage variations however cause additional amplitude modulation of the RF signal (re modulation) as illustrated in figure 6-2. Moreover, when the impedance of the bias network is reactive (not short [15]), the additional amplitude modulation will be out of phase compared to the original RF signal resulting in memory effects or envelope frequency dependent and asymmetrical of the output signal.

To reduce the power supply variation effect in the amplifier, the bias networks should be carefully designed in order to isolate the current variations drawn from the dc power supply. Imperfections in the design can increase the variation in the dc voltage and consequently the memory effects will appear [15].

6.2.4 Mismatching of Even Harmonics

Generally, in the amplifier design, the input/output matching networks are designed to overcome the mismatching between active nonlinear device (transistor) and input/output termination (almost 50-ohm) at fundamental frequency. Theoretically, any signal reflected from the active device at any frequency should be absorbed in the matching networks but practically; this is not the case in common matching networks [18], because they are designed at RF amplifier bandwidth (fundamental frequencies) which means band limited.

Consequently, in the two-tone input signal case, the signals at harmonic zone 0, zone 2, zone 3, … zone *K* (figure 6-3) generated from the active device due to its nonlinearity (first mixing process) are reflected back to the input side rather than absorbed by the input

matching network resulting. These reflected signals are mixed again in the active device with the two-tone input signal (second mixing process) and generates an additional nonlinearity in the output signal as modification of the output spectrum (figure 6-3) [14].
In the second mixing process, it is important to note that, the active device two-tone input signal is mixed with the reflected signal at even harmonic zones resulting in a modification of the odd order IMD (zone 2 in figure 6-3) and besides that, mixing the two-tone input signal with the reflected signal at odd harmonic zones will not result in a modification of the odd order IMD.

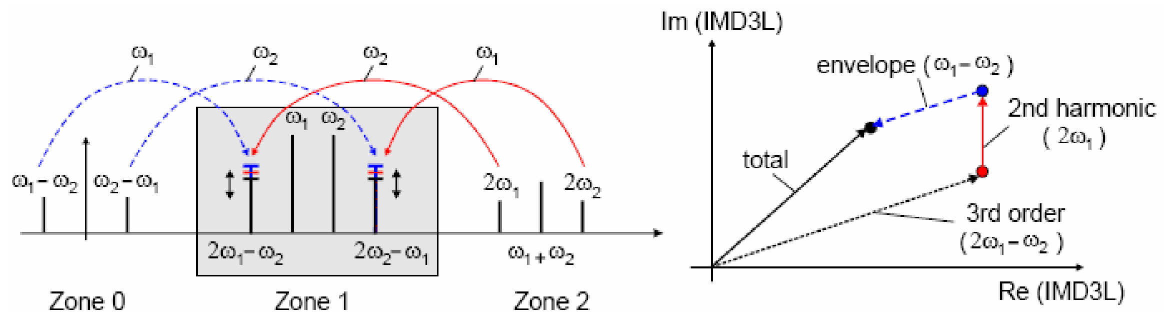

Figure 6-3: Memory effects due to mismatching of even harmonics

As shown in figure 6-3, the resultant 3rd order IMD is a vector sum of the signals at IMD produced from the 3rd order nonlinearity (first mixing process) and the signals at IMD produced from the second order nonlinearity (second mixing process) in the active device.

6.3 Simulated Results of Memory Effects in the Power Amplifier

The simulations were done for class-A and class-AB operation. Operating points were V_{CE} = 2.75 V, I_B = 75 µA for class A and V_{CE} = 2.75 V, I_B = 20 µA for class AB.
Two-tone stimulus input signal with center frequency of 2.4 GHz was used. The frequency spacing was varied between two tones from 10 KHz to 5 MHz and input power sweep from -18 dBm to 3 dBm was considered. Figures 6-4a and 6-4b shows that in both classes, the output signal at the third order intermodulation don't have a power variation as function of the envelope frequency, which means that, this power amplifier doesn't exhibit memory effects.

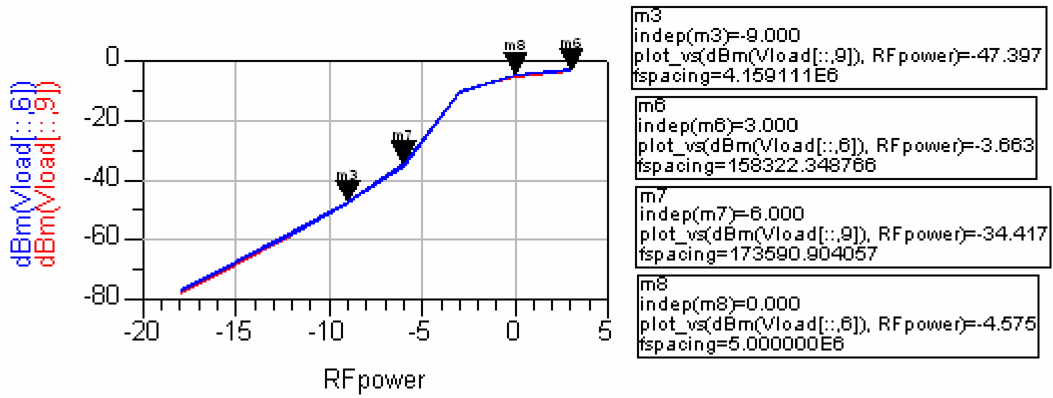

(a)

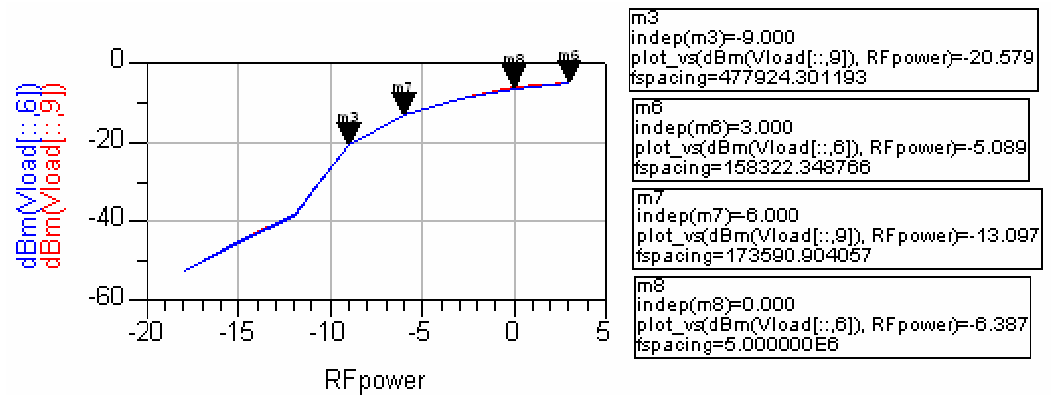

(b)

Figure 6-4: Measured upper and lower IMD3 as function of input power and frequency spacing (Δf) of a two-tone input signal: (a) class-A, (b) class-AB

.

Figure 6-5 shows the measured memory effects in the HBT Power Amplifier device at fundamental output powers and third intermodulation for class-A operation. We can notice that this power amplifier have low memory effects since it shows

- Less than 0.01dB variation in the output power at fundamental frequencies.
- Less than 0.2 dB variations in the third order IMD.

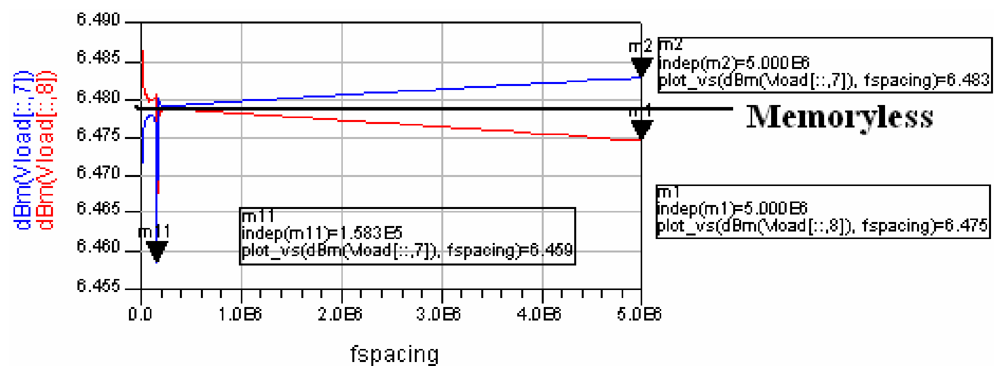

(a)

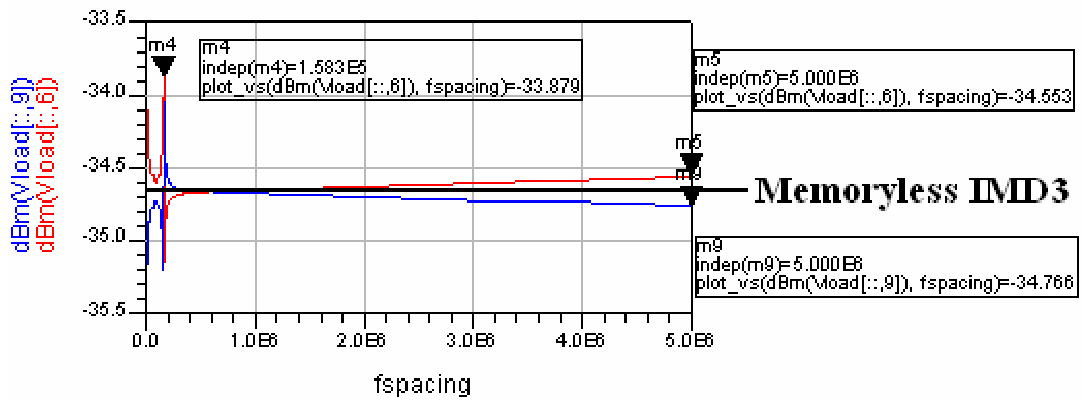

(b)

Figure 6-5: Measured output signal at (a) fundamental frequencies, (b) upper and lower IMD3 as function of frequency spacing (Δf) of a two-tone input signal (input power =-6 dBm).

We notice that the highest memory effect is located at frequency spacing of 158.6 KHz. Since the HBT device is of small size, we do not expect significant heating or power dissipation and, thus, we do not expect that the memory arises from thermal heating.

This phenomena is explained in [16], it is proved that if the information bandwidth spans from dc to a few MHz and the impedance of the base-band matching network changes over that frequency range, the PA response over that same bandwidth will present some kind of memory effects that can be visible in the variation of the IMD when performing two-tone tests with different frequency separation.

To prove that the impedance of the base-band matching network changes over the frequency range of the information bandwidth we have performed a simulation of the load impedance shown in figure 6-6 and of the source impedance shown in figure 6-8.

The load and source impedances simulated for frequencies from 1 MHz to 20 MHz are shown in figures 6-7 and 6-9 respectively.

We notice from these plots important variations of the impedances with resonance situated around of 158.6 KHz.

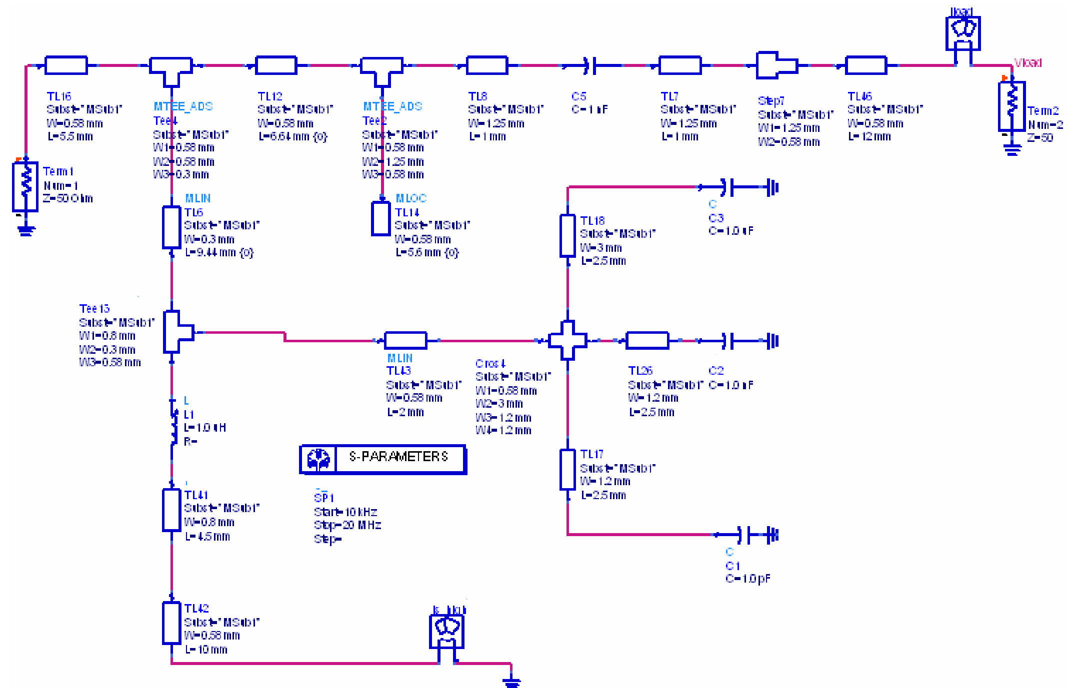

Figure 6-6: Schematic of the load impedance

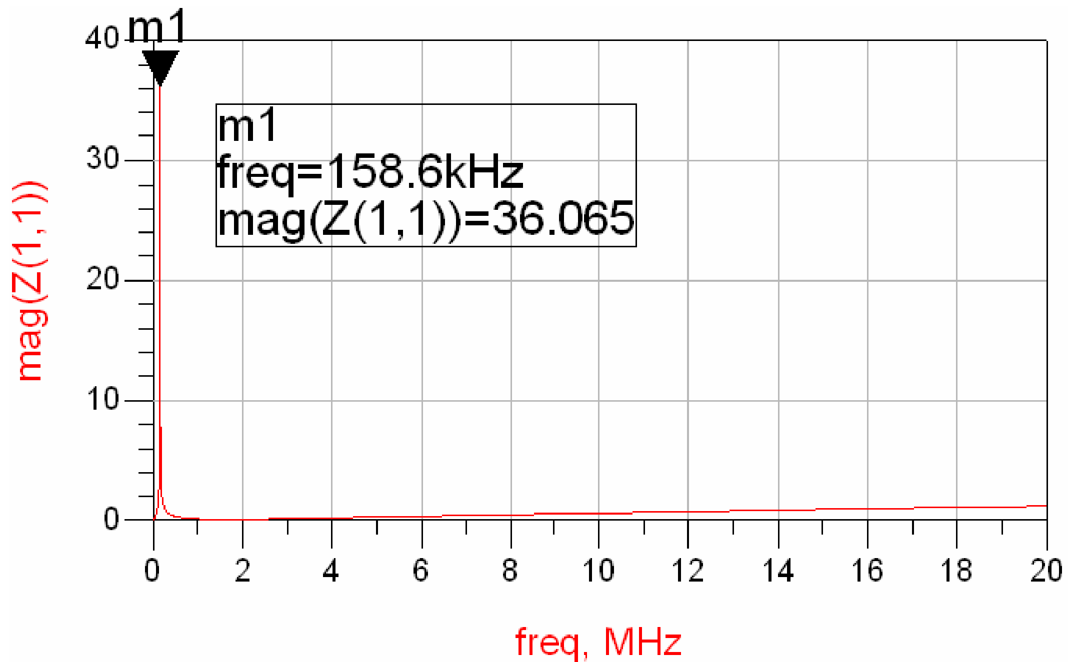

Figure 6-7: Output impedance

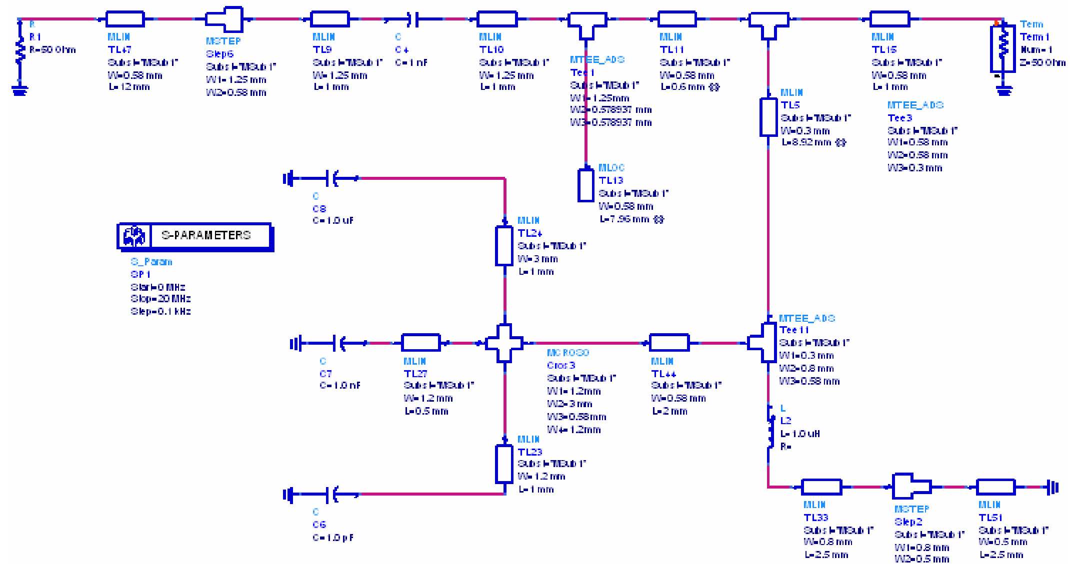

Figure 6-8: Schematic of the source impedance

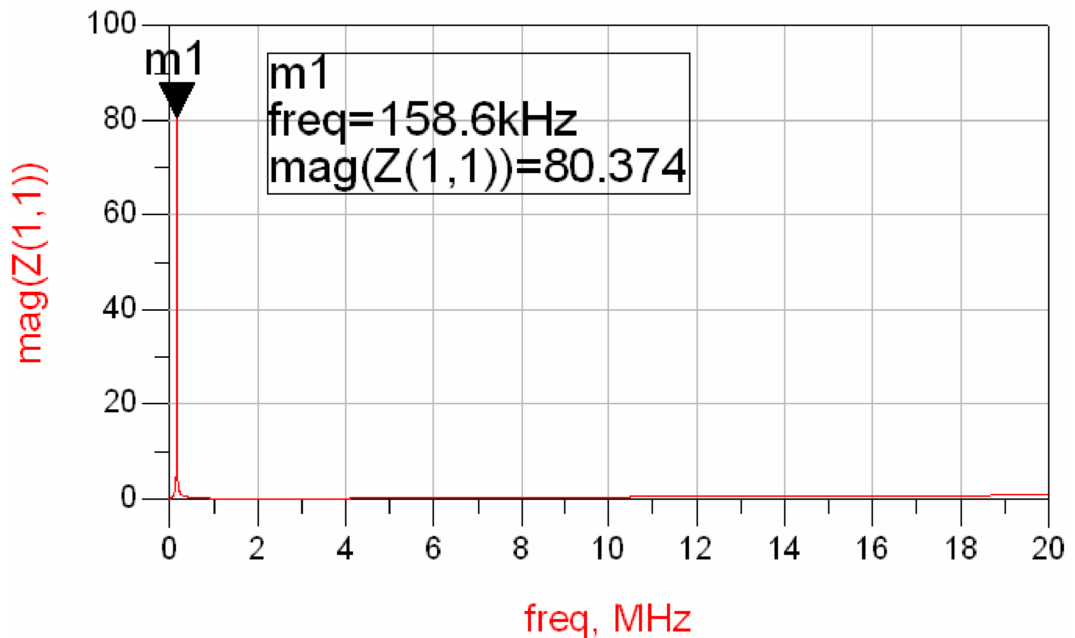

Figure 6-9: Input impedance

7 CHAPTER 7

MEASUREMENTS

7.1 Introduction

An essential part of every circuit design is the measurement of an IC chip. The physical manifestation of a circuit design is often very different from even the most detailed and intricate simulations. For power amplifiers, which are perhaps the most empirical of all RF designs, this is especially true. This chapter will discuss the specifics of measuring this power amplifier design. The power gain, filtered output power, linearity, efficiency, power added efficiency, the input and output reflection coefficients and the memory effects of the PA were measured and are presented in the following sections.

7.2 Matching measurement

Matching of the circuit was measured by its input and output reflection coefficients using a Vector Network Analyzer, VNA, and a source voltage in order to bias the power amplifier in class A as is shown in figure 7-1. A perfect match at the output or input of a circuit would imply a zero reflected power at the two ports. S11 and S22 of -10 dB suggest an acceptable level of matching. A lower value than -10 dBm for the reflection coefficients implies a good match. Figure 7-2 illustrates the input and output reflection coefficients of the circuit versus frequency. S22 is below -10 dB and S11 is below -20 dB over a wide band of 200 MHz approximately which mean that we have a very good match.

Figure 7-2 shows also the gain S21 of the PA which is the transmitted power from the input port to the output port. We notice a wide band gain around our frequency of interest of 17 dB approximately.

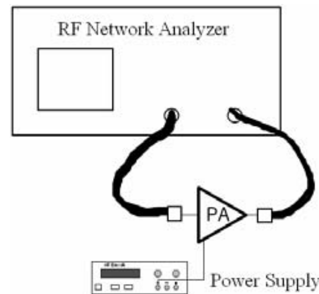

Figure 7-1: Setup for the matching measurement

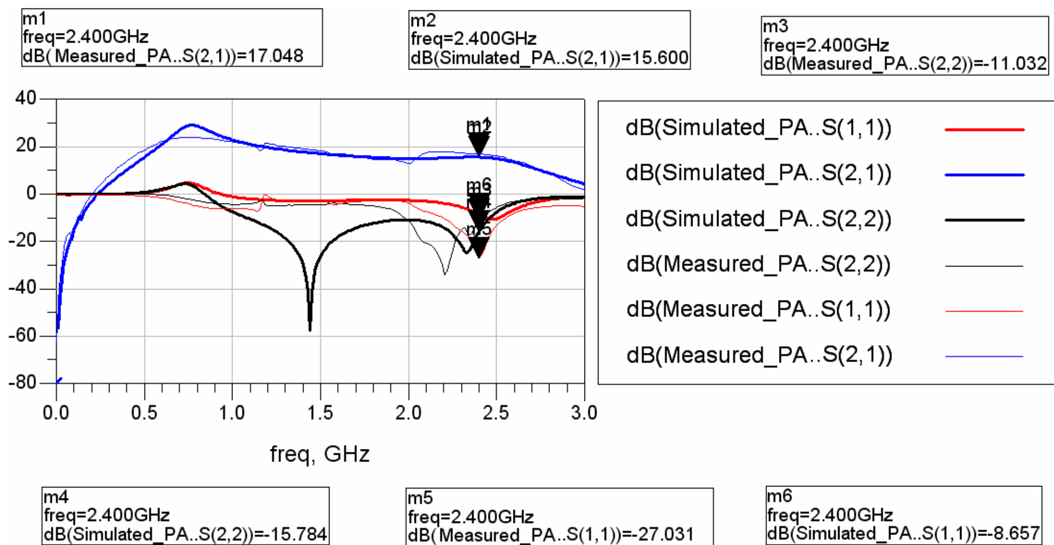

Figure 7-2: Input, output reflection coefficients (S11, S22) and transmission coefficient (S21)

7.3 Power Gain and Compression Characteristic Measurement

Power Gain of the amplifier was measured using the setup shown in figure 7-3. The spectrum analyzer is employed in the test setup to measure the power spectrum of the Fundamental frequency generated by the signal generator, the power supply is used to bias the power amplifier in class A.

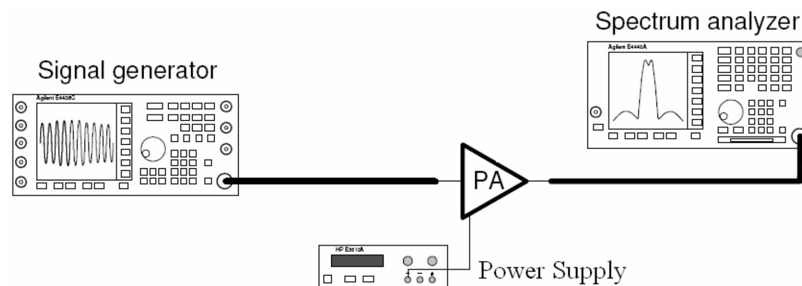

Figure 7-3: Power Gain setup measurements

To calculate the power gain we perform a power sweep from -30 dBm to 0 dBm with 0.5 dB step. For each input power we read the output power from the spectrum analyzer, we substrate the input power from the output power and hence we get the power gain. Figure 7.4 shows the power gain versus the input power.

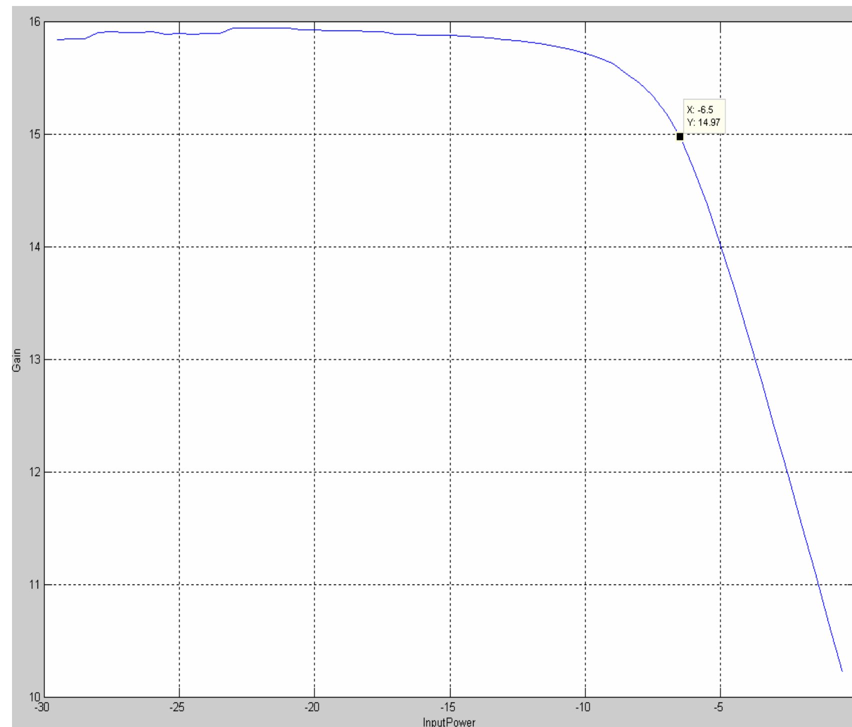

Figure 7-4: Power Gain versus Input Power

Every power amplifier gets saturated after a certain input power. The PA was measured for its compression point. The output 1 dB compression point of the class A power amplifier was measured at 2.4 GHz with a 2.75 V power supply. Figure 7-5 shows the output power versus the input power of the power amplifier. The output 1 dB compression point is shown in figure 7-4 and in figure 7-5 to be approximately at -6.5 dBm input power and +8.468 dBm output power.

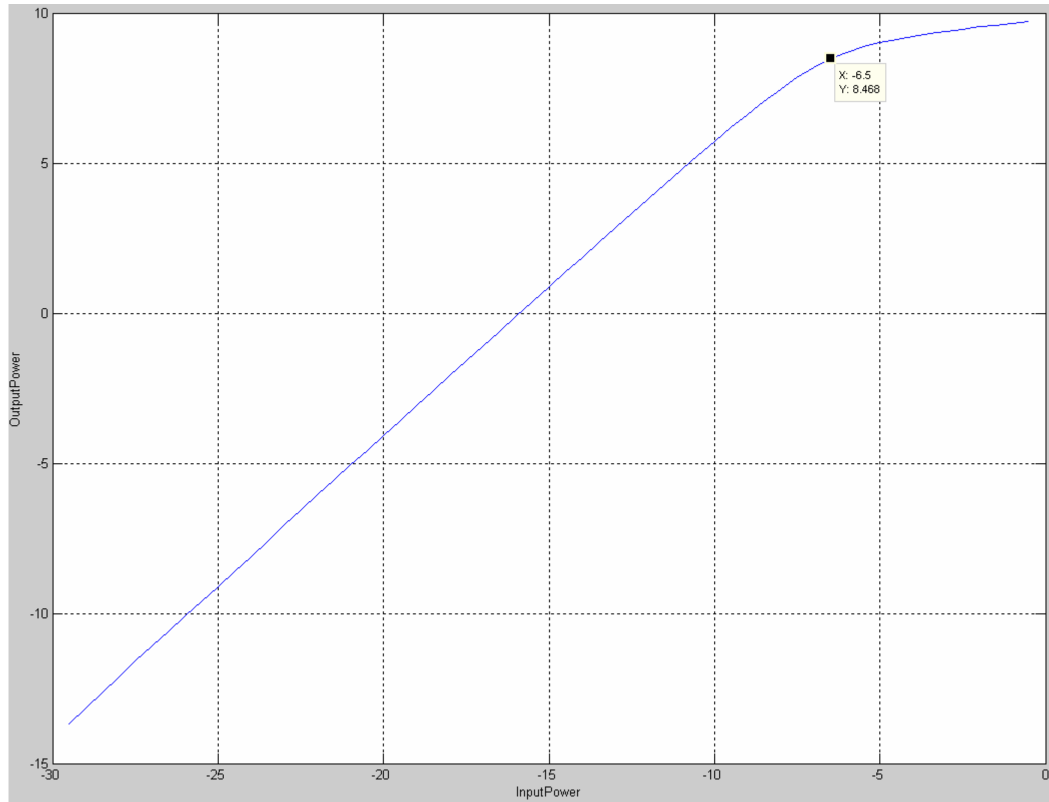

Figure 7-5: Output Power versus Input Power

7.4 Adjacent Channel Power Ratio Measurement

The Adjacent Channel Power Ratio (ACPR) of the amplifier was measured using the setup shown in figure 7-3. Adjacent channel power ratio (ACPR) characterizes how the main channel power spills over into the adjacent channels due to the nonlinearity of the PA. The problem that we have faced in this measurement was that our signal generator doesn't generate WIFI signals. We have performed this measurement with 3GPP WCDMA signals. The power in the WCDMA carrier is measured using a 5MHz measurement bandwidth. The total power in the adjacent channel and in the alternate from the center of the outermost carrier is measured and compared to the carrier power. The result is expressed in dBc.

For the adjacent channel we got -54 dBc and for the alternate channel we got -60 dBc which meet with the specifications for 3GPP and the specifications of WIFI and imply that we have a good linearity.

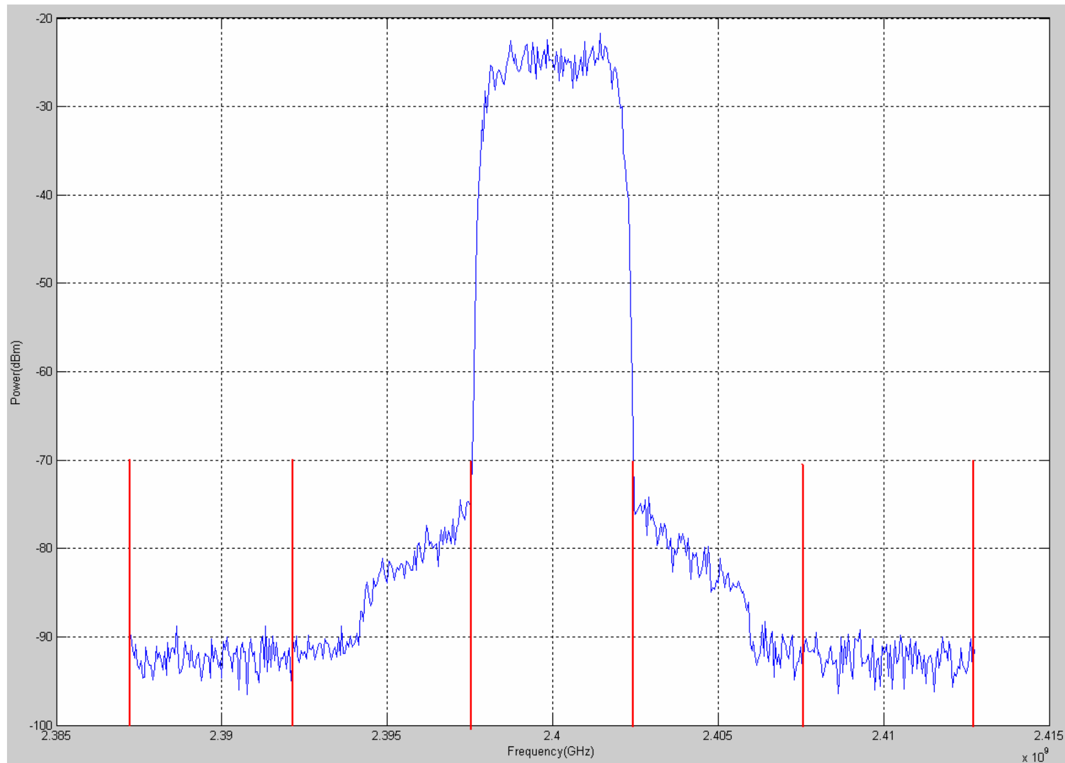

Figure 7-6: 3GPP ACPR measurement

7.5 Efficiency and Power Added Efficiency measurements

Power conversion efficiency of the PA was also measured under the same conditions with a 2.75v power supply at 2.4 GHz. The efficiency was measured by taking the ratio of the output power seen on the spectrum analyzer to the total DC power consumed from the power supply. The power added efficiency was measured by taking the ratio of the output power seen on the spectrum analyzer minus the input power to the total DC power consumed from the power supply. Figure 7-7 shows the efficiency (red) and the power added efficiency (blue) of the power amplifier versus the output power of the circuit. As the output power increases, the PAE and the Efficiency also increases. A maximum power efficiency of almost 28.4% was measured and a maximum PAE of 26% was measured when the input power is -0.5 dBm.

We notice that at 1-dB compression point the power efficiency is approximately 21.3% and the power added efficiency is 20.62%

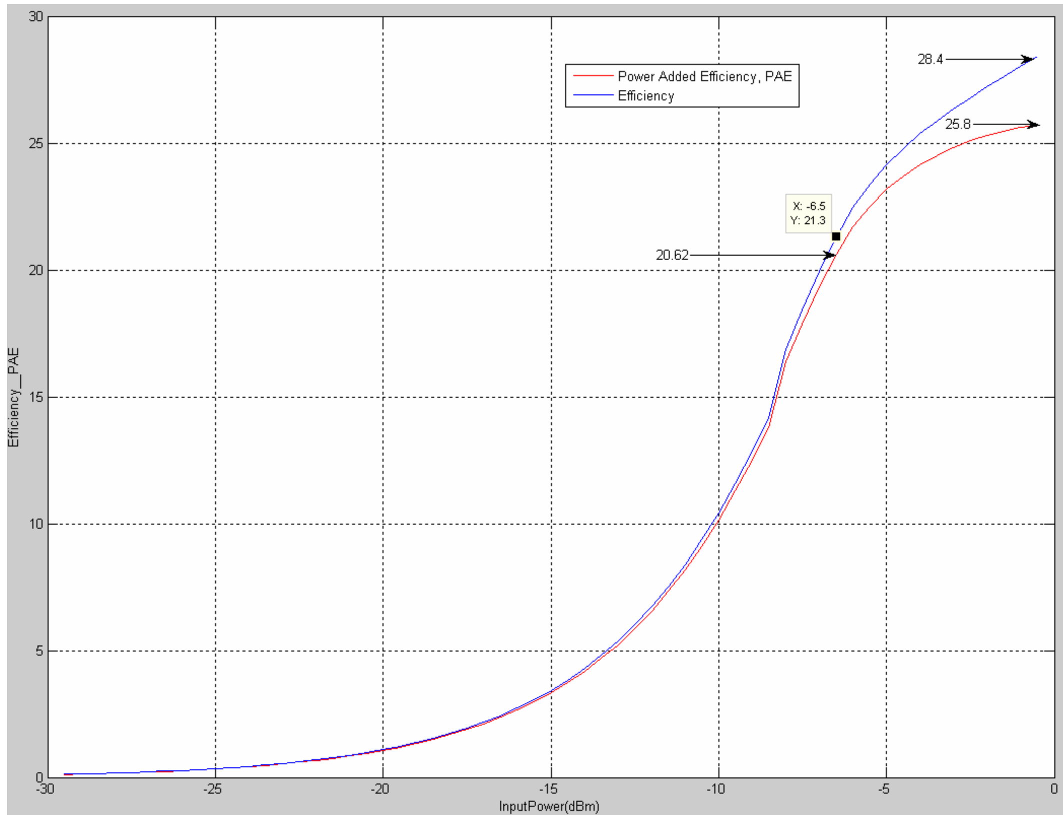

Figure 7-7: Power efficiency and PAE versus output power

7.6 Linearity measurement

Linearity of the power amplifier was measured by its two-tone intercept point. The measurement setup is shown in figure 7-8. For accurate measurement, the power loss of the power combiner, the cables and the connectors were measured in advance.

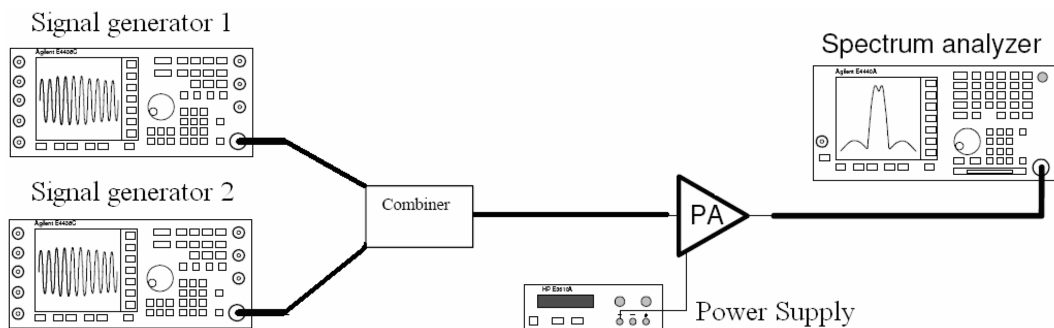

Figure 7-8: Two Tones measurement setup

Two closely spaced equal amplitude input tones were applied to the circuit at 2.4 GHz and 2.4001 GHz. The intermodulation products of the two signals would lie at 2.3999 GHz and 2.4002 GHz. These two intermodulation products are hard to filter out because

they are in the operating band of the amplifier. Figure 7-9 shows the fundamental and intermodulation products at the output versus the input power. We notice that the 1-dB compression point now is around -10 dBm input power, which is 3 dB below the 1-dB compression point of the one tone measurement.

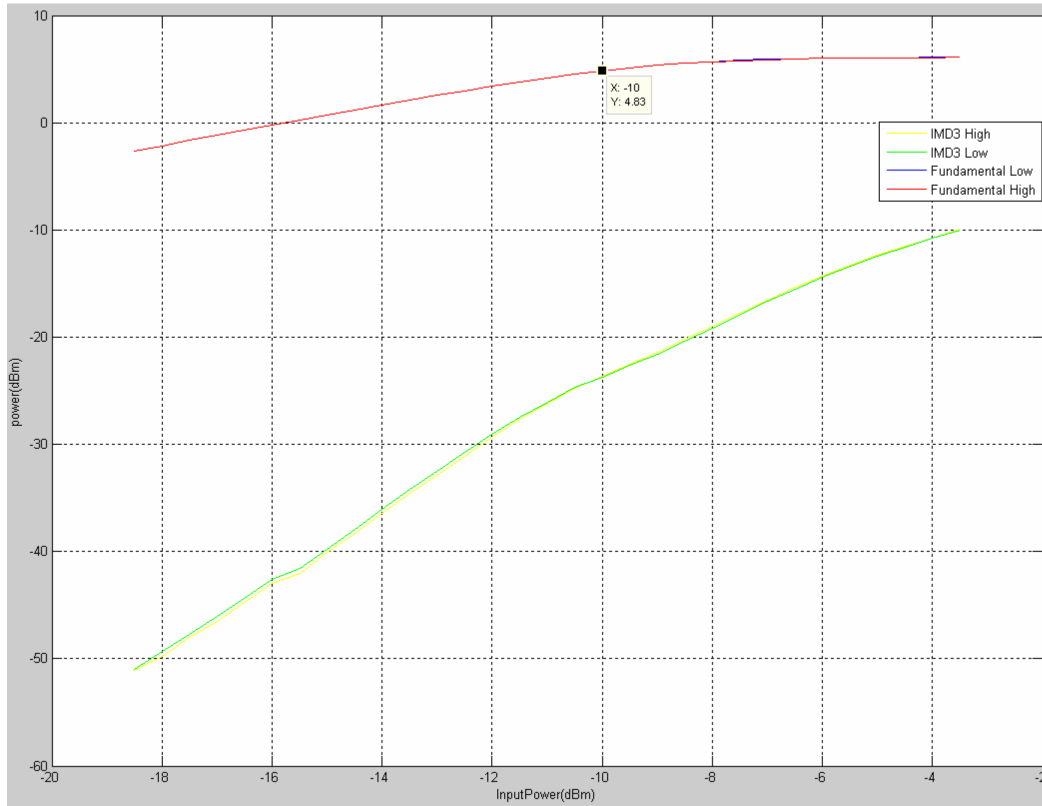

Figure 7-9: The two fundamentals and the third order intermodulation products

The two-tone intercept point of the PA was measured to be 16 dBm at the output and 1 dBm per tone at the input this measurement is done by linear extrapolation of the fundamentals and the third order intermodulation products as shown in figure 7-10.

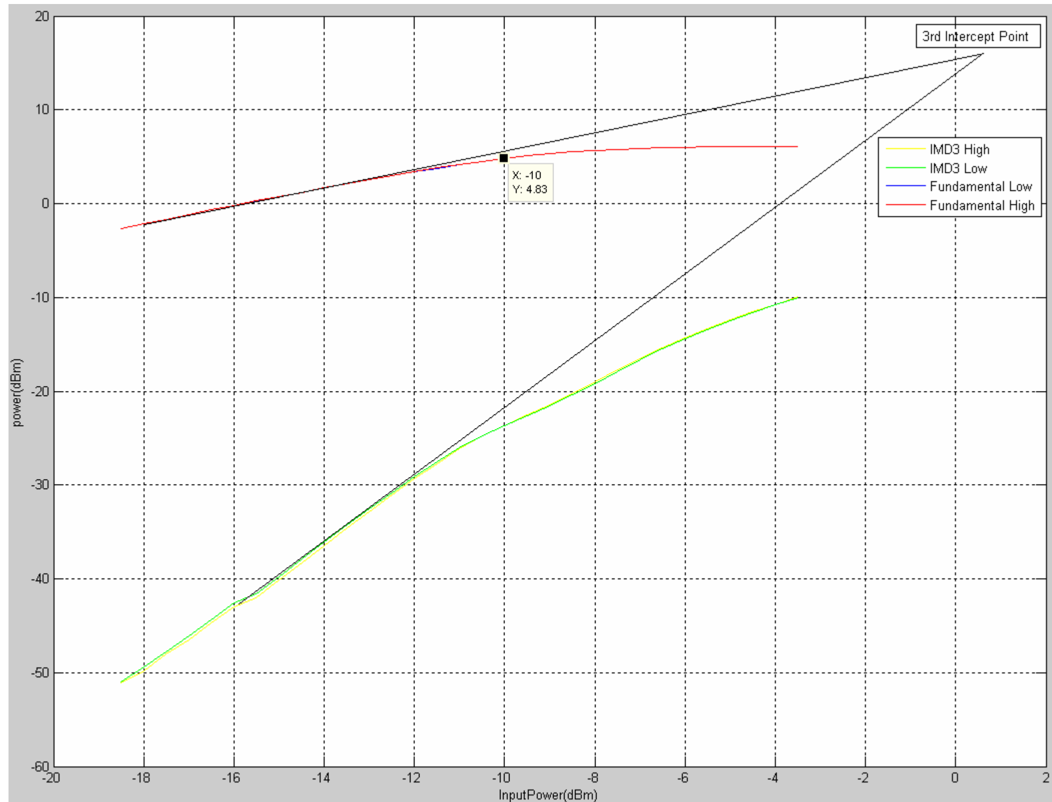

Figure 7-10: Two-Tones intercept point

7.7 Memory Effects

Memory effects of the PA were also measured under the same conditions and same setup measurement of the linearity measurement shown in figure 7-8. Two-tone stimulus input signal with centre frequency of 2.4 GHz was used. The frequency spacing was varied between two tones from 10 KHz to 2MHz and the input power is swept from -30 dBm to 0 dBm.

Figure 7-11 shows the measured memory effects in the Power Amplifier device at fundamental output powers and third intermodulation for class-A operation. Figure 7-12 shows the difference between the two fundamentals and the difference between the third order intermodulation products in 3D view. We can notice that this power amplifier have low memory effects since it shows

- Less than 0.2 dB variation in the output power at fundamental frequencies.
- Less than 1.5 dB variations in the third order IMD.

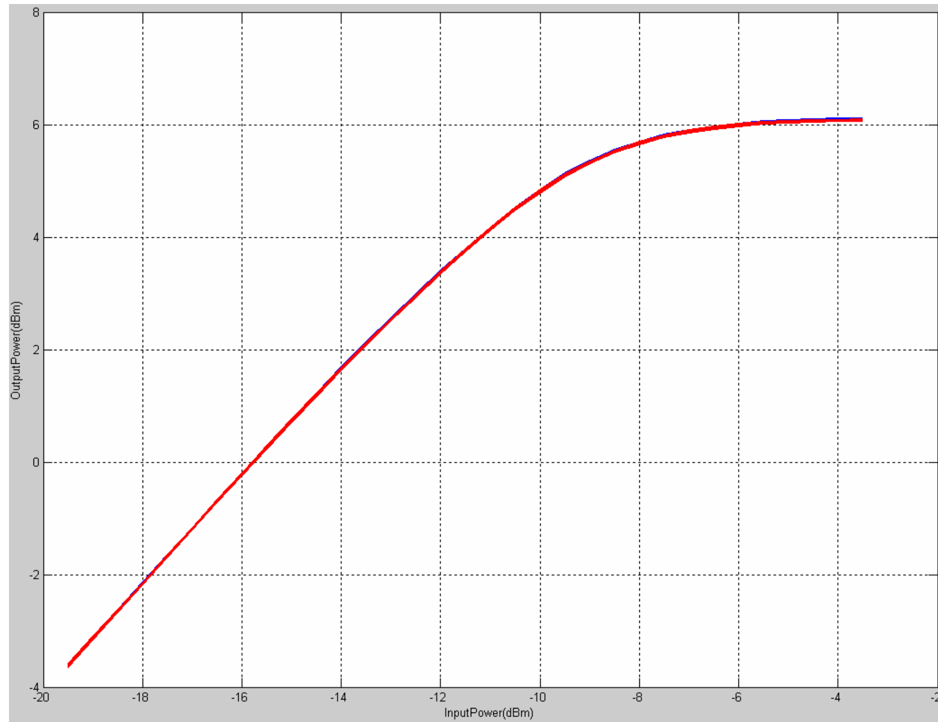

(a)

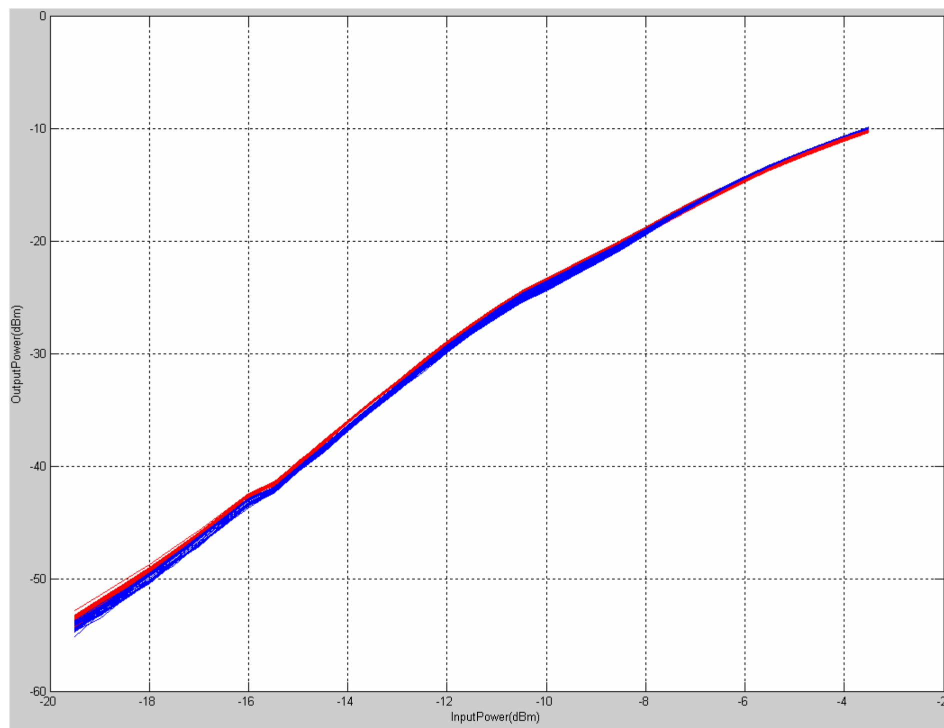

(b)

Figure 7-11: Measured output signal at (a) fundamental frequencies, (b) upper and lower IMD3 as function of frequency spacing (Δf) of a two-tone input signal and input power sweeping

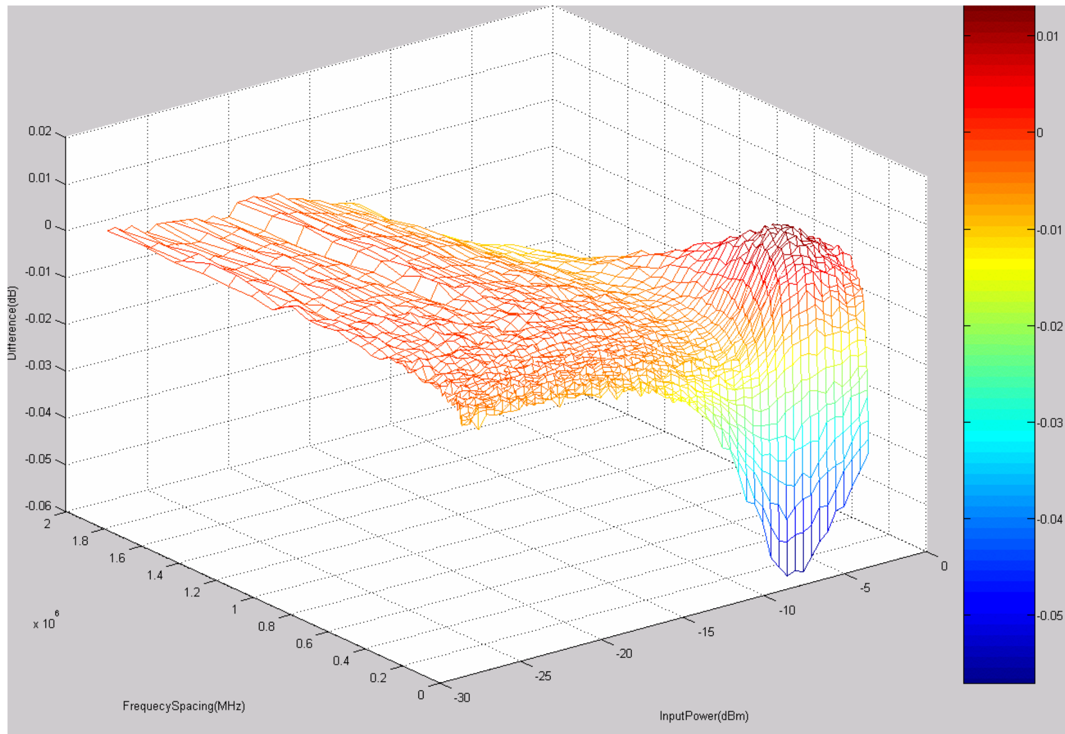

(a)

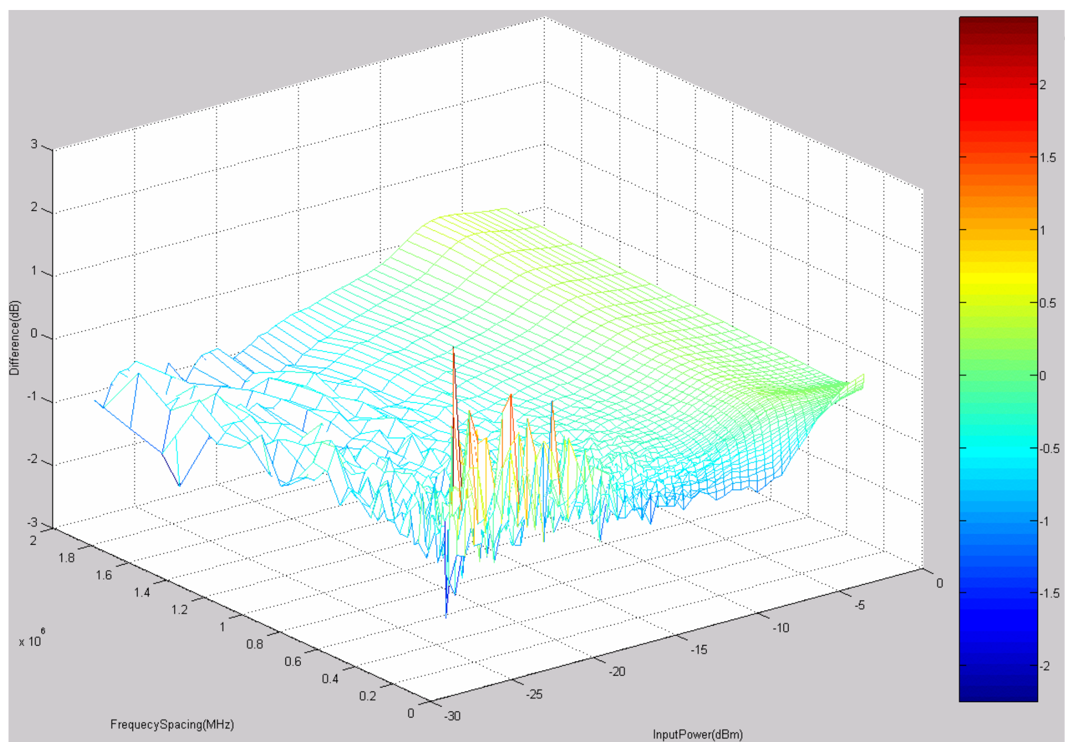

(b)

Figure 7-12: 3D View of the difference measured output signal at (a) fundamental frequencies, (b) upper and lower IMD3 as function of frequency spacing (Δf) of a two-tone input signal and input power sweeping

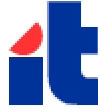

8 CHAPTER 8

CONCLUSION AND THE FUTURE WORK

8.1 Introduction

There are many issues surrounding power amplifier design that can make or break practical implementation. Given the empirical nature of power amplifier design, there are many issues that should be explored in future work. This chapter gives a brief overview of some of these issues and gives some conclusions for this research.

8.2 Conclusion

The primary goal of the project, that HBT transistors can replace widely used CMOS technology in RF applications, has been fulfilled in the modelling of an HBT power amplifier. Based on the results we got, HBT technology gives more advantage in terms of higher power gain and better thermal capabilities, than CMOS.

Many aspects of the PA were considered when presenting the final results, as the power gain, filtered output power, linearity, efficiency, power added efficiency, the input and output reflection coefficients and the memory effects.

At 1-dB compression point the power efficiency found is approximately 21.3% and the power added efficiency is 20.62%, which meets the practical efficiency of the class A Power Amplifiers. Linearity of the power amplifier was measured by its two-tone intercept point, and showed good results, and we can also notice that this power amplifier has low memory effects since it shows less than 0.2 dB variations in the output power at fundamental frequencies.

In overall, this gives a solid base for the future work in popularization of the HBT based PA.

8.3 Future Work

Future work related to the topics and innovations presented in this thesis can be divided into two categories: theoretical research and practical areas. The first includes all issues related to modelling, analysis and extraction, and partially those related to simulations

and measurements, while the latter is considered here to include real world problems in PAs that can be solved by the circuit techniques.

Several research directions for the future work, using this thesis as a starting point can be identified:

- increasing the efficiency and the PAE more with increasing the IMD performance at the same time
- understanding the sources of the memory effects and try to minimize them
- optimizing the design to get best results

One of the possible directions in the future work is multiple stage PA design.

In any practical PA implementation, multiple stages are necessary to amplify the signal from the small- signal regime to a high power level. This is implemented in multiple stages, as illustrated in Fig. 8.1, with each stage providing on the order of 10 dB of power gain.

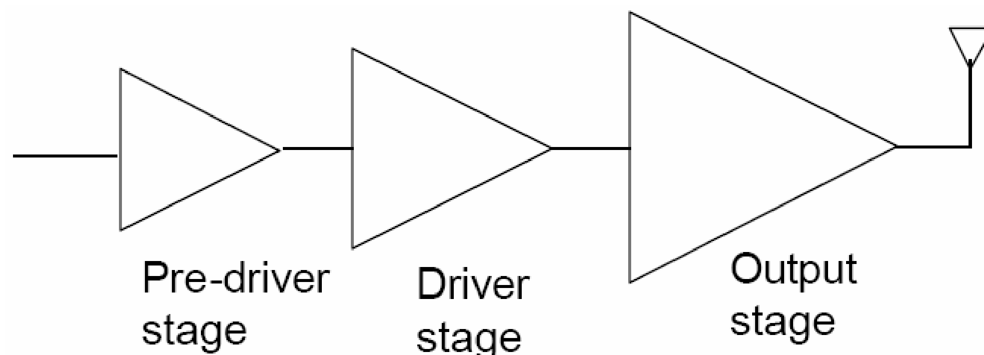

Figure 8-1: Multiple stage power amplifier

It is believed that the future development of a HBT PAs with many more elements and active devices integrated, is able to provide an increase in gain for signals as well as better performance in RF applications.

As such, further work can be aimed at producing inexpensive and well-manufactured applications for the purpose of power combining and amplification.

Appendix

Manufacturing

We printed out the design on a paper then we took a photo with a special machine to get the circuit on a film. We notice that we have printed the layout in the dark field polarity (negative process). Then we have followed the following steps.

- Put the film on the board and let it be subject to Ultraviolet rays for about 40 to 60 seconds. The ultraviolet rays will fix the copper where the film is transparent.

- Plunge the board in a chemical solution for about 10 minutes to remove the unusable copper from the board and get our circuit.

- Let the board to be subject to ultraviolet rays to dry it on the both sides.

- Solder the components of the circuits (Transistors, Resistances, Capacitors, Inductors and Connectors).

The following figure shows the final power amplifier board.

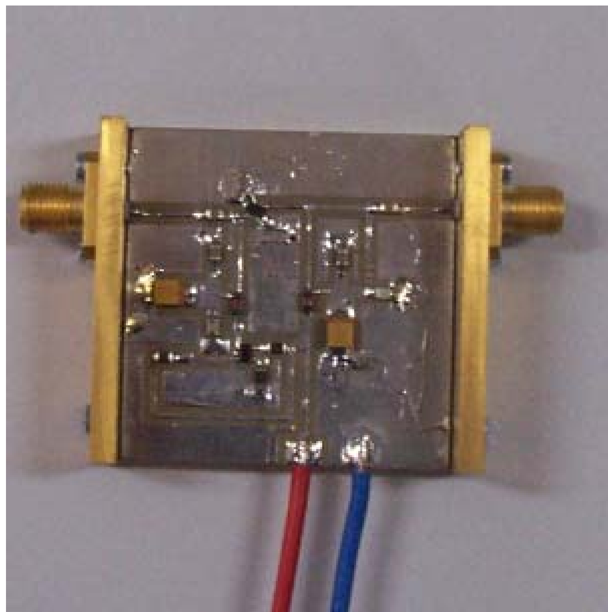

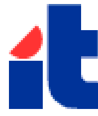

References

[1] http://hyperphysics.phy-astr.gsu.edu/hbase/solids/pnjun.html

[2] Sheng S. Li, "*Semiconductor Physical Electronics*", Plenum, New York, 1993

[3] S.M.Sze, "*Semiconductor Devices Physics and Technology*", 2nd Edition, John Wiley & Sons, New York, INC., 2001

[4] http://www.cellular.co.za/wifi.htm

[5] http://www.answers.com/topic/wifi

[6] Peter B. Kenington, "*High-linearity RF amplifier design*", Artech House, INC., 2000.

[7] S.C. Cripps, "*RF Power Amplifiers for Wireless Communications*", Artech House, Norwood, MA, 1999.

[8] H.L. Krauss, C.W. Bostian and F.H. Raab, "*Solid State Radio Engineering*", John Wiley & Sons, New York, NY 1980.

[9] N. Sokal and A. Sokal, Class E-A New Class of High-Efficiency Tuned Single Ended Switching Power Amplifiers, "*IEEE Journal of Solid State Circuits*", Vol. SC10, June 1975, pp. 168-76.

[10] M. Albulet, "*RF Power Amplifiers*", Noble Publishing, Atlanta, GA, 2001.

[11] Jose Carlos Pedro and Nuno Borges Carvalho, "*Intermodulation Distortion in Microwave and Wireless Circuits*", Artech House, INC., 2003.

[12] David M.Pozar, "*Microwave Engineering*", John Wiley & Sons, INC., 2005.

[13] A. Ahmed, M. Endalkachew, and G. Kompa: Power Amplifier Linearization Using Memory Polynomial Predistorters with Non-uniform Delay Taps, "*IEEE MTT-S Int. Microwave Symp. Dig.* ", Fort Worth, TX, USA, June 2004, pp. 1871-1874.

[14] J. Vuolevi and T. Rahkonen, "*Distortion in RF Power Amplifier*", Norwood, MA: Artech House, 2003.

[15] A. Khanifar, N. Maslennikov, and B. Vassilakis: Bias Circuit Topologies for Minimization of RF Amplifier Memory Effects, "*33rd European Microwave Conference*", Germany, October 2003, pp. 1349-1352

[16] Pedro Miguel Cabral, Jose Carlos Pedro and Nuno Borges Carvalho, "*A unified Theory for Nonlinear Distortion Characteristics in Different Amplifier Technologies*", Instituto de telecomunicações Aveiro, 2005.

[17] Kate A. Remley, Dylan F. Williams, Dominique M. M., P. Schreurs and John Wood Jose, "*Simplifying and Interpreting Two-Tone Measurements*", IEEE Transactions on Microwave Theory and Techniques, VOL. 52, N0.11, November 2004

[18] http://www.cel.com/pdf/datasheets/nesg2031m05.pdf